(12) LEVEL II

DNA 4593T

(6) GROUND OPTICS MEASUREMENTS OF PROJECT STRESS HIGH ALTITUDE BARIUM RELEASES

Technology International Corporation
75 Wiggins Avenue
Bedford, Massachusetts 01730

(12) 108 p.

(11) April ~~1978~~ (10) W. P. /Boquist, T. J. /Fitzgerald
G. T. /Best

(9) Topical ~~Report, for~~ Period 1 Oct~~ober~~ 1977—30 April ~~1978~~

CONTRACT No. DNA 001-76-C-0275

(15)

(14) TIC-795

(16) I25AAXH

(17) X635

THIS WORK SPONSORED BY THE DEFENSE NUCLEAR AGENCY
UNDER RDT&E RMSS CODE B322078462 I25AAXHX63532 H2590D.

(18) DNA, SBIE (19) 4593T, AD-E300 259

Prepared for
Director
DEFENSE NUCLEAR AGENCY
Washington, D. C. 20305

389 334

DISCLAIMER NOTICE

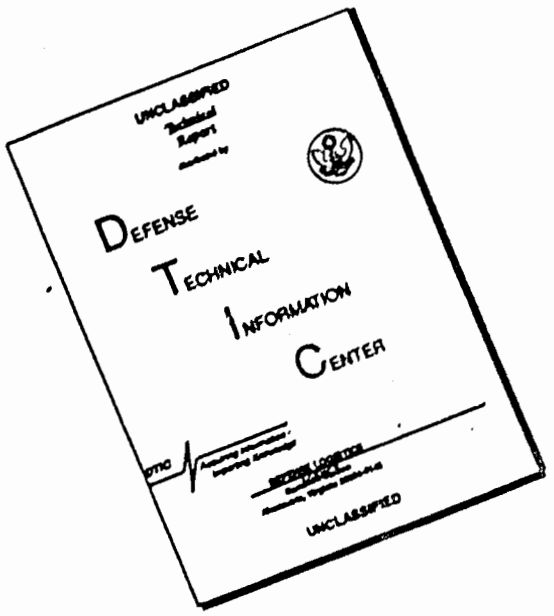

THIS DOCUMENT IS BEST QUALITY AVAILABLE. THE COPY FURNISHED TO DTIC CONTAINED A SIGNIFICANT NUMBER OF PAGES WHICH DO NOT REPRODUCE LEGIBLY.

Destroy this report when it is no longer needed. Do not return to sender.

PLEASE NOTIFY THE DEFENSE NUCLEAR AGENCY, ATTN: TISI, WASHINGTON, D.C. 20305, IF YOUR ADDRESS IS INCORRECT, IF YOU WISH TO BE DELETED FROM THE DISTRIBUTION LIST, OR IF THE ADDRESSEE IS NO LONGER EMPLOYED BY YOUR ORGANIZATION.

UNCLASSIFIED

SECURITY CLASSIFICATION OF THIS PAGE *(When Data Entered)*

REPORT DOCUMENTATION PAGE		READ INSTRUCTIONS BEFORE COMPLETING FORM
1. REPORT NUMBER DNA 4593T	2. GOVT ACCESSION NO.	3. RECIPIENT'S CATALOG NUMBER
4. TITLE *(and Subtitle)* GROUND OPTICS MEASUREMENTS OF PROJECT STRESS HIGH ALTITUDE BARIUM RELEASES		5. TYPE OF REPORT & PERIOD COVERED Topical Report for Period 1 Oct 77—30 Apr 78
		6. PERFORMING ORG. REPORT NUMBER TIC 795
7. AUTHOR(s) W. P. Boquist T. J. Fitzgerald G. T. Best		8. CONTRACT OR GRANT NUMBER(s) DNA 001-76-C-0275
9. PERFORMING ORGANIZATION NAME AND ADDRESS Technology International Corporation 75 Wiggins Avenue Bedford, Massachusetts 01730		10. PROGRAM ELEMENT, PROJECT, TASK AREA & WORK UNIT NUMBERS NWET Subtask I25AAXHX635-32
11. CONTROLLING OFFICE NAME AND ADDRESS Director Defense Nuclear Agency Washington, D.C. 20305		12. REPORT DATE April 1978 13. NUMBER OF PAGES 110
14. MONITORING AGENCY NAME & ADDRESS*(if different from Controlling Office)*		15. SECURITY CLASS *(of this report)* UNCLASSIFIED 15a. DECLASSIFICATION DOWNGRADING SCHEDULE

16. DISTRIBUTION STATEMENT *(of this Report)*

Approved for public release; distribution unlimited.

17. DISTRIBUTION STATEMENT *(of the abstract entered in Block 20, if different from Report)*

18. SUPPLEMENTARY NOTES

This work sponsored by the Defense Nuclear Agency under RDT&E RMSS Code B322078462 I25AAXHX63532 H2590D.

19. KEY WORDS *(Continue on reverse side if necessary and identify by block number)*

Barium
Cloud Triangulation
Radiometric Analysis
Striations

20. ABSTRACT *(Continue on reverse side if necessary and identify by block number)*

Optical measurements of six barium releases at high altitude are presented.

DD FORM 1 JAN 73 1473 EDITION OF 1 NOV 65 IS OBSOLETE

UNCLASSIFIED

SECURITY CLASSIFICATION OF THIS PAGE *(When Data Entered)*

CONTENTS

SECTION 1

INTRODUCTION

A two-phase field experiment was conducted by DNA during the Fall of 1976 and the Winter of 1977 to provide an operational simulation of communication transmission path effects produced by an intervening single ionized plasma cloud in the upper atmosphere. These experiments, known as Project PRESTRESS and Project STRESS, consisted of a single and a series of five rocket borne barium release experiments, respectively.

The participation of Technology International Corporation in DNA Project STRESS was for the purpose of providing general optical coverage of the barium release phenomenology during the time period a given cloud would be visible from the ground. Such coverage included:

1) A photographic history of the morphological development of the neutral and ion clouds and evolving structure.
2) Radiometric measurements of the ion cloud radiance and minimum column density.
3) Two-station triangulation measurements of the observable cloud motion(s).
4) High resolution coverage of plasma striations and spatial frequency.

The end requirement of this data acquisition was to aid in the interpretation and correlation of data obtained by other DNA experimenters in the areas of radar track and satellite transmission experiments. In addition, of course, an inherent result of the optical coverage is the general augmentation of the barium release phenomenological data base, particularly for the condition of early (pre-sunset) releases.

Table 1.1 summarizes the release parameters for the PRESTRESS (one event) and STRESS (five events) experiments. All events were a 48 kgm payload of barium reactant mixture and were programmed for a nominal 185 km release altitude. The time of release with respect to a nominal 96^{o} solar zenith angle was varied from zero up to 90 minutes before time corresponding to 96^{o}, as shown in Table 1.1. Thus, the last two events were actually released before sunset, as will be seen in more detail later. Optical observations of barium clouds at these altitudes are limited in a practical sense to solar angles of between about 96^{o} to about 102^{o} regardless of the release times.

The STRESS events, as well as other similar experiments, are released at an altitude range of 180 to 190 km to optimize ion production while minimizing ion depletion due to the formation of barium oxide. Figure 1.1 shows diagrammatically the buildup of BaO with time as a function of altitude at three different altitude regimes.

The satellite(s) used in conjunction with the STRESS transmission experiments were the Lincoln Lab LES-8 and LES-9 semi-synchronous satellites. LES-9 (to the east) was used on events Anne, Betty, Carolyn, and Dianne. LES-8 (to the west) was used on events Esther and Fern. A total of six ion cloud sounding rockets were fired from the Eglin launch complex against the last three events.

Figure 1.2 is a map of the Eglin Gulf Test Range area showing the locations of the sub-release point of each event and the relative locations of the ground optics sites. Eglin C-6 and Tyndall 9702 sites were for primary data acquisition. A mobile site was operated at different positions between the Eglin and Tyndall vicinities as dictated by predictions for each event. A fourth site was operated by SRI for TIC at Barin Field, Alabama, and an AFAL crew member on board A/C 662 operated a fifth camera station for supplementary data.

Table 1.1

PROJECT STRESS OPERATIONAL PARAMETERS

EVENT	DATE	YIELD	HOB	RELEASE ANGLES	REMARKS
ANNE	1 DEC.1976	48KG	181±.5KM	96°	LES 9
BETTY	26 FEB.1977	48KG	(179)	96°-13 MIN.	LES 9
CAROLYN	2 MAR.1977	48KG	(191)	96°-15 MIN.	LES 9
DIANNE	7 MAR. 1977	48KG	(185.5)	96°-11 MIN.	LES 9
ESTHER	13 MAR.1977	48KG	(189)	96°-75 MIN.	LES 8
FERN	14 MAR.1977	48KG	(186)	96°-90 MIN.	LES 8

( ) INDICATES UNTRIANGULATED DETERMINATION

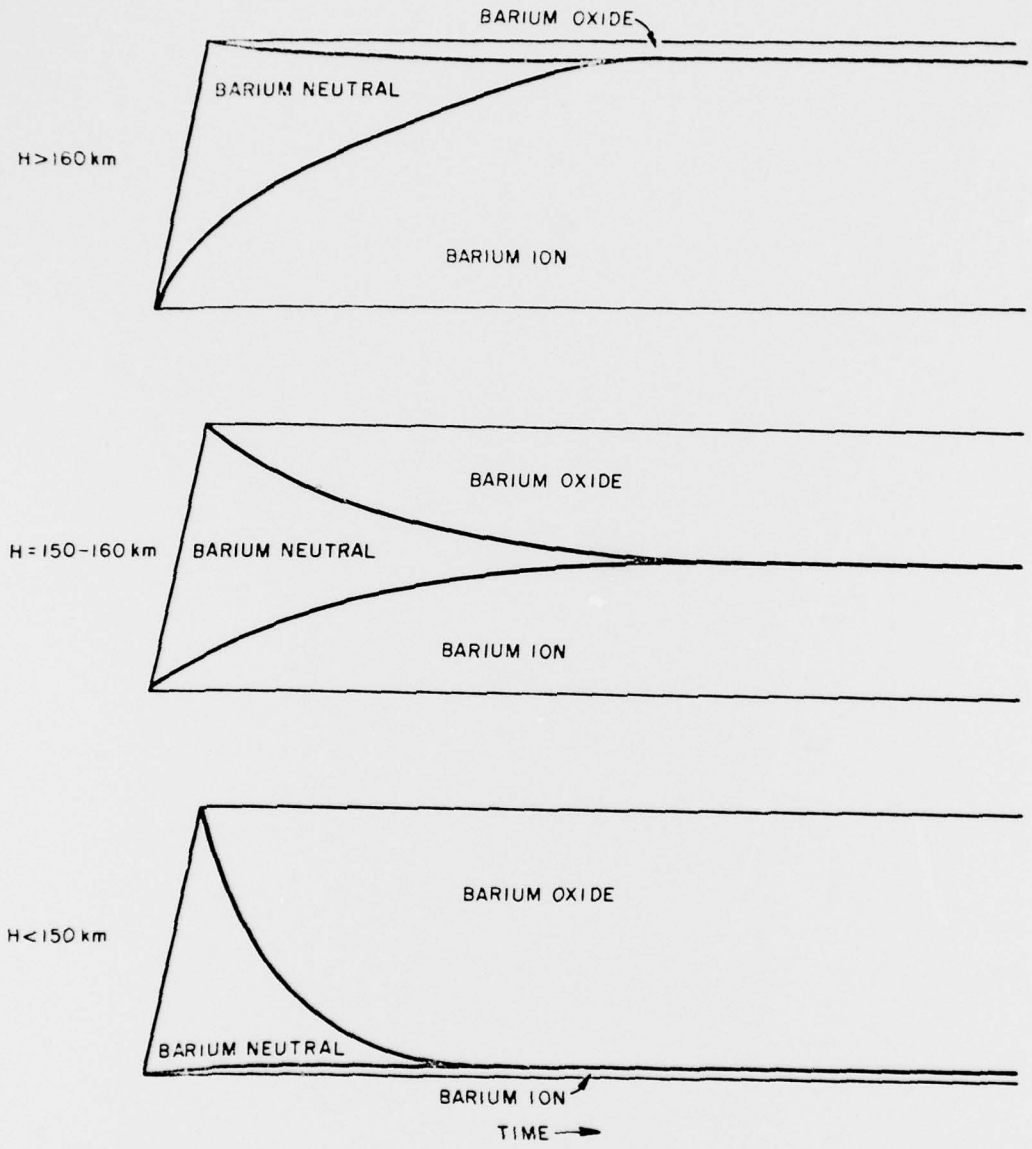

Figure 1.1 Barium Oxide Production vs Altitude

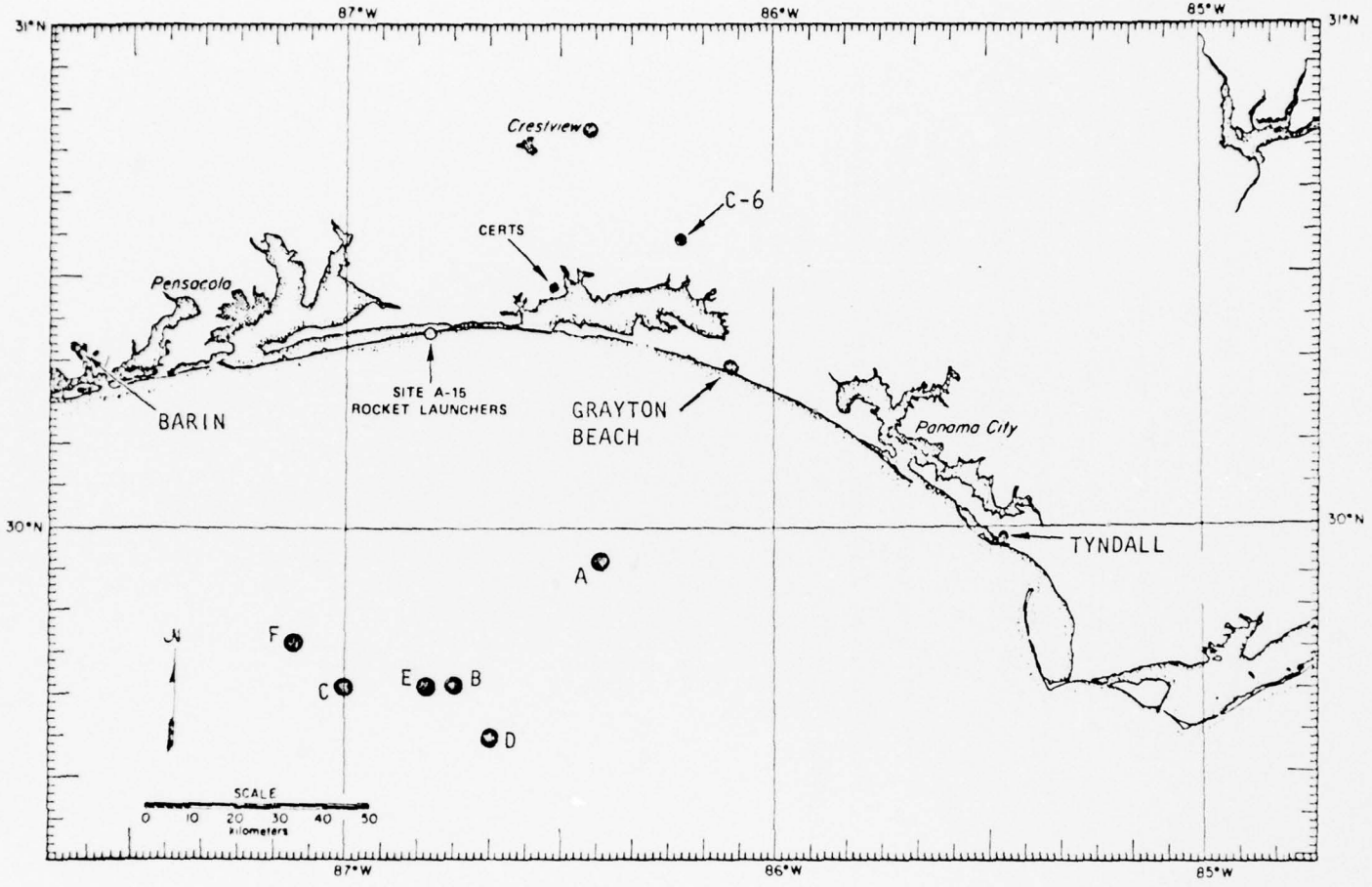

Figure 1.2 Project STRESS Sub-Release Points

Table 1.2 presents the actual release time for each STRESS event together with the relative release angle and local sunset time. Figure 1.3 plots, as a function of local time, the extent of optical coverage relative to sunset times, and the times of rocket penetration in the ion cloud. The circles indicate the release time of a given experiment. When the release point was observed, the circle is shown as a solid. In the case of event Betty, natural clouds obscured the burst point, whereas for events Esther and Fern the ambient (pre-sunset) sky background negated recording the release expansion.

Table 1.3 summarizes the various optical sites and their geographic coordinates. These coordinates for the triangulation sites include the site elevation in addition.

Table 1.2

PROJECT STRESS RELEASE TIMES

EVENT	DATE (LOCAL/GMT)	RELEASE TIME (LOCAL/GMT)	RELEASE ANGLE (SOLAR ZENITH)	TIME OF 96° (LOCAL/GMT)	SUNSET (LOCAL)
ANNE	1 DEC 1976	5 11 43 PM (23 11 43)	96°	5 12 PM (23 12)	4 45 PM
BETTY	26 FEB 1977	5 52 29 PM (23 52 29)	96° - 13 MIN (93°)	6 06 PM (00 06)	5 39 PM
CAROLYN	2 MAR 1977	5 54 10 PM (23 54 10)	96° - 15 MIN (93°)	6 09 PM (00 09)	5 42 PM
DIANNE	7 MAR 1977 (8 MAR 1977)	6 01 10 PM (00 01 10)	96° - 11 MIN (93 1/2°)	6 12 PM (00 12)	5 45 PM
ESTHER	13 MAR 1977	5 01 08 PM (23 01 08)	96° - 75 MIN (79°)	6 16 PM (00 16)	5 49 PM
FERN	14 MAR 1977	4 46 09 PM (22 46 09)	96° - 90 MIN (76°)	6 16 PM (00 16)	5 49 PM

LOCAL TIME = GMT - 6 HOURS

SOLAR RATE = APPROX. 4.4 MIN/DEGREE

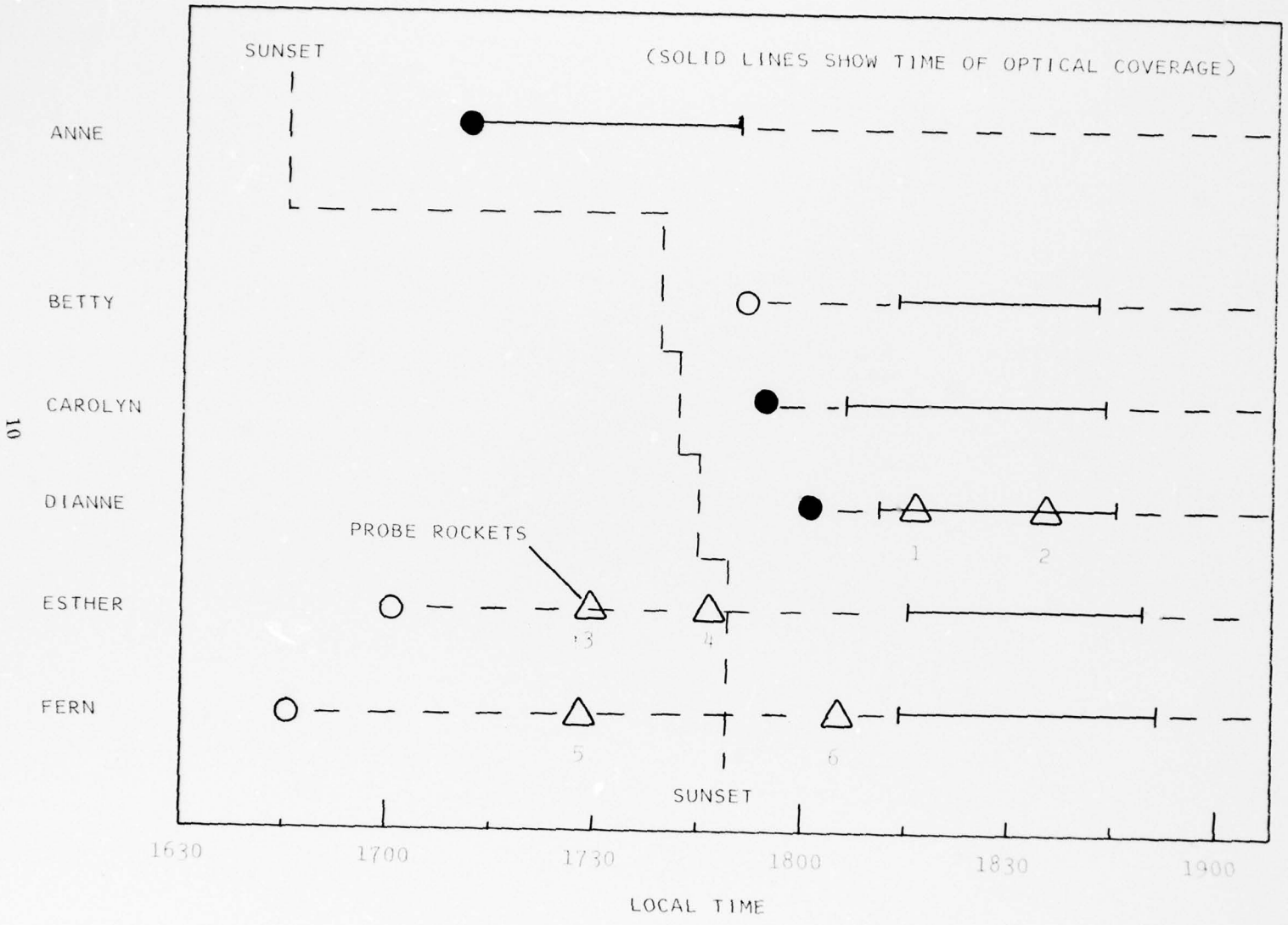

Figure 1.3 Project STRESS Optical Data Coverage

Table 1.3

GROUND OPTICS SITE LOCATIONS

Primary Sites		
Eglin AFB, Fla. C-6 Site	Elevation: 140.07' above m.s.l. 30°34'21.93"N	86°13'0.48"W
Tyndall AFB, Fla. 9702 Site	Elevation: 8.57' above m.s.l. 29°58'02.92"N	85°28'11.03"
Secondary Sites		
Mobile Optics		
A - De Funiak Springs, Fla.	30°44.6' N	86°03.7' W
B - (Clouded in)		
C - Crestview, Fla.	30°47.0' N	86°25.7' W
D - Grayton Beach, Fla.	30°18.5' N	86°05.8' W
E - Carabelle, Fla.	29°50.8' N	84°39.7' W
F - Panacea, Fla.	29°58' N	84°22' W
Barin Field, Ala.	30°23'28.3"N	87°38'12.7"W
Linson F	30°18.5' N	86°05.8' W
A/C 662 - Refer to AFAL Report		

SECTION 2

PHOTOGRAPHIC TIME HISTORY

Extensive photographic coverage of the PRESTRESS and STRESS high altitude chemical releases was obtained by the DNA ground optics sites. The coverage included color and black and white morphology data, large format triangulation data, high resolution data, and narrow band filter and spectroscopic data. This section presents selected data frames from the morphology records from each of the two primary triangulation sites, Eglin AFB C-6 site, and Tyndall AFB 9702 site, grouped in sets of four frames for each event at each site. The data frames were selected to portray the maximum extent of cloud development during the period of cloud visibility which corresponded generally to between 96^{o} and 102^{o} solar zenith angle (regardless of the actual time of release).

The reader will be able to nominally compare the two perspectives of each cloud at approximately the same times in most instances. In some cases (Event Betty particularly), natural clouds obscurred some of the coverage and only nominal comparisons can be made. In general the "normal" releases (i.e., releases at or near the time of 96^{o} SZA) will be seen to exhibit a more or less spherical neutral cloud initially, a developing ion cloud as the neutral atoms are (singly) ionized, and a late time ion cloud often sans neutral cloud as the latter will, having drifted further east (all clouds behaved in this manner), extend beyond the solar sunset line and not be visible.

Perhaps the most striking facet of the photographic history series for a given event is how different the ion clouds appear from the C-6 and Tyndall sites at comparable times.

2.1 Event Anne

Event Anne was released as part of Project PRESTRESS on 1 December 1976 at a solar depression angle of 6^{o}. Coverage was obtained from release until approximately R + 37 minutes. Figure 2.1 shows the Anne history as seen from the C-6 site looking south between R + 11 seconds and R + 26 minutes. In Plate (d) the upper left portion of the striation image is the northern most (lower) end, while the lower right portion of the image is the southern most (upper) end of the striations.

Figure 2.2 shows the Anne development from R + 3 minutes to R + 20 minutes as seen from the Tyndall site. In this perspective, the striation image slope from upper left to slightly lower right corresponds to the upper southern end and the lower northern end.

2.2 Event Betty

Event Betty was released on 26 February 1977 as the first of a series of five events in Project STRESS. The release took place at a solar depression angle of 3^{o}. At this low depression angle, the sky background negated good coverage for about the first 15 minutes. Coverage was obtained from about R + 20 minutes to R + 50 minutes. Figure 2.3 shows the development history of Betty as seen from the C-6 site from R + 23 minutes until R + 42 minutes. Considerable natural cloud cover existed at times throughout the visible portion of this event.

Figure 2.4 shows event Betty as seen from the Tyndall site at R + 30 minutes and R + 38 minutes. Relatively little data is available from this site due to the adverse effects of both intermittent cloud cover and the moon's proximity to the line of sight to the object. In this series of photographic plates, the left hand edge of the striation image corresponds to the lower northern edge of the striations while the right hand edge corresponds to the upper southern edge.

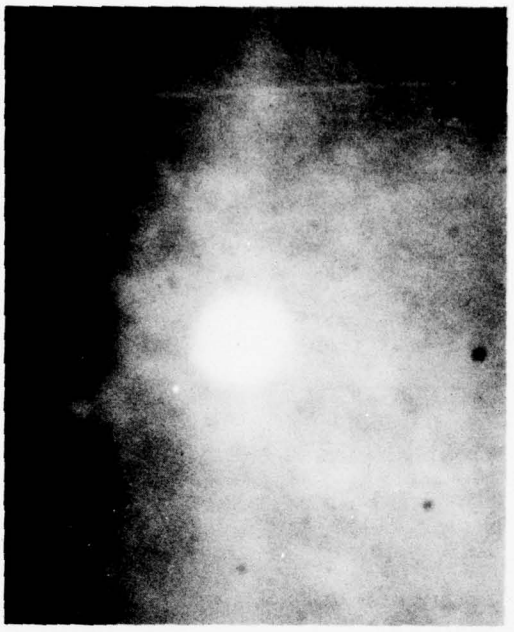

a) R + 11 sec (Frame 7)

b) R + 7 min (Frame 82)

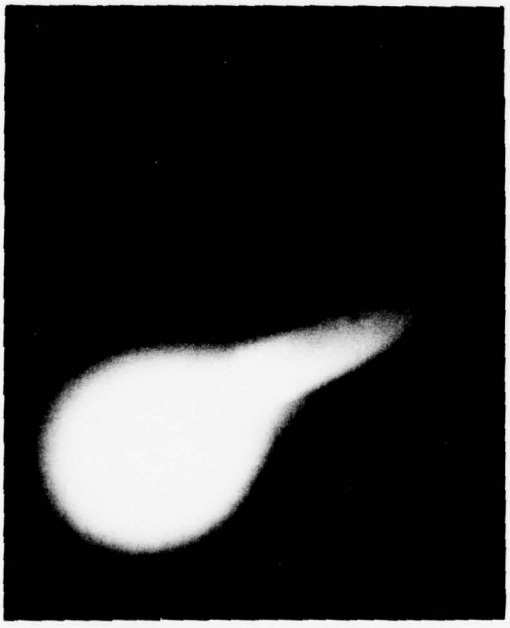

c) R + 19 min (Frame 129)

d) R + 26 min (Frame 154)

Figure 2.1 Event Anne, Eglin C-6 Site, Record 73313

a) R + 3 min (Frame 47)

b) R + 11 min (Frame 97)

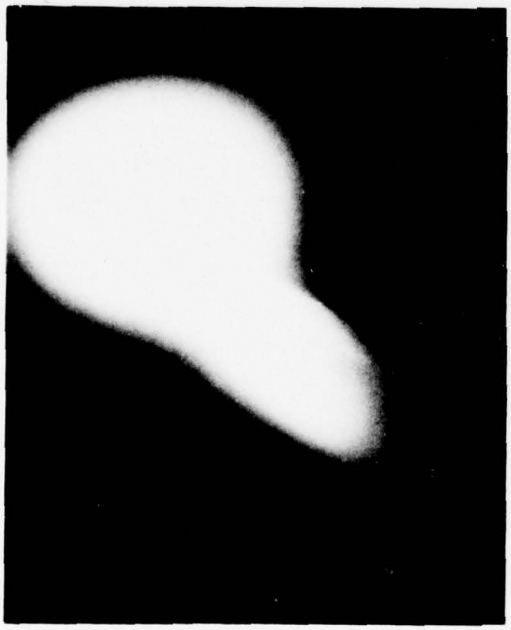

c) R + 21 min (Frame 131)

d) R + 30 min (Frame 161)

Figure 2.2 Event Anne, Tyndall 9702 Site, Record 73323

a) R + 23 min (Frame 24)

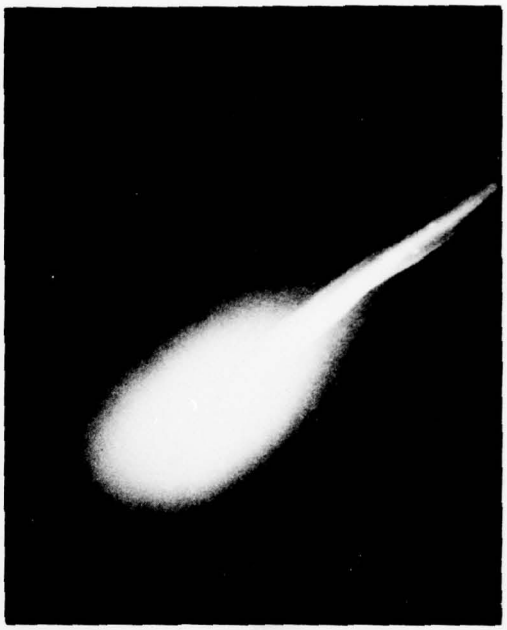

b) R + 33 min (Frame 91)

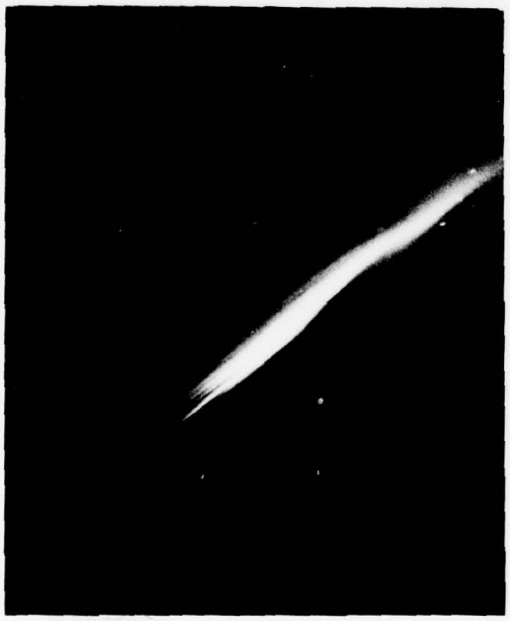

c) R + 37 min (Frame 119)

d) R + 42 min (Frame 149)

Figure 2.3 Event Betty, Eglin C-6 Site, Record 73413

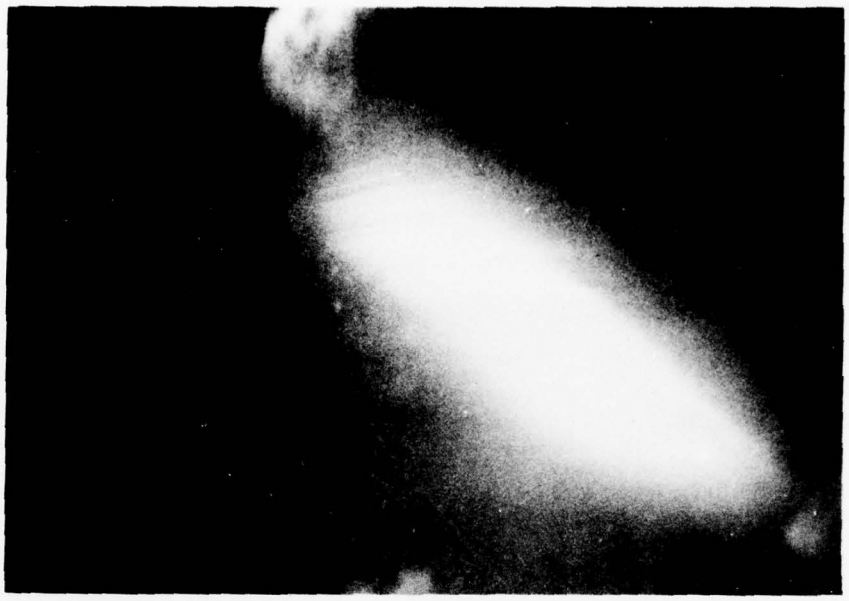

a) R + 30 min (Frame 37)

b) R + 38 min (Frame 87)

Figure 2.4 Event Betty, Tyndall 9702 Site, Record 73423

2.3 Event Carolyn

Event Carolyn was released on 2 March 1977 at a solar depression angle of about 3^{o}. Coverage was obtained from about R + 12 minutes until about R + 50 minutes. Figure 2.5 shows the ion cloud development history from R + 22 minutes to R + 40 minutes as seen from the C-6 site. In the latter plates the neutral cloud is not evident due to both dissipation and an earlier sunset on the cloud, being east of the ion cloud.

The corresponding development of the Carolyn cloud from the Tyndall perspective is shown in Figure 2.6 from R + 22 minutes to R + 43 minutes. As the ion cloud drifted east with respect to the Tyndall site, the cloud approached and then passed through the magnetic zenith, providing, respectively, the above average delineation of the striations as seen in Plates (b) and (c) and, just before sunset on the cloud, the zenith view of Plate (d).

2.4 Event Dianne

Event Dianne was released on 7 March 1977 at a solar depression angle of $3\ 1/2^{o}$, the last in a series at this nominal depression. Coverage of this event was obtained from about R + 10 minutes to about R + 45 minutes. During the period of optical coverage, two rocket probes were launched into the ion cloud from the A-15 launch site. Figure 2.7 shows the event Dianne ion cloud development history from R + 16 minutes to R + 35 minutes, as seen from the C-6 site. Dianne exhibited a significant amount of mid-cloud striation as seen to some extent in Plate (d), but shown in much greater detail in the high resolution photograph in Figure 6.10 of Section 6.

Figure 2.8 shows the Dianne time history as seen from the Tyndall site from R + 17 minutes to R + 34 minutes. Although the detailed striation contrast is not readily apparent from this perspective, the unusual deformation of the ion cloud is highlighted in this series.

a) R + 22 min (Frame 176)

b) R + 28 min (Frame 221)

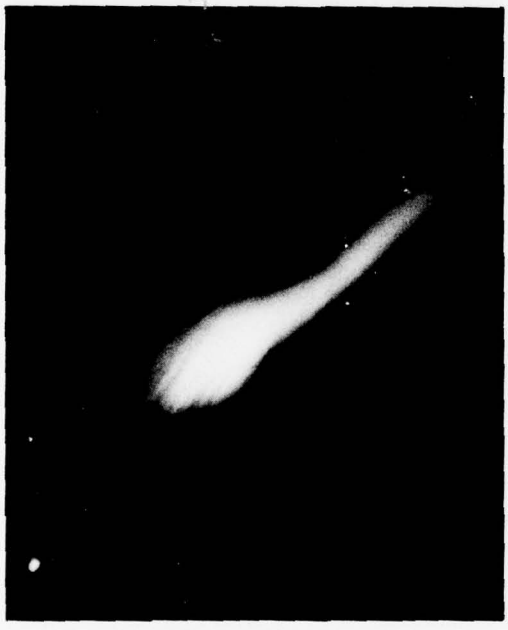

c) R + 35 min (Frame 270)

d) R + 40 min (Frame 302)

Figure 2.5 Event Carolyn, Eglin C-6 Site, Record 73513

a) R + 22 min (Frame 170)

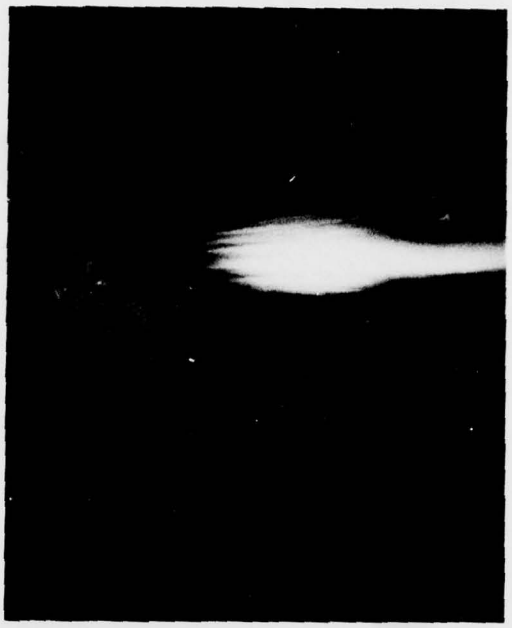

b) R + 30 min (Frame 242)

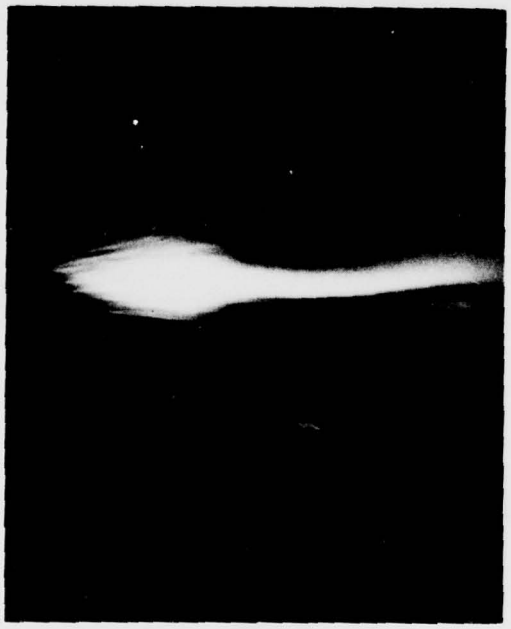

c) R + 36 min (Frame 281)

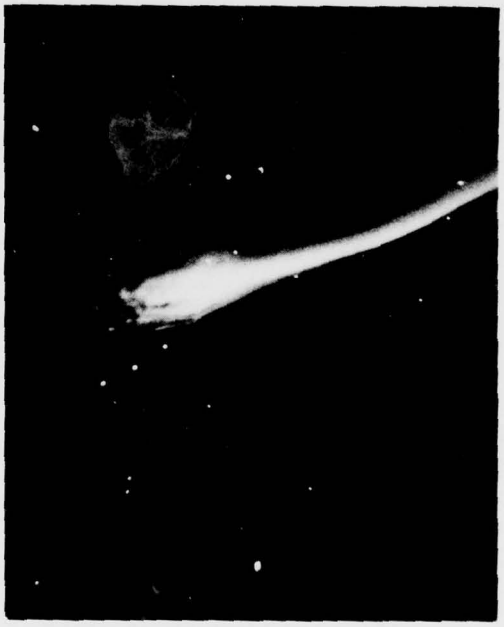

d) R + 43 min (Frame 319)

Figure 2.6 Event Carolyn, Tyndall 9702 Site, Record 73523

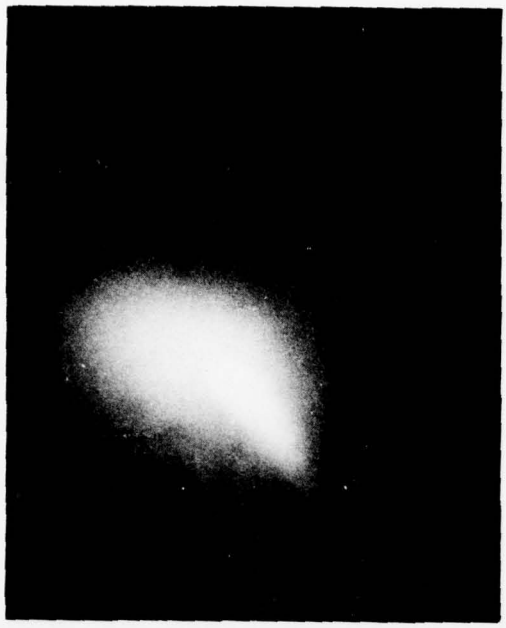

a) R + 16 min (Frame 46)

b) R + 22 min (Frame 92)

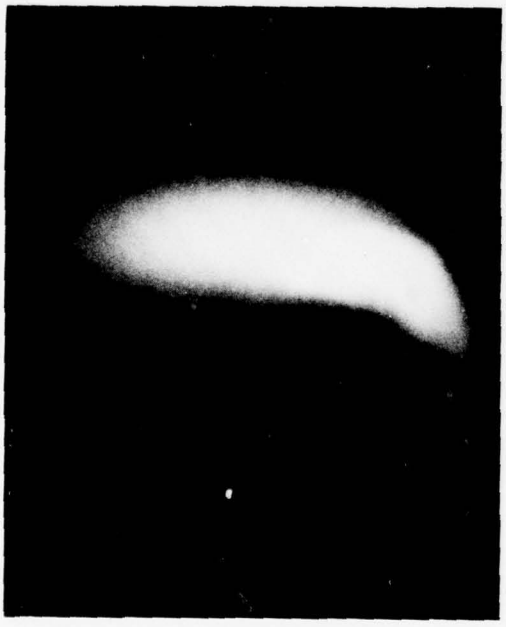

c) R + 29 min (Frame 136)

d) R + 35 min (Frame 178)

Figure 2.7 Event Dianne, Eglin C-6 Site, Record 73613

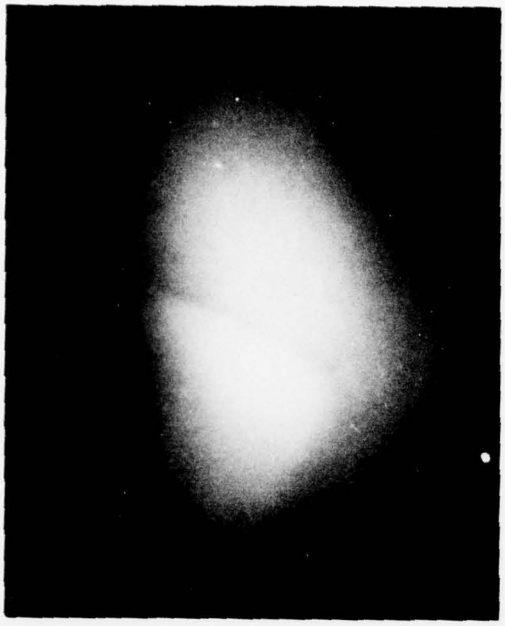

a) R + 17 min (Frame 84)

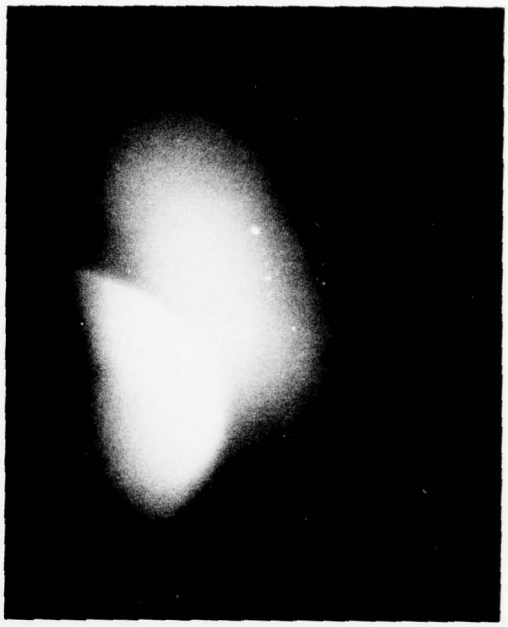

b) R + 24 min (Frame 142)

c) R + 30 min (Frame 183)

d) R + 34 min (Frame 210)

Figure 2.8 Event Dianne, Tyndall 9702 Site, Record 73623

2.5 Event Esther

Event Esther was released on 13 March 1977 at a solar zenith angle of 79^{o} -- well before sunset at the earth's surface. Coverage of this event was obtained from about 1 hour 15 minutes to 1 hour 50 minutes. Prior to the period during which the cloud was visible, two sounding rockets were fired into the ion cloud (see Figure 1.3). Figure 2.9 shows the ion cloud striation activity between R + 1 hour 22 minutes and 1 hour 38 minutes from the C-6 site. The Esther cloud motion during this period was relatively slow as noted by the celestial background reference.

Figure 2.10 shows event Esther as seen from the Tyndall site from R + 1 hour 20 minutes to R + 1 hour 38 1/2 minutes. The perspective is such that while not looking directly at the magnetic zenith (in these plates), the angle is close enough to enhance the detail of a significant portion of the striations in comparison with the C-6 perspective.

2.6 Event Fern

Event Fern was released on 14 March 1977 at a solar zenith angle of 76^{o}, comparable to that for event Esther. Coverage of this event was slightly greater than that of Esther, from about R + 1 hour 28 minutes until about R + 2 hours 6 minutes. Two sounding rockets were fired into the ion cloud for event Fern, again prior to the period for which optical coverage was possible. Figure 2.11 shows the Fern ion cloud from between R + 1 hour 42 minutes and R + 2 hours 02 minutes from the C-6 site. The Fern cloud was generally non-descript insofar as apparent visible structure from the C-6 perspective, except at late times (within the viewing window) broad longitudinal structure was evident (Plate (d)).

In Figure 2.12 the Fern event ion cloud is seen from R + 1 hour 39 minutes until R + 1 hour 52 minutes from the Tyndall site. As with event Carolyn, the Tyndall perspective encompassed a portion of the cloud through

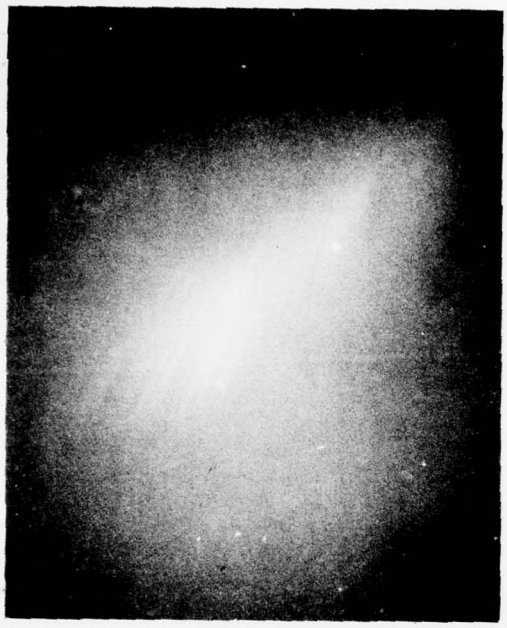

a) R + 1 hr 22 min (Frame 36)

b) R + 1 hr 28 min (Frame 82)

c) R + 1 hr 33 min (Frame 113)

d) R + 1 hr 38 min (Frame 149)

Figure 2.9 Event Esther, Eglin C-6 Site, Record 73713

a) R + 1 hr 20 min (Frame 67)

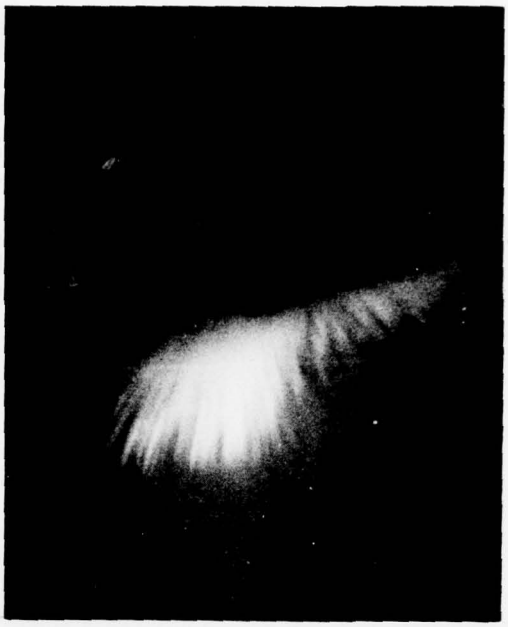

b) R + 1 hr 26 min (Frame 115)

c) R + 1 hr 30 min (Frame 143)

d) R + 1 hr 38 1/2 min (Frame 197)

Figure 2.10 Event Esther, Tyndall 9702 Site, Record 73723

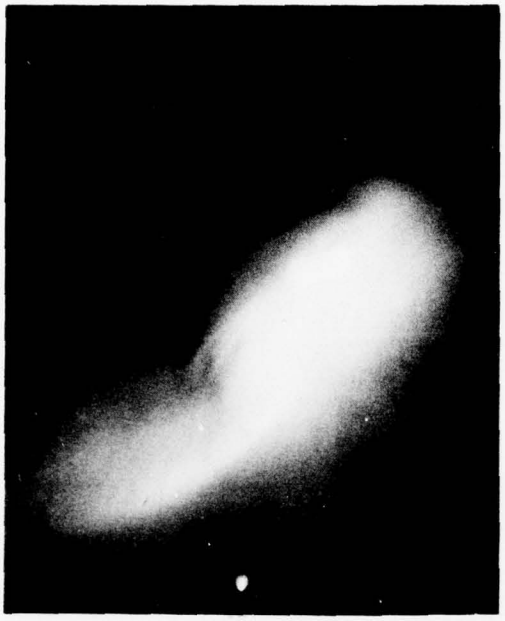

a) R + 1 hr 42 min (Frame 59)

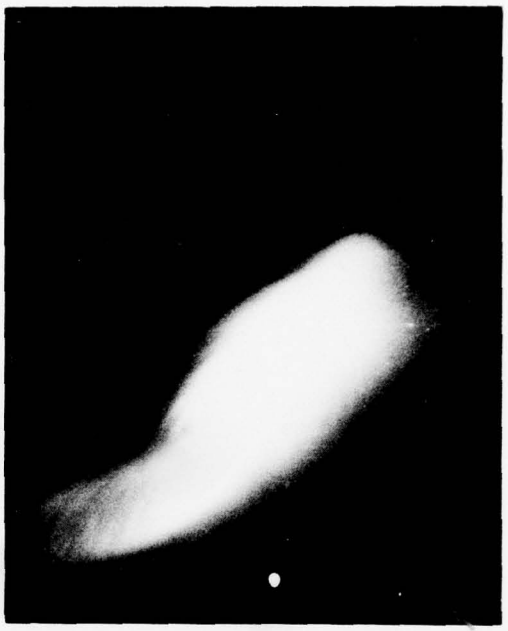

b) R + 1 hr 49 min (Frame 103)

c) R + 1 hr 54 min (Frame 136)

d) R + 2 hr 02 min (Frame 166)

Figure 2.11 Event Fern, Eglin C-6 Site, Record 73813

a) R + 1 hr 39 min (Frame 88)

b) R + 1 hr 45 min (Frame 133)

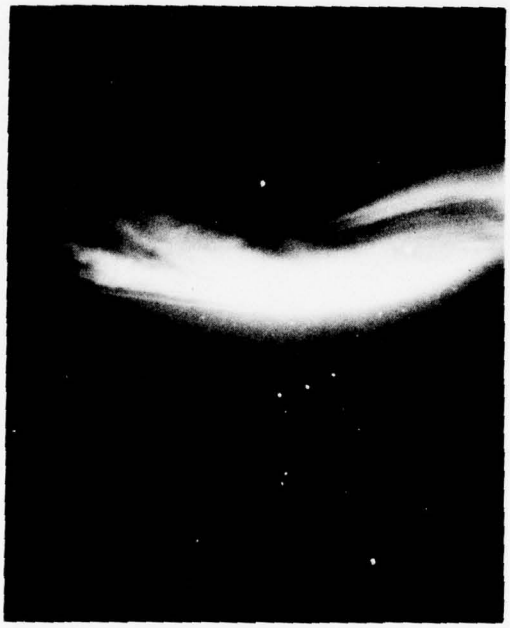

c) R + 1 hr 48 min (Frame 152)

d) R + 1 hr 52 min (Frame 176)

Figure 2.12 Event Fern, Tyndall 9702 Site, Record 72823

magnetic zenith. The uniquely distinctive line structure in the lower portion of the images (in Plates (b) and (c) particularly) is apparent due to this relatively unusual perspective. The Fern cloud, as with Esther, moved relatively slowly during the time within which it was observed.

SECTION 3

EARLY TIME CLOUD EXPANSION

As part of the overall measurements performed on the STRESS photographic data, the early cloud radius versus time was determined for events Anne, Carolyn, and Dianne. Event Betty was not observed due to natural cloud cover at release time, and events Esther and Fern were released with sky background conditions too bright to record the initial release.

The early time data was obtained with a slow cine camera running at 6 fps. The lens-film-exposure sensitivity was such that the order of 5 - 6 seconds of data was obtained.

Figure 3.1 shows the event Anne expansion curve as measured from the 6 fps cine record. The diameter dimensions are given in kilometers, assuming a 200 km nominal slant range to the detonation point. Figures 3.2 and 3.3 show similar data for events Carolyn and Dianne.

Figure 3.1 incorporates representative velocity calculations for event Anne at the initial expansion phase (3 km/sec) through the region at which stabilization is predominating (1 km/sec). Comparable magnitudes were exhibited by the other releases. At higher altitudes a faster expansion is observed, and at lower altitudes significant slower expansion is observed (Boquist et al., 1971).

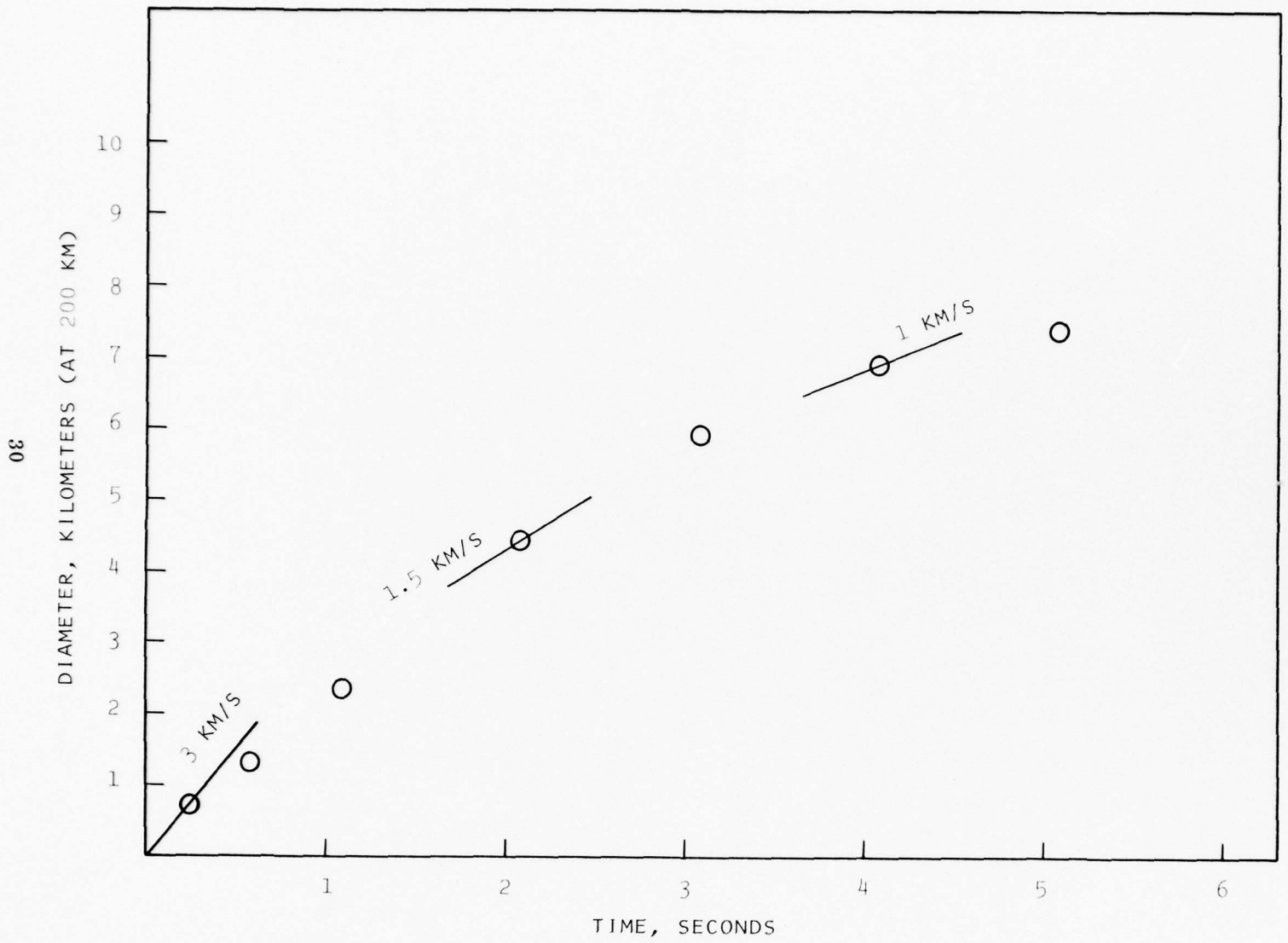

Figure 3.1 Event Anne Early Release Diameter Time History

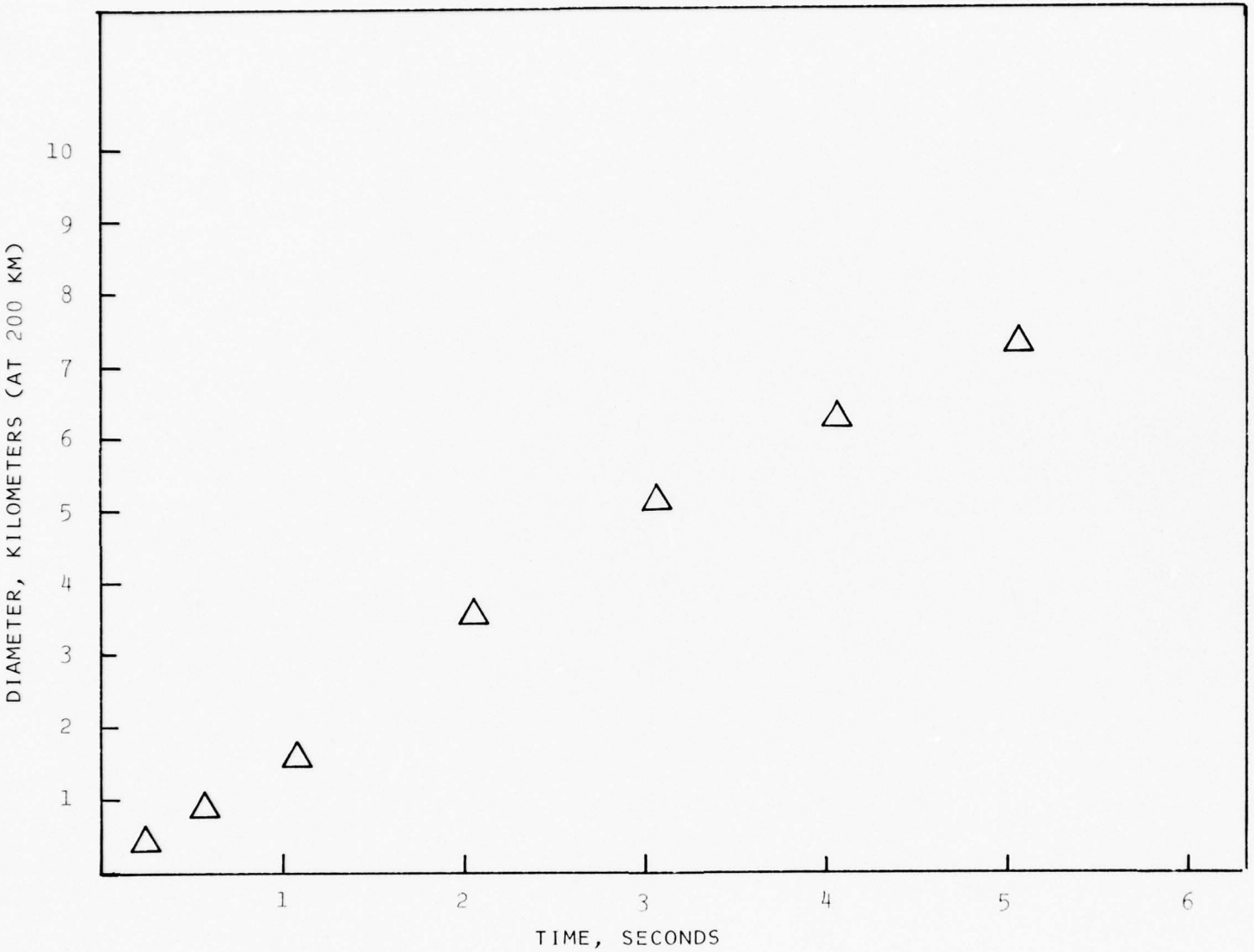

Figure 3.2 Event Carolyn Early Release Diameter Time History

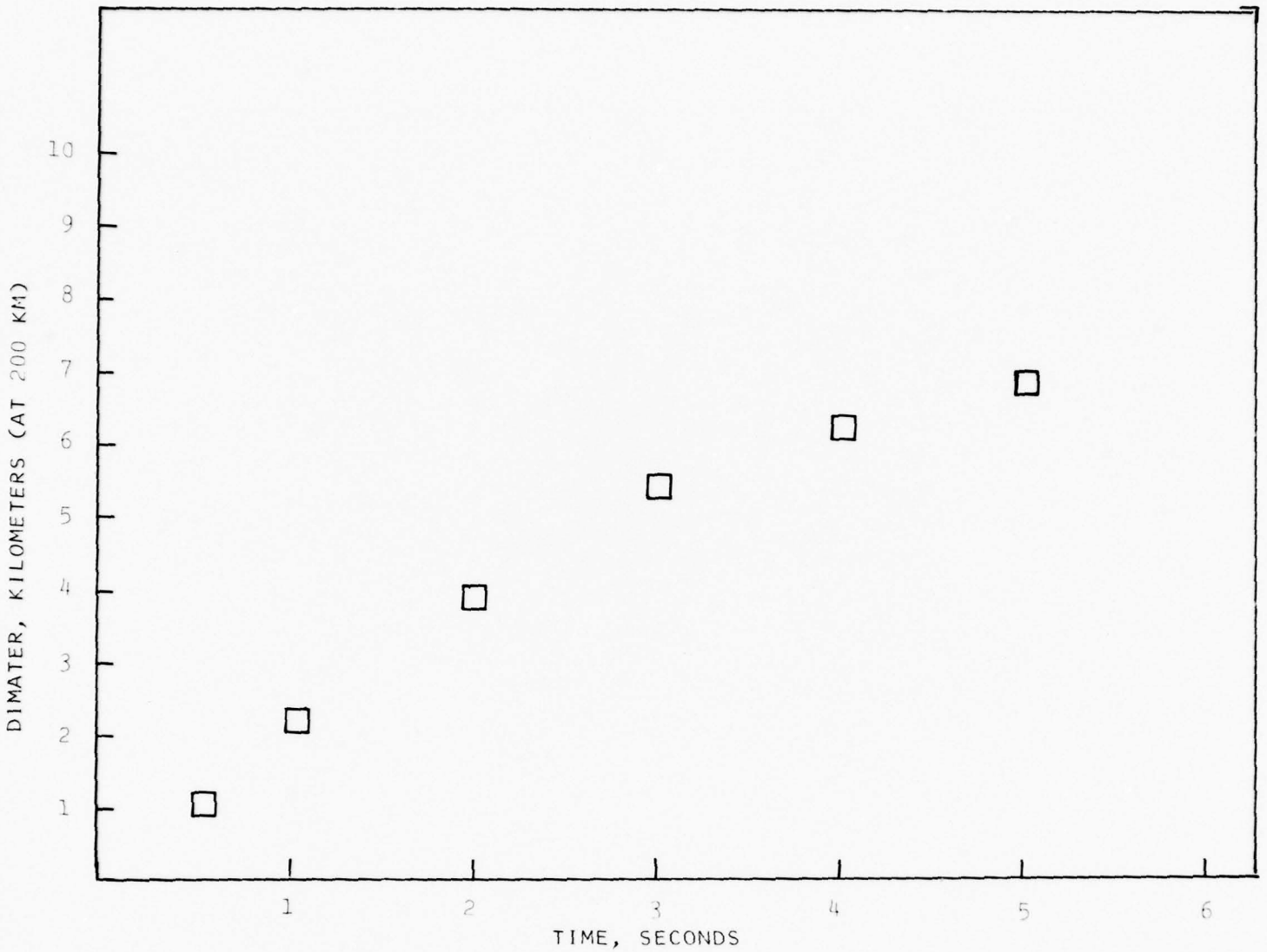

Figure 3.3 Event Dianne Early Release Diameter Time History

SECTION 4

RADIOMETRIC MEASUREMENTS AND ANALYSIS

4.1 Background

As part of the overall objectives of the Project STRESS ground optics measurements program, calibrated radiometric and spectrographic measurements were made to determine the peak and integrated radiance history of the barium ion clouds. To this end a narrow band interference filter camera system was operated at the C-6 triangulation site and a spectral survey spectrograph was operated at the Tyndall triangulation site for each STRESS event.

Solar radiation incident on a neutral barium vapor cloud in the upper atmosphere will, by virtue of its ultraviolet radiation content, ionize a portion of the neutral barium. Visible solar radiation incident on the resulting two (neutral and ion) clouds will undergo solar resonnance scattering and the clouds will emit wavelengths peculiar to either ion or neutral states of barium atoms. Ionized barium scatters light at five discrete wavelengths. The relative intensities of the cloud at each of these wavelengths will vary due to the geometry of illumination and optical thickness of the cloud. Thus, in order to determine the absolute peak and integrated ion radiance history of a barium cloud, radiometrically calibrated photography of the ion cloud, isolated by use of a narrow band interference filter, is performed. Ideally, all five emission wavelengths are observed and correlated to obtain the total ion radiance. When fewer are measured, the total must be obtained by scaling relative intensities. Moreover, when an optically thick ion cloud is photographed, the calculated results will be indicative of a lower bound of contributing ions.

Figure 4.1 presents a typical spectral density profile of a STRESS ion cloud spectrogram. Four of the five primary ion line emissions are clearly observed. The fifth line at 6497A is barely detectable due to the low long wavelength spectral sensitivity of the high speed type 2484 film used for the STRESS program. Table 4.1 identifies the known neutral and ion radiation of excited barium atoms.

The STRESS ion filter camera system incorporated a narrow band interference filter designed to isolate the 4934A ion line. The transmission of this filter as a function of wavelength is shown in Figure 4.2. Because off-axis incident ion light is transmitted less efficiently with increasing angle (the peak transmission wavelength shifts to shorter wavelengths for increasing off-axis angles), the filter was actually constructed for a normal incidence peak transmission at 4965A to permit an effective field of view of better than 24^{o} commensurate with the camera field of view of 21^{o}. The theoretical maximum field of view for an on-axis 4934A filter is about 16^{o}. The variation of transmission with incidence angle is shown in Figure 4.3 for the 6 1/2" diameter 68A bandwidth DNA filter. Figure 4.4 shows a sample two-dimensional density trace of a filter camera data frame which graphically illustrates with equal stepped density contours the edge fall-off of optical sensitivity due to the combined effect of filter shift and lens transmission at increasing field of view.

Photographic filter data was obtained for all of the STRESS events. For event Betty, however, there were sufficient natural clouds to prevent a proper time history analysis as with the other events. Thus the radiometric analysis reported here covers events Carolyn, Dianne, Esther and Fern.

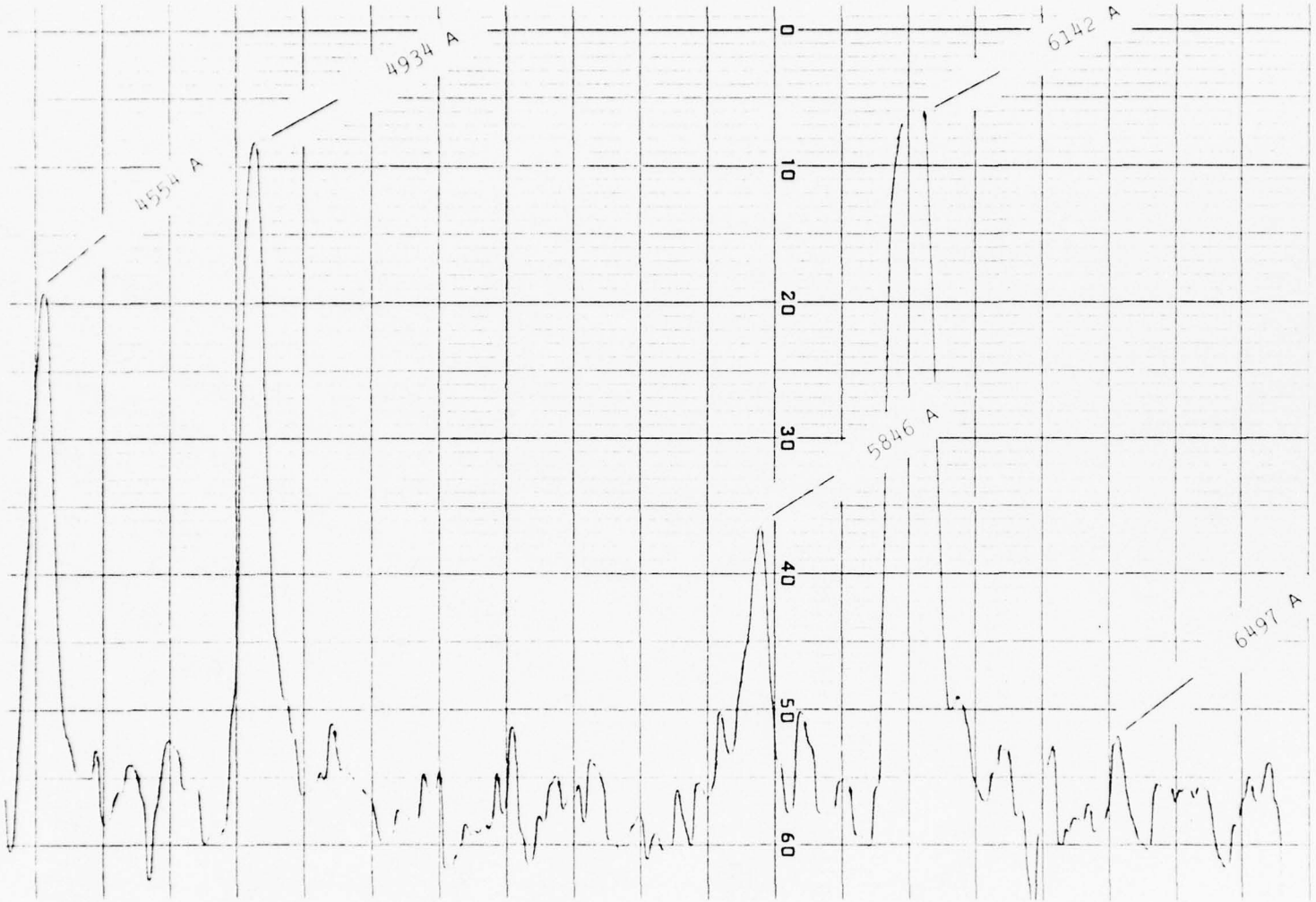

Figure 4.1 Ion Cloud Spectra Sample

Table 4.1

BARIUM CLOUD SPECTRA

STRESS OPTICAL MEASUREMENTS

Neutral Emissions	Ionized Emissions
4283	
	4554
4607 (SR)	
4726	
	4934
5535	
5778	
5806	
5826	
	5854
5907	
5972	
5997	
6019	
6063	
6111	
	6142
6342	
6450	
6483	
6498.7	6496.9
6527	
6595	
6675	
6694	

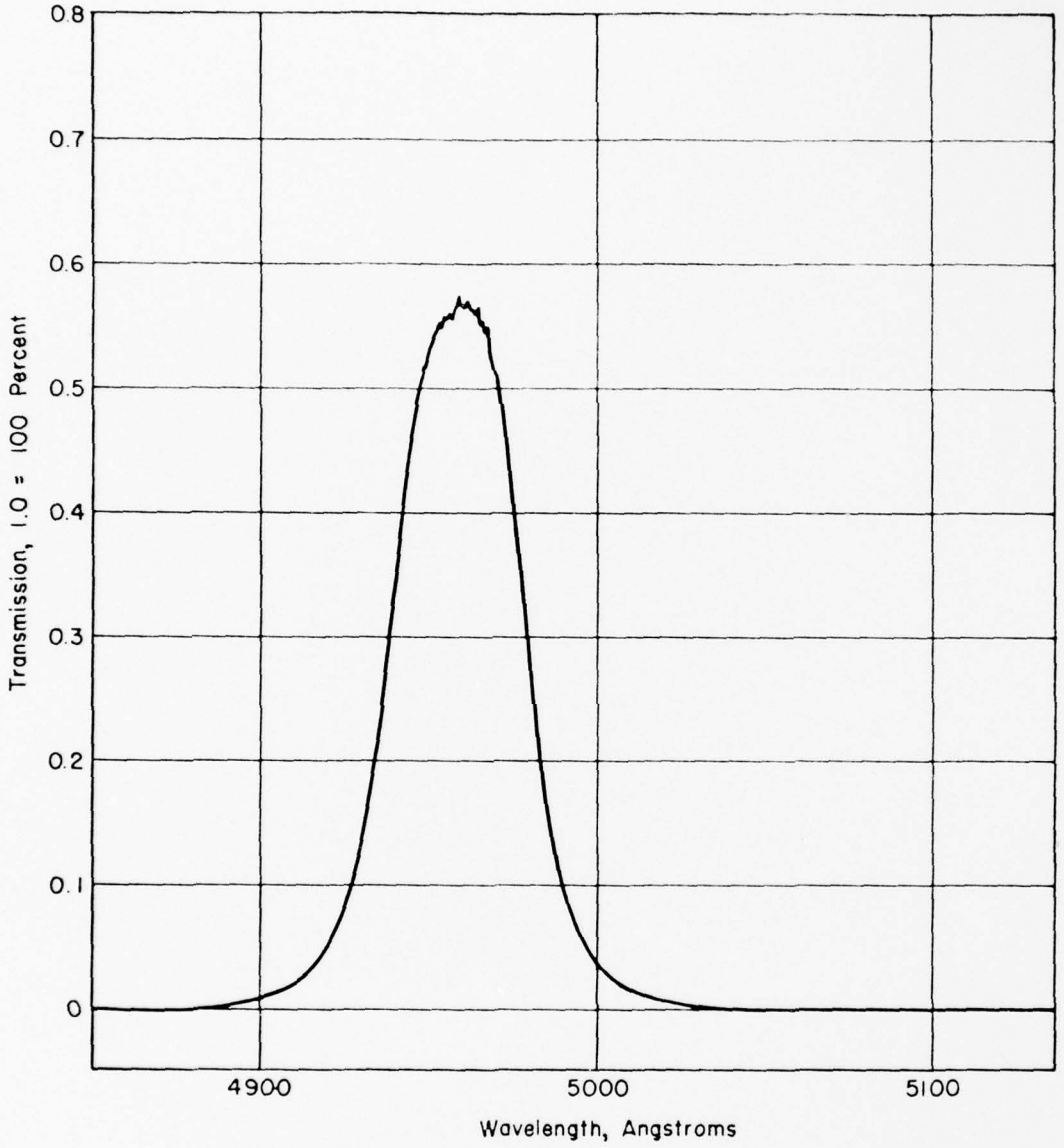

Figure 4.2 Transmission of DNA 6" diameter 4934A interference filter centered at 4960A at zero incidence angle.

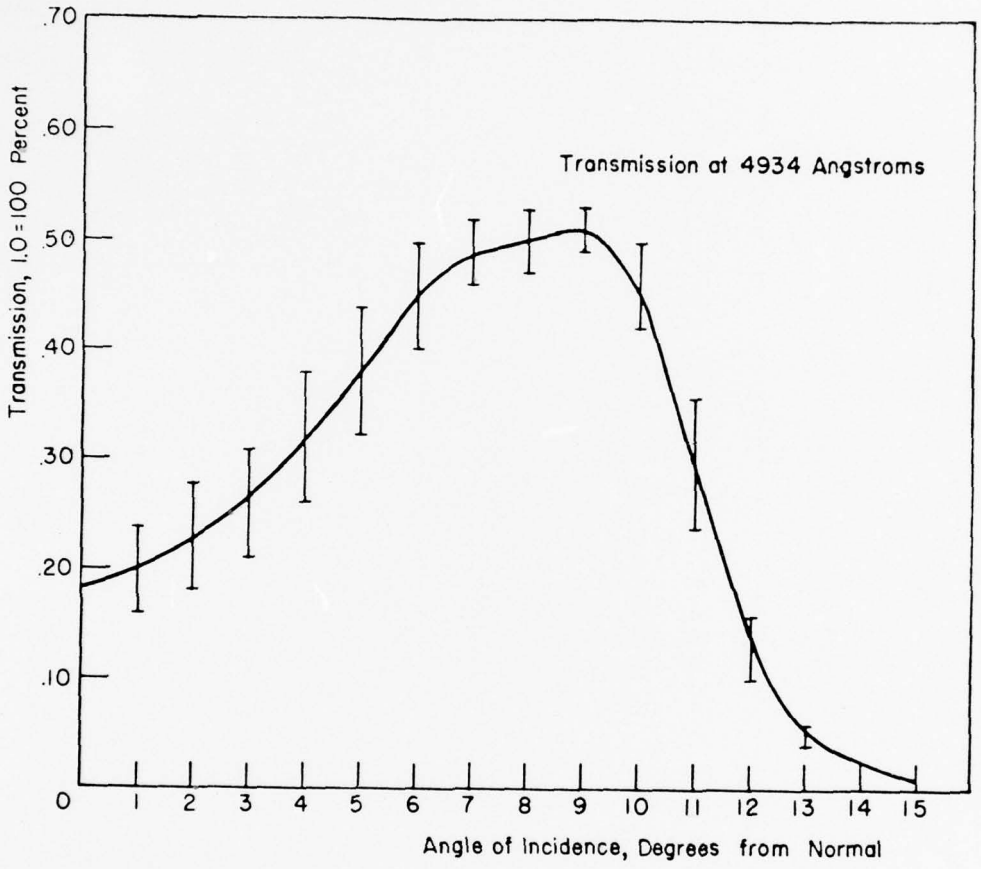

Figure 4.3 Variation of transmission with angle of incidence for DNA 4934A filter.

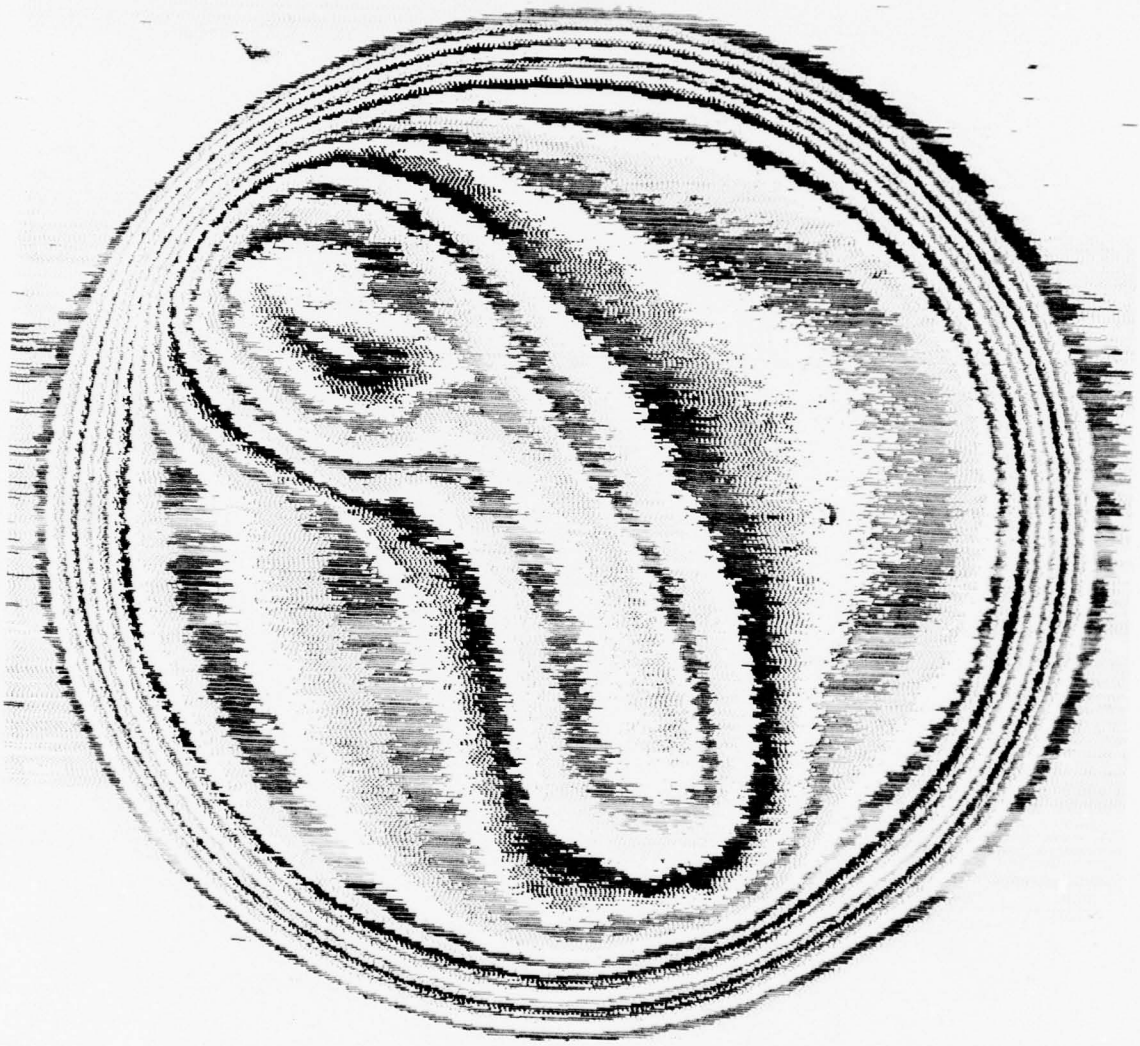

Figure 4.4 Sample Isodensitrace of Barium Cloud

4.2 Radiometric Analysis

4.2.1 Calibration Procedures

Each photographic picture element of our image (pixel) has a certain density and corresponds to a particular exposure (ergs cm^{-2} of the illumination involved). Calibration is performed by making a sequence of incrementally stepped images of known exposures at the same wavelength on the film record before processing. After processing it is then possible to uniquely relate each image element density value to an absolute exposure value. In practice the absolute density need not necessarily be measured as an intermediary such as the response (cms deflection) of the scanning densitometer to that density can be used.

The sequence of stepped images of known exposures is produced by exposing the film in a calilbration sensitometer. The sensitometer contains a standard or calibrated lamp of known spectral irradiance, and makes a contact print of a Kodak step tablet on the film to be calibrated. The step tablet consists (usually) of 21 images whose diffuse density increases in steps of 0.15 so that from step to step in the image, the exposure increases by approximately $\sqrt{2}$. The twenty steps involved thus permit a dynamic range of 1000:1 to be calibrated. The calibration exposure duration in the sensitometer is best chosen to be close to that of the field exposures. In this way the effects of reciprocity failure are minimized. In practice the exposures chosen for analysis cover a range of durations, yet only one exposure duration is available on each stepwedge. Thus the reciprocity correction factor for exposures of other durations must be known.

A convenient way to handle raw radiometric data is to define a unit exposure ($1\ E_u$) as the time-integrated irradiance in a standard duration exposure relative to which all other exposure values are measured. In this case, 0.2 second was chosen as standard, and a filtered step wedge image

was processed with all records produced by the filtered camera. This produced a range of standard exposures between 1 and 1000 E_u. The filter is necessary in the sensitometer to define a narrow wavelength range over which the sensitivity is being measured. It need not necessarily be the same filter as used in the field, as long as characteristics of both are known, but it should peak at approximately the same wavelength as the source. Since there is a finite density in the "clear" portion of any step wedge, the irradiance at step 1 (the clearest step of the wedge, and densest step at the tablet image) will not equal that of the irradiance source alone, but is, in this case, $10^{-0.19} = 0.65$ of the irradiance source.

4.2.2 Data Reduction Procedure

The data image is scanned by a double beam densitometer incorporating a mechanism which develops two-dimensional contour maps of the photographic image as a function of density. The double-beam feature permits data image film density to be compared with the density in a linear density reference wedge. The position of the wedge is continuously adjusted automatically so as to maintain a density balance. Thus, the position of the wedge is recorded by a pen operating in several possible modes. As the output record moves under the pen (in unison with the film record moving through the measuring beam), these modes write respectively "space," "dot," or "line." A sequence of three characteristics is required to distinguish increases from decreases. In practice three separate colored pens are also alternated so that one complete density cycle has 9 coded levels. As many cycles as desired may be used so that the position of the wedge may be recorded with as much resolution as is justified. Since each wedge position corresponds to a particular density, it is possible to convert directly from isodensitrace contour to Relative Exposure (E_u) without determining absolute density. For each frame scanned (i.e., for each setting of the densitometer) the cms. deflection of the wedge is recorded separately for each level of the step wedge

image.

The area within each contour of the densitometered image is planimetered and the exposure (in E_u) corresponding to each contour is also tabulated. The peak radiance of the cloud is obtained by simply determining the peak exposure of the cloud, subtracting the background and converting to absolute radiance units with the aid of the absolute E_u calibration data and the effective exposure duration.

The measurement of the integrated radiance can be treated much like determining the volume of a mountain of which the isodensitrace is a contour map and exposure corresponds to altitude. The "mountain" may be considered as a stack of progressively smaller slabs, or as a nested set of irregular cylinders; the latter concept was used in this analysis. Again background is removed by using only the volume of each cylinder above the background level.

Each cylinder has a mean exposure ("altitude") which is taken to be geometric mean of its outer and inner contours. Thus $E_{rel} = 10^{1/2}(\text{Log } E_o = E_i)$, where the subscripts refer to the outer and inner contour respectively. The cylinder area is simply the difference in total areas of successive contours. Table 4.2 illustrates a typical peak and integrated radiance calculation. Note that background subtraction occurs after exposure (rather than Log (exposure)) has been determined.

Absolute Calibration. Since the same calibration source and exposure duration were used for all sensitometric calibrations of the data records, the relative peak and integrated radiances (in E_u) can be converted to absolute peak and integrated radiances, by using constant multiplying factors, derived as follows:

The irradiance produced at the film plane by the sensitometer has been determined, through comparison with an N.B.S. standard, to be 0.165864

Table 4.2

SAMPLE PEAK AND INTEGRATED RADIANCE CALCULATION

Contour	Acm^2	ΔAcm^2	Log E_{rel}	E_{rel}
GBR	-			
GB	-			
R 1	-			
2	-			
3	325.5	10.0	1.38	24.55
G 1	315.5	13.0	1.40	26.00
2	302.5	22.05	1.43	27.70
3	280.45	22.65	1.455	29.34
B 1	257.8	32.15	1.46	31.26
2	225.65	44.0	1.51	33.50
3	181.65	37.15	1.54	35.69
R 1	144.5	15.6	1.565	37.80
2	128.9	25.2	1.59	40.27
3	103.7	16.45	1.62	43.15
G 1	87.25	17.05	1.65	45.97
2	70.2	20.5	1.675	48.70
3	49.7	15.1	1.70	51.88
B 1	34.6	13.8	1.73	55.27
2	20.8	8.4	1.755	58.55
3	12.4	6.9	1.78	62.37
R 1	5.5	2.95	1.81	66.83
2	2.55	2.3	1.84	70.96
3	.25		1.862	72.78

micro watts cm^{-2} nm^{-1} at 4965 A. The integrated transmission band of the interference filter isolating this wavelength is 3.336 nm. Thus the unattenuated exposure, E (i.e., without a step wedge in the sensitometer), is for 0.2 second calibration duration.

$$E = 0.2 \times 3.336 \times 0.165864 \times 10 \text{ ergs cm}^{-2} = 1.106647 \text{ ergs cm}^{-2}.$$

Since the step wedge does not go from density 0 to density 3, but rides on an average baseline of density 0.19, the unit exposure scale can vary from 1 to 1,000 E_u where unit exposure E_u is given by,

$$\text{One } E_u = 1.06647 \times 10^{-0.19} \times 10^{-3} \text{ ergs cm}^{-2} = 7.145 \times 10^{-4} \text{ erg cm}^{-2}.$$

Peak Radiance Calibration Factor. An extended source of radiance N ergs cm^{-1} $ster^{-1}$ sec^{-1} at a large distance, when imaged by a lens of relative aperture F for an effective exposure duration T_{eff}, produces an exposure of:

$$E = \frac{\pi N}{4F^2} T_l T_f T_a T_{eff}.$$

where T_l is the lens transmission at the wavelength of interest,

T_f is the filter transmission at the wavelength of interest, and

T_a is the atmospheric transmission at the wavelength of interest and at the zenith angle used.

Thus $$N = \frac{E}{T_{eff}} \frac{4F^2}{\pi T_c T_f T_a}$$

Expressing E in exposure units and taking $T_1 = 0.8$, $T_f = 0.35$, $T_a = 0.6$ and E_u as derived above,

$$N = \frac{E\ (E_u)}{T_{eff}}\ 3.046 \times 10^{-3}\ cm^{-2}\ ster^{-1}\ sec^{-1}\ .$$

Integrated Radiance Calibration Factor. The total power scattered by the cloud is given by Best (1972) as

$$P = \frac{\left[\Sigma_n A_n\ (E_n - E_b)\right]_{E_u}\ R^2}{T_{eff}}\ (1.3887 \times 10^5)\ ergs\ sec^{-1}$$

Effective Exposure Duration (T_{eff}). Photographic reciprocity failture can be accommodated by treating each exposure of duration other than that used for sensitometric calibration, as if it had an equivalent duration T_{eff}. T_{eff} can be determined by producing a sequence of step wedge images of different exposure durations. To maintain similar density range, a compensating neutral density filter is used. Density or step number is plotted for each wedge image. The average exposure offset $\overline{\Delta\ Step}$ (in steps) relative to the 0.2 second reference exposure is determined for each other exposure. Since each step corresponds to a change in log (Exposure) of 0.15, we may write

$$\overline{\Delta Log_{10}}(Exposure) = 0.15\ \overline{\Delta Step}$$

$\Delta\ Log_{10}\ (E_{rel})$ is obtained by N.D. - $\overline{\Delta\ Log_{10}}$ Exposure and represents the change in the logarithm of the exposure of duration T sec necessary to produce the same density as 0.2 second exposure. Since Exposure = Irradiance x Time (effective), and the irradiance remains constant, the value of Time (effective)

for each actual exposure duration can be determined as

$$T_{eff} = 0.2 \times 10 \left(\Delta \text{Log}_{10} \langle E_{rel} \rangle \right)$$

as given in Table 4.3. By graphical interpolation, T_{eff} for 1 second was found to be 0.69 sec. These values of T_{eff} have been used as required in evaluating peak and integrated radiances.

Table 4.3

EFFECTIVE EXPOSURE DURATION

Exposure (sec)	N. D.	$\overline{\Delta \text{Log}_{10}}$(Exposure)	$\Delta \text{Log}_{10}(E_{rel})$	T_{eff} (rel 0.2 sec)
0.2	0	0	0	0.2
2	.9	0.119	0.781	1.207
4	1.2	0.225	0.975	1.888
8	1.5	0.437	1.063	2.315
16	1.8	0.538	1.262	3.656
32	2.1	0.585	1.515	6.547

4.3 Radiometry Results for STRESS Events

4.3.1 Peak and Integrated Radiance Calculations

Peak and integrated radiances for the last four STRESS events of 1977 were evaluated as discussed in Section 4.2. For these events, the background contour was selected by comparing the isodensitrace with the actual film record. Figures 4.5 through 4.8 show the isodensitraces of events Carolyn, Dianne, Esther, and Fern at 18:25:16 hours, 18:31:01 hours, 18:34:18.5 hours, and 18:40:21 hours, respectively, as typical of the data obtained. The background values selected showed an appropriate rate of decrease with time and the absolute values compared satisfactorily with expected twilight sky radiances at the solar depression angles involved.

The numerical results of the peak radiance calculations are plotted in Figure 4.9 for events Carolyn, Dianne, Esther and Fern at 4934A. The data points for each event are connected by a straight line to aid the viewer. In general, minor fluctuations in the amplitude of a given event are not signifcant and merely reflect data scatter. The fall-off of each curve near the end of the data is due to sun-set on the cloud.

Figure 4.10 shows the integrated radiance of the same four events at the same release plus times.

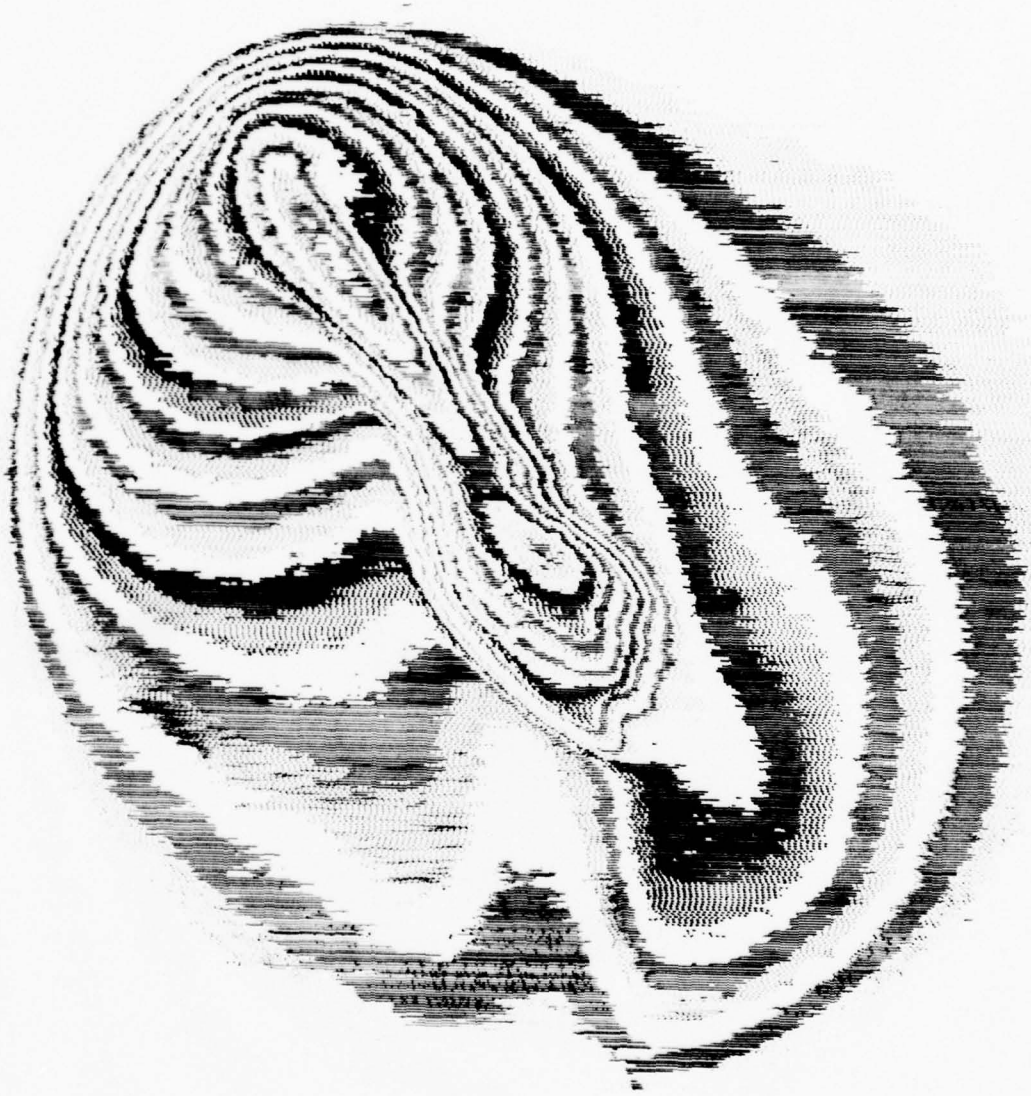

Figure 4.5 Event Carolyn IDT at R + 31:06

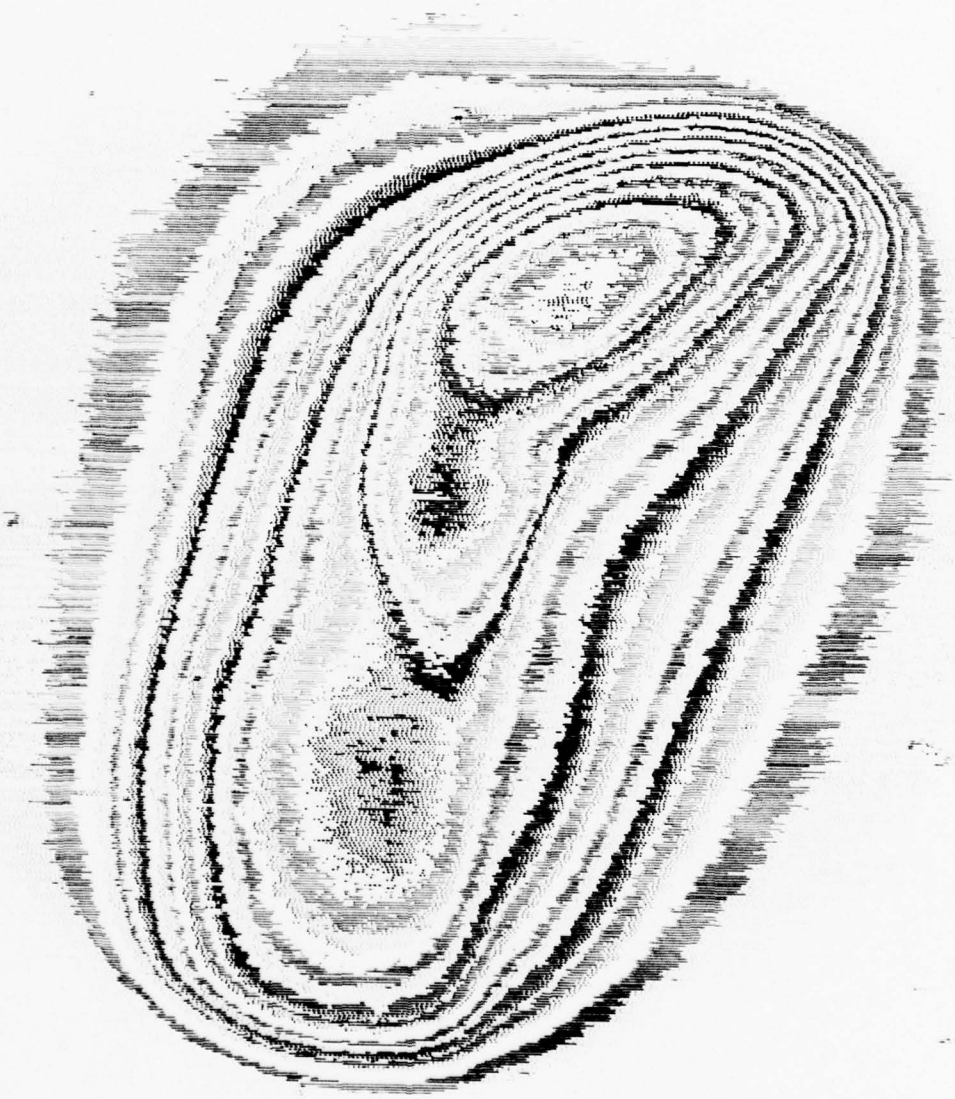

Figure 4.6 Event Dianne IDT at R + 29:51

Figure 4.7 Event Esther IDT at R + 1:33:10

Figure 4.8 Event Fern IDT at R + 1:54:12

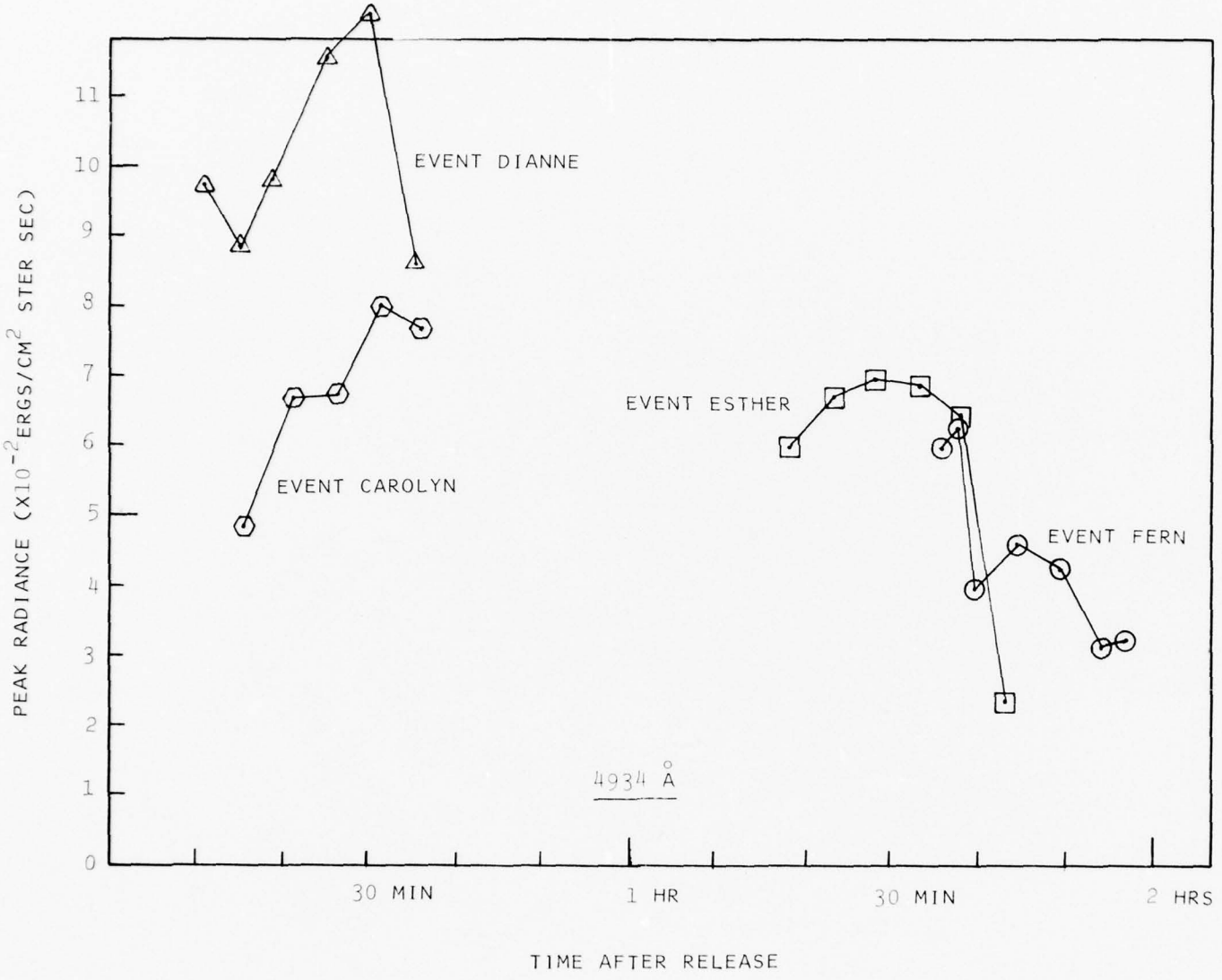

Figure 4.9 STRESS Peak Radiance

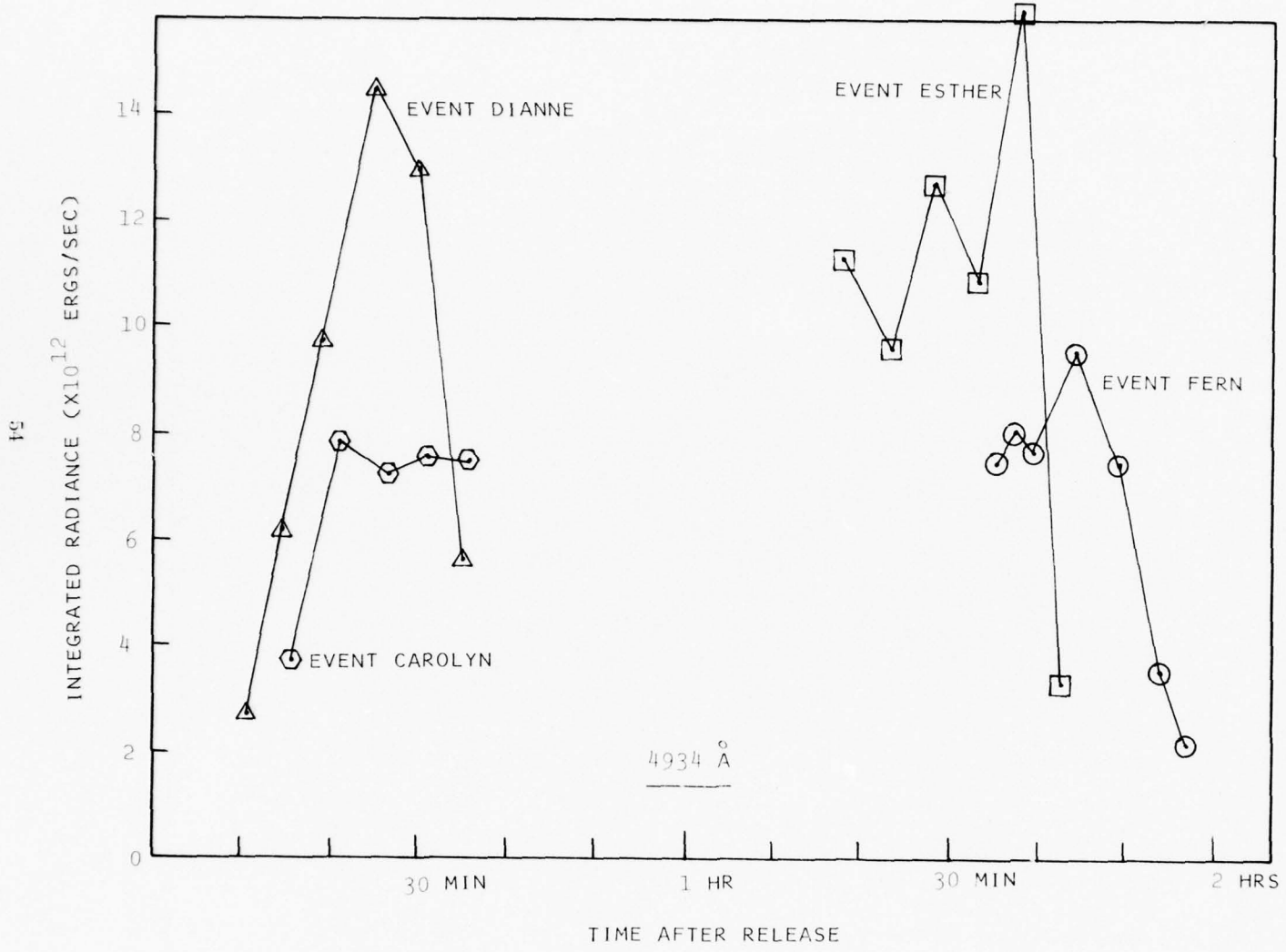

Figure 4.10 STRESS Integrated Radiance

4.3.2 Calculations of Column Density and Yeild

The peak and integrated radiance data shown in Figures 4.9 and 4.10 was converted, respectively, to maximum column density (ions cm^{-2}) and yield (ions). The conversion of peak radiance to maximum column density was performed using the optically thick model of Kivel, et al. (1972). However, since the radiance units used by Kivel refer to a Lambertian surface (Figure 4.11), the radiances tabulated in this section must be multiplied by π before entering the ordinate of Figure 4.4. Kivel uses two different sources of solar radiation data (Allen and Utrect). Best (1972) has shown that the observations fit well between the two models and a mean of the Kivel models was generated and used for this analysis.

The calculated peak ion column densities (ions/cm^2) for events Carolyn, Dianne, Esther, and Fern are presented in Tables 4.4 through 4.7 as a function of both local time and time after release. The column densities given are the order of 10^{12} ions/cm^2. The increase after the ionization phase has been completed may be due to diffusion permitting broader solar illumination of the observed column; the final decrease is due to sunset across the ion cloud, as observed earlier.

The integrated radiance data can also be converted to integrated yield. In principle the radiance value at each contour interval should be converted to ions $(cm^2 col)^{-1}$ before the summation is performed. In practice this effort is not here justified so the integrated radiance of the cloud as a whole is converted to an ion inventory as if the cloud were optically thin. Thus, the ion yield so determined represent minimum values. It has been shown (Best and Rosenberg, 1970) that there are 3.34 ions for every photon sec^{-1} scattered at 4934A. The minimum ion yields thus calculated are included in Table 4.4 through 4.7.

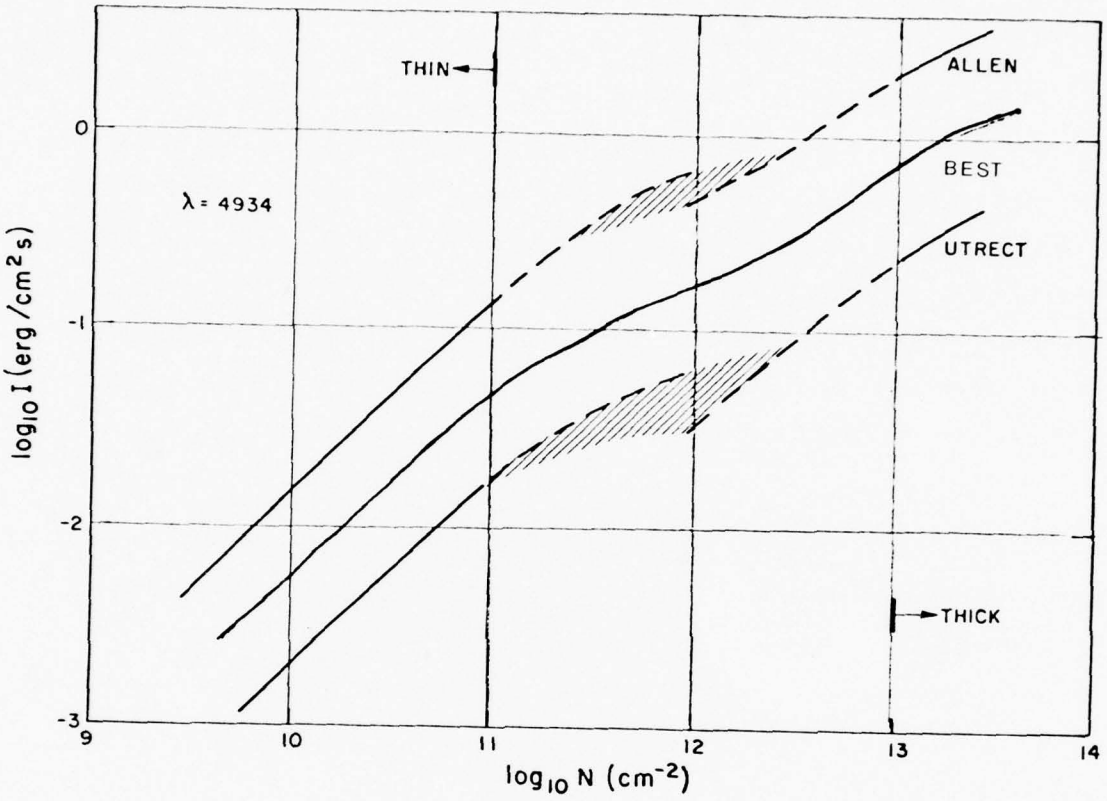

Figure 4.11 Kivel Model for Conversion of Peak Radiance to Maximum Column Density (1972)

Table 4.4

EVENT CAROLYN - ION COLUMN DENSITY AND YIELD

Time (Local)	Time (Release)	Peak Column Density (ions/cm^2)	Minimum Yield (ions)	Minimum Yield (%)
18:10:04	00:15:54	8.5×10^{11}	3.16×10^{24}	8.4
18:15:37	00:21:27	$.65 \times 10^{12}$	6.59×10^{24}	17.5
18:20:30	00:26:20	1.7×10^{12}	6.05×10^{24}	16.1
18:25:16	00:31:06	2.3×10^{12}	6.29×10^{24}	16.7
18:29:58	00:35:48	2.1×10^{12}	6.15×10^{24}	16.4

Table 4.5

EVENT DIANNE - ION COLUMN DENSITY AND YIELD

Time (Local)	Time (Release)	Peak Column Density (ions/cm^2)	Minimum Yield (ions)	Minimum Yield (%)
18:12:20	00:11:10	3.0×10^{12}	2.29×10^{24}	7.07
18:16:08	00:14:58	2.7×10^{12}	5.12×10^{24}	15.8
18:20:03	00:18:53	3.2×10^{12}	8.06×10^{24}	24.9
18:25:52	00:24:42	4.1×10^{12}	1.20×10^{25}	37.0
18:31:01	00:29:51	4.3×10^{12}	1.08×10^{25}	33.3
18:36:00	00:34:50	2.55×10^{12}	4.65×10^{24}	14.4

Table 4.6

EVENT ESTHER - ION COLUMN DENSITY AND YIELD

Time (Local)	Time (Release)	Peak Column Density (ions/cm^2)	Minimum Yield (ions)	Minimum Yield (%)
18:19:20	1:18:12	1.3×10^{12}	9.36×10^{24}	26.3
18:24:12	1:23:04	1.65×10^{12}	8.03×10^{24}	22.6
18:29:13	1:28:05	1.7×10^{12}	1.05×10^{25}	29.5
18:34:18	1:33:10	1.7×10^{12}	9.03×10^{24}	25.4
18:39 01	1:37:53	1.5×10^{11}	7.73×10^{24}	21.7
18:44:14	1:43:06	1.9×10^{11}	2.75×10^{24}	7.72

Table 4.7

EVENT FERN - ION COLUMN DENSITY AND YIELD

Time		Peak Column Density	Minimum Yield	
(Local)	(Release)	(ions/cm^2)	(ions)	(%)
18:21:42	1:35:33	1.3×10^{12}	6.29×10^{24}	19.1
18:23:46	1:37:37	6.0×10^{11}	6.76×10^{24}	20.5
18:25:51	1:39:42	4.8×10^{11}	6.42×10^{24}	19.5
18:30:31	1:44:22	7.0×10^{11}	8.03×10^{24}	24.4
18:35:16	1:49:07	6.0×10^{11}	6.22×10^{24}	18.9
18:40:21	1:54:12	3.0×10^{11}	3.07×10^{24}	9.3
18:42:50	1:56:41	3.2×10^{11}	1.84×10^{24}	5.6

The STRESS chemical payloads consisted of 48kg of Ba/Ba $(NO_3)_2$ in a 12/1 molar ratio. (About 200 gm of barium/copper oxide was used as starter, but this has little effect on the yield.) The reaction involved is

$$12\,Ba + Ba(NO_3)2 \longrightarrow 7\,Ba + 6\,BaO + N_2$$

Thus one mole of chemical mix (1.9094 kg) can generate 7 moles of free barium and the total available barium in 48 kg is 175.97 moles or 1.0598×10^{26} barium atoms.

Of the released barium vapor, an altitude dependent fraction is oxidized by reaction with O_2 and the remaining part is ionized. We assume a near-average atmosphere and determine the altitude dependent part from Figure 4.12 which is as given by Best (1972).

Table 4.8 shows the release altitudes, the fraction of vapor expected to be ionized, and the maximum potential yields of ions. Dividing the actual yields by the potential yields gives the efficiencies of the releases, as shown in the last column of Table 4.4 through 4.7. The barium/barium nitrate chemistry contains only slightly more available barium atoms compared with the 2.46 barium/copper oxide mix (175.97 or 167.7 moles per 48 kg, ref. Table 4.9). However, the yields observed for the STRESS releases are consistently high and are at least as good as the old mix without the wide scatter of integrated inventories.

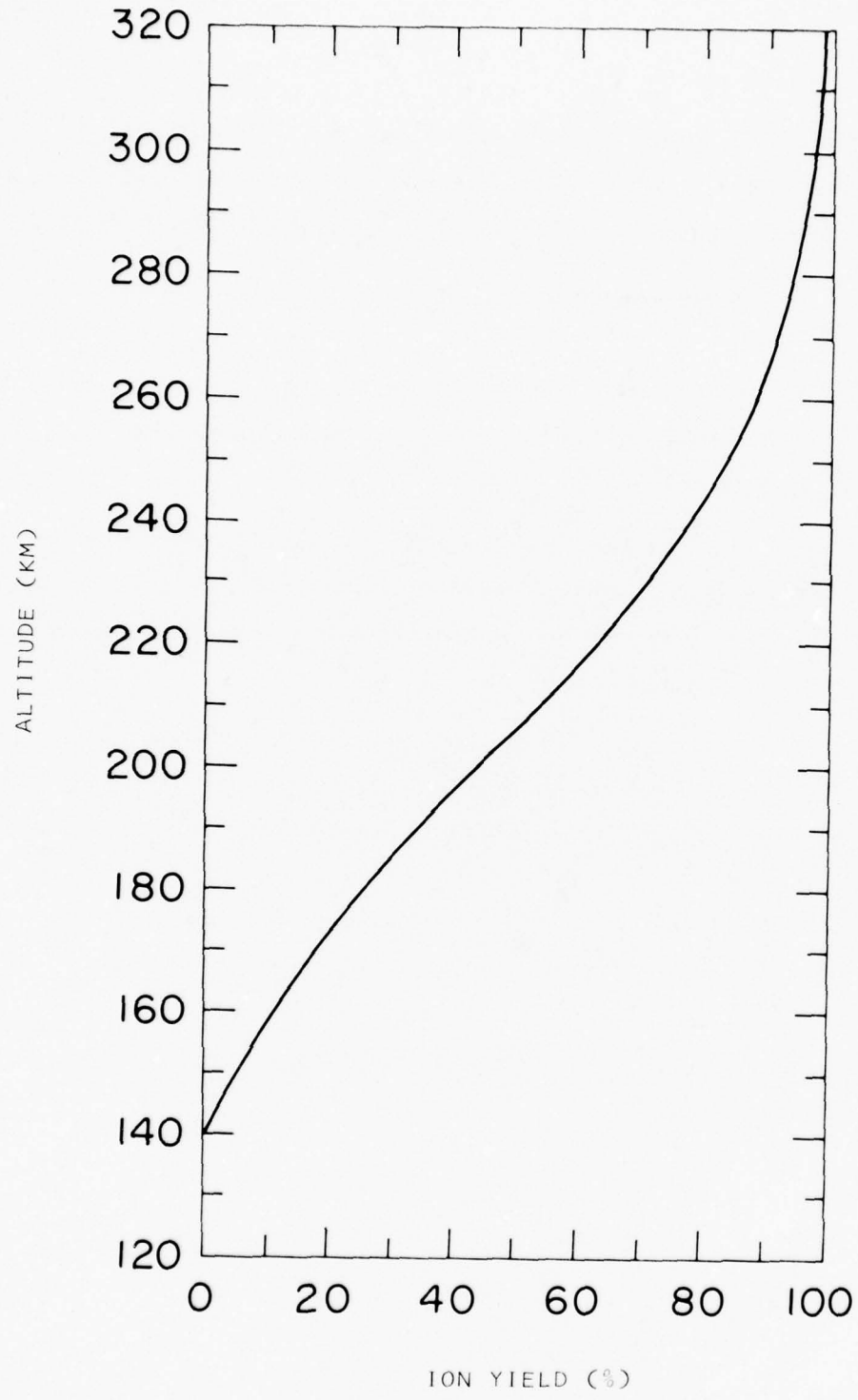

Figure 4.12 Ion Yield as Percentage of Barium Vapor

Table 4.8

MAXIMUM POSSIBLE ION YIELD FOR EACH EVENT

Event	Altitude (km)	Fraction Ionized	Potential Yield (ions)
Anne	181	0.265	2.81×10^{25}
Betty	179	0.25	2.65×10^{25}
Carolyn	191	0.355	3.76×10^{25}
Dianne	185.5	0.306	3.24×10^{25}
Esther	189	0.336	3.56×10^{25}
Fern	186	0.310	3.29×10^{25}

Table 4.9

CHEMICAL MIXES USED IN BARIUM RELEASES

Mix	A	A2	A3	A4	A5	A6	A7	A8	B	C
% Mass Ba	75	69	79.8	74	72.7	79	96.3	79.85	86.3	33.3
CuO	25	31	18.4	25	24.5	20	--	18.50	--	--
$Ba(N_3)_2$	--	--	1.8	--	1.8	--	--	--	--	--
Added Sr.	--	--	--	1	1	1	--	--	--	--
$Ba(NO_3)_2$	--	--	---	--	--	--	--	--	13.7	--
$Na\ NO_3$	--	--	---	--	--	--	--	1.65	--	--
O_2	--	--	---	--	--	--	3.74	--	--	--
Ti	--	--	---	--	--	--	--	--	--	45.93
B	--	--	---	--	--	--	--	--	--	20.73
Mole Ration Ba: Oxidizer	1.7:1	1.3:1	2.5:1	1.7:1	1.7:1	2.3:1	6.1	2.5:1	12:1	**
Moles Excess Ba/km Mix	2.24	1.12	3.48	2.22	2.17	3.24	4.67	3.49	3.67*	2.42

* This figure for mix as given. When 15 kg mix B plus 1 kg mix A as starter, there are 57.28 moles excess Ba/16 kg can (Average = 3.577 moles excess Ba per kg).

** 9.59 moles Ti + 19.17 moles B → 9.59 moles TiB_2.

SECTION 5

CLOUD TRIANGULATION

5.1 Calculational Method

The triangulation calculation routine developed by TIC determines -- for a common definable feature in the photographic image from each triangulation site -- the geodetic position in latitude, longitude, and altitude above sea level in kilometers.* A calculated miss-distance of the triangulation vectors is also obtained. If this value is greater than 1 to 1 1/2 km, the triangulation is repeated. (This check loses validity for the special case where one station views an elongated feature, e.g., striation, directly along its axis.)

In general, the triangulation records are first timed to $\pm$ 1 sec; the camera pointing attitude is then determined using iterated groups of images of identified known celestial bodies. The selected feature position is then measured with respect to the thus determined optical axis and plotted as a function of time for each triangulation site record. (The triangulation lenses have a maximum displacement distortion of 0.3 mm over a 41^{o} field.) At this point the plot is smoothed, if required, and image feature positions for each site determined for selected common times. A target vector is then developed mathematically (in geocentric coordinates) for each site/feature at a common time and the two vectors triangulated to obtain the feature position which is finally transformed into geodetic coordinates for mapping.

The accuracy of the STRESS triangulation measurements are varied in that some events presented distinct features which could be easily identified from each site and readily triangulated, whereas some events presented very diffuse indistinctive images for which only approximate edges could be identified.

---

* Based upon the Clarke spheroid model of 1866.

Whenever possible it was attempted to triangulate the following features in this analysis:

- The center of the neutral cloud.
- The sharp (trailing) edge of the ion cloud, or end-most striation.
- The diffuse end (leading) edge of the ion cloud.

For each event triangulated a comparative set of photographic plates is presented, side by side, of the developed ion cloud as seen from each of the two triangulation sites (Eglin C-6 and Tyndall 9702). This data is included in order to aid in the interpretation of the triangulated features and, more generally, to illustrate for a given event the contrast in cloud appearance as a function of perspective.

On the accompanying plots of barium cloud motion the nominal sub-release point is drawn as a solid circle with the release time in hours and minutes. The symbols for cloud feature position as a function of time are shown as minutes after the (same) hour (not release-plus times), except for Esther and Fern which are shown as minutes after the following hour.

A summary table of calculated cloud velocities is presented at the conclusion of this section. This data is qualified and attention should be paid to the relevant discussion at that point.

5.2 Event Anne

Figure 5.1 shows both the neutral and ion clouds at R + 21 and R + 26 minutes for PRESTRESS Event Anne, from Tyndall and C-6 sites, respectively. In the Tyndall photograph the slope of the field aligned (and striated) ion cloud from upper left to upper right corresponds to higher (southern) and lower (northern) altitudes along the field lines. In the C-6 photograph, however, because of the critical perspectives with respect to the field lines, upper left is the lower (northern) end of the ion cloud striations, while lower right is the upper (southern, converging) end of the striations.

Figure 5.2 shows the neutral and ion cloud tracks of Event Anne from release to R + 24 minutes (neutral) and R + 30 minutes (trailing striation). At R + 30 minutes, (23:42) the striation was measured to extend from 150 km at the northern lower end to an altitude of 205 km at the southern upper end, as shown in this figure. The triangulated vertical motion of the cloud features in general is plotted in Figure 5.3. The sweep of the curves upward beyond R + 25 minutes is indicative of the sun setting on the lower extremities of the cloud which thus appear to be higher in altitude.

5.3 Event Betty

In Figure 5.4 the ion cloud of Project STRESS Event Betty is shown at R + 42 minutes as seen from both Tyndall and C-6 sites. In the Tyndall photograph the lower portion of the image represents the lower, northerly end of the ion cloud. This corresponds to the lower left (striated) portion of the image representing the C-6 perspective.

Figure 5.5 shows the cloud tracks of the Event Betty neutral cloud to R + 32 minutes and the lower end of a striation, identified at "A", to

a) R - 21 min, Tyndall Site

b) R - 26 min, C-6 Site

Figure 5.1 Project PRESTRESS, Event Anne, Release Time 05:11:43 L

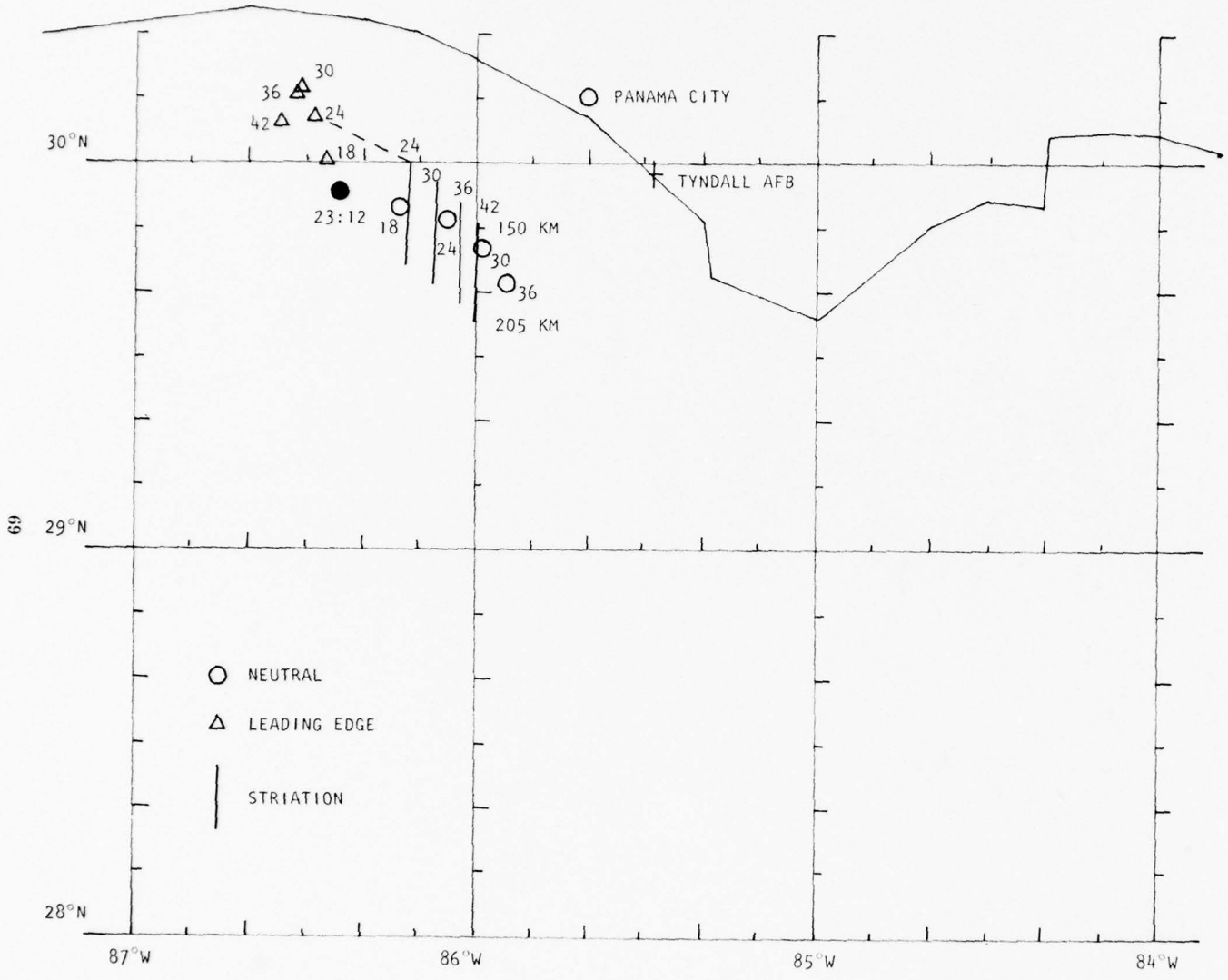

Figure 5.2 Event Anne Cloud Tracks

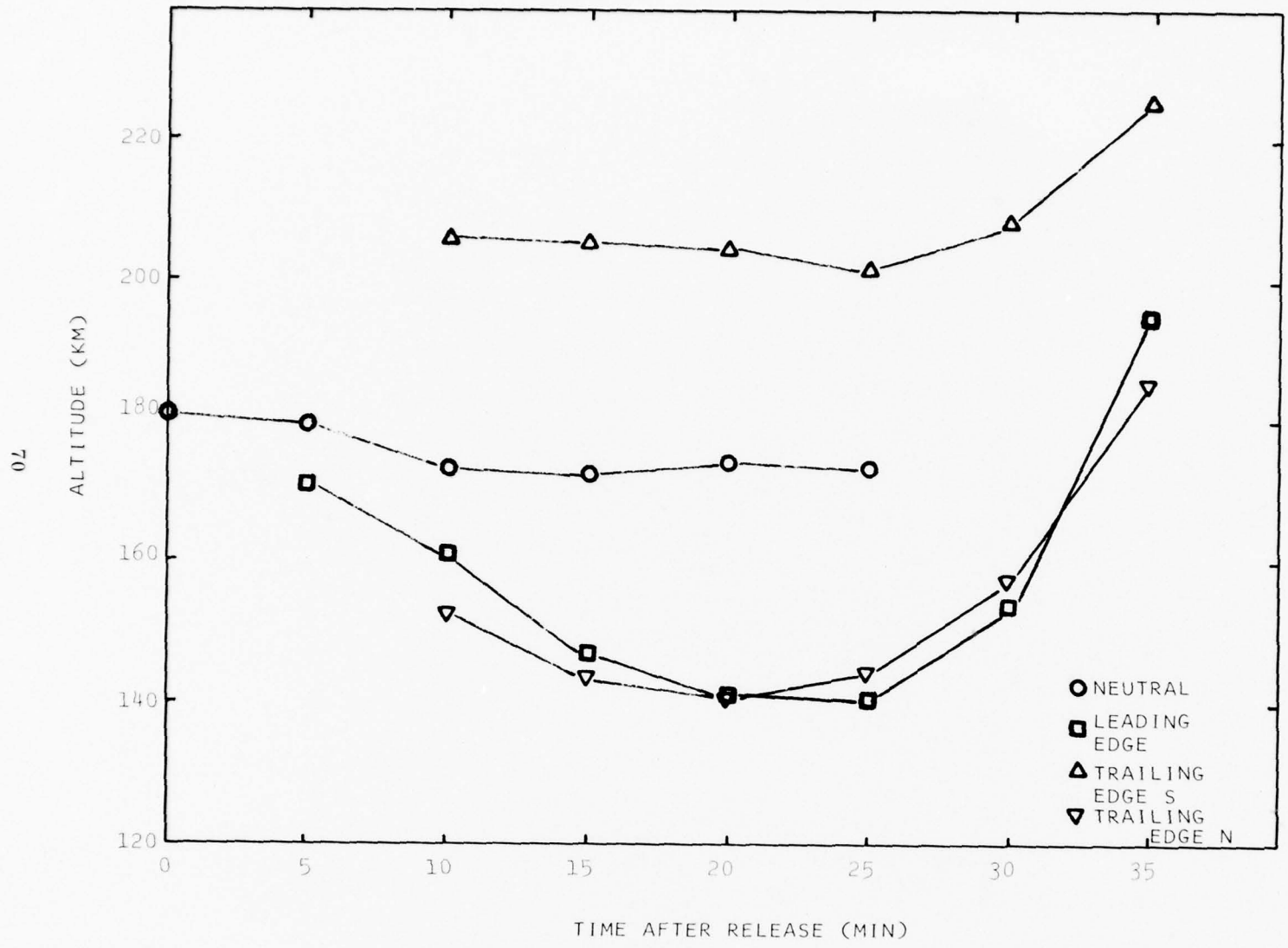

Figure 5.3 Event Anne Cloud Altitude History

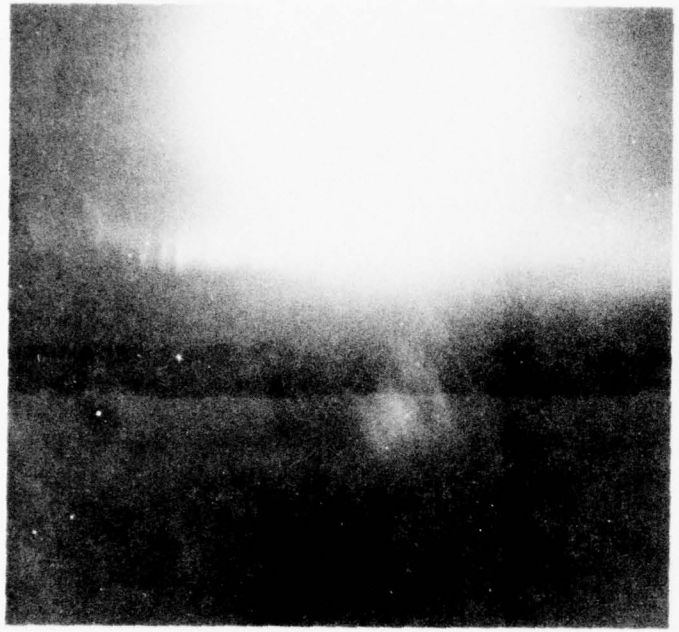

a) R + 42 min, Tyndall Site

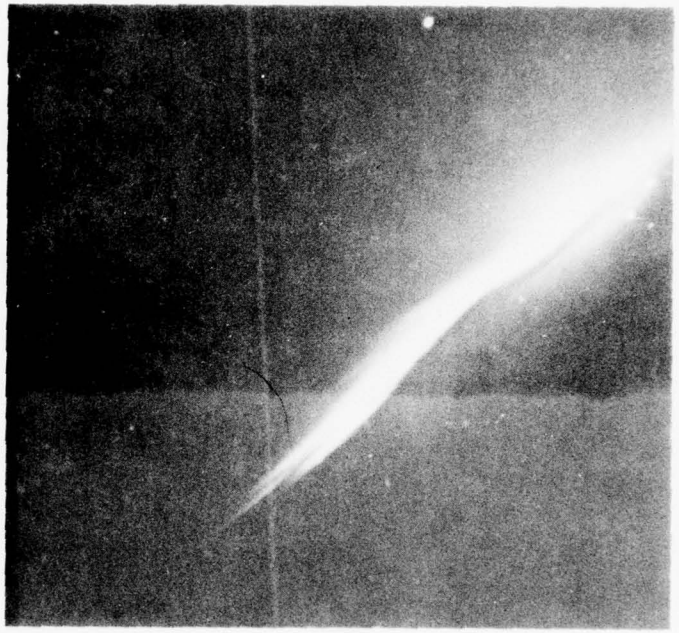

b) R + 42 min, C-6 Site

Figure 5.4 Project STRESS, Event Betty, Release Time 05:52:29 I.

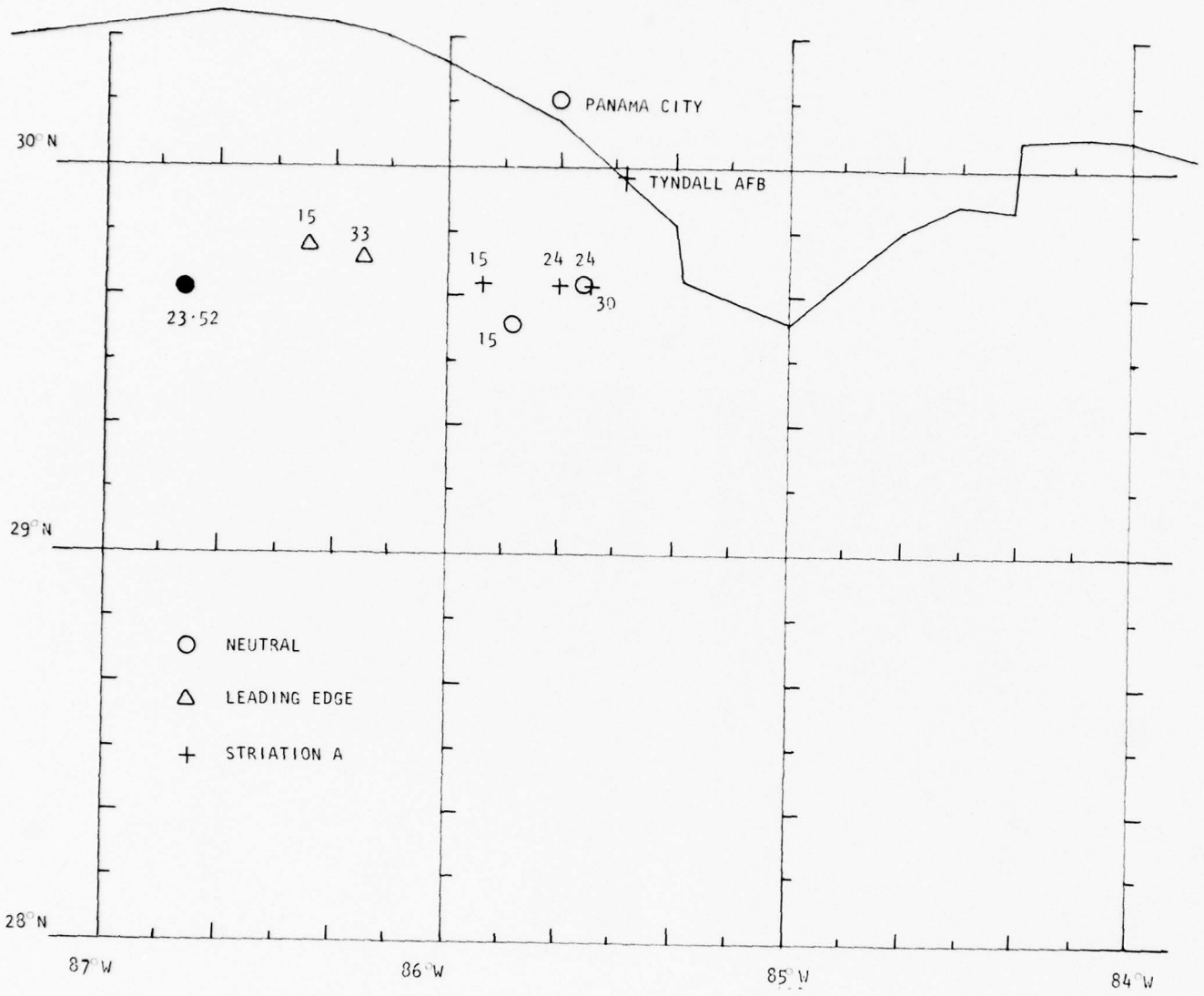

Figure 5.5 Event Betty Cloud Tracks

R + 38 minutes. Also shown is the last measurable position of the leading edge at R + 41 minutes. Both the center of the neutral cloud and the trailing edge of the ion cloud moved very nearly due east during this event.

5.4 Event Carolyn

Figure 5.6 shows the comparative views of Event Carolyn at R + 36 and R + 40 minutes. In both the Tyndall and C-6 photographs, the left most end of the striations is down and to the north. No neutral cloud is evident in these photographs. At later times, the Tyndall site was able to view the ion cloud essentially up the field lines passing through the striated cloud for a short period just before the sun set on the cloud.

Figure 5.7 plots the motion of the Event Carolyn neutral cloud center, the western (leading) edge of the ion cloud, and the upper end (only) of the foremost eastern (trailing) striation (U). The neutral cloud was measured out out to R + 33 minutes, and the ion cloud to R + 39 minutes. In this instance the overall cloud motion was east southeast.

5.5 Event Dianne

The complementary perspectives of Event Dianne from Tyndall and C-6 are shown in the Figure 5.8 ion cloud photographs at R + 34 and R + 35 minutes. This event was somewhat unique relative to the two previous events released at about the same solar depression angle in that the cloud exhibited both significant east-west longitudinal distortion as well as detailed striated structure in its mid-section at later times. This latter observation is more clearly evidenced in Figure 6.10 taken from a C-6 high resolution photographic record.

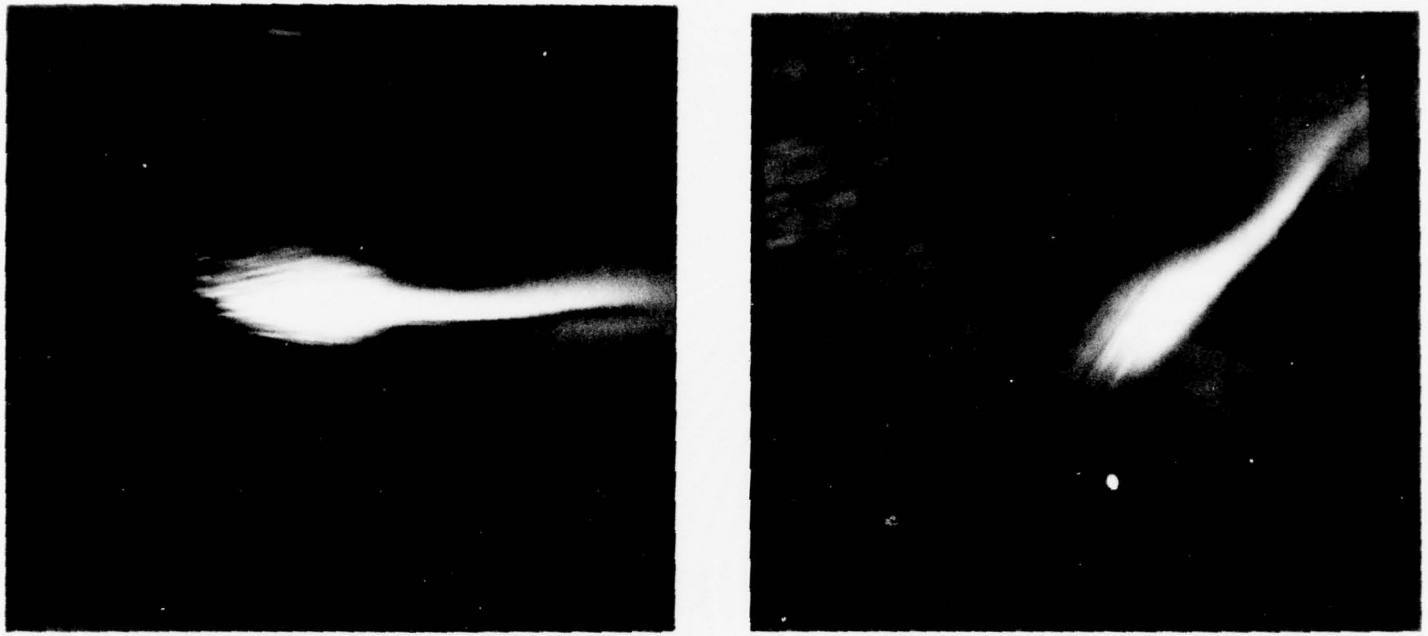

a) R + 36 min, Tyndall Site

b) R + 40 min, C-6 Site

Figure 5.6 Project STRESS, Event Carolyn, Release Time 05:54:10 L

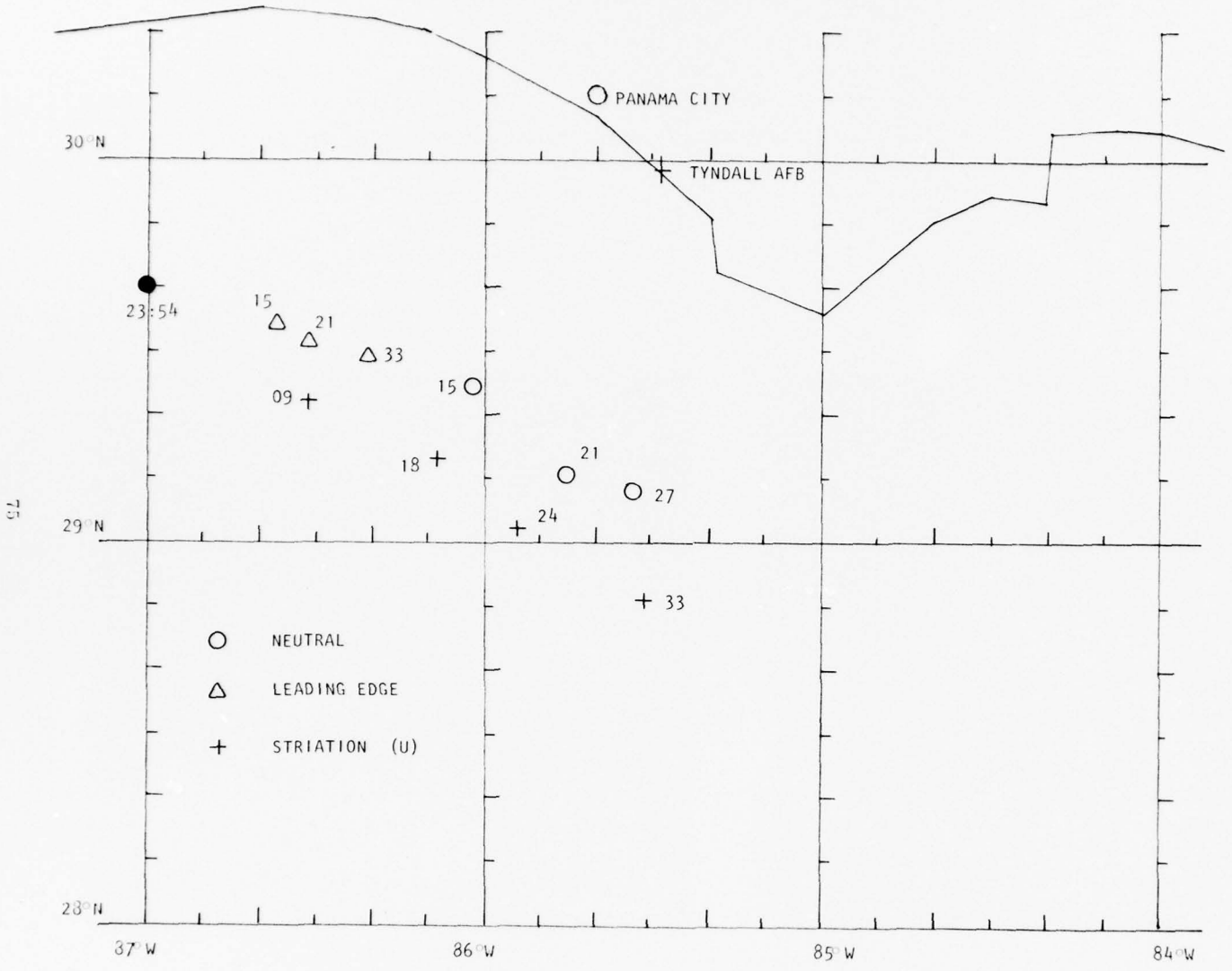

Figure 5.7 Event Carolyn Cloud Tracks

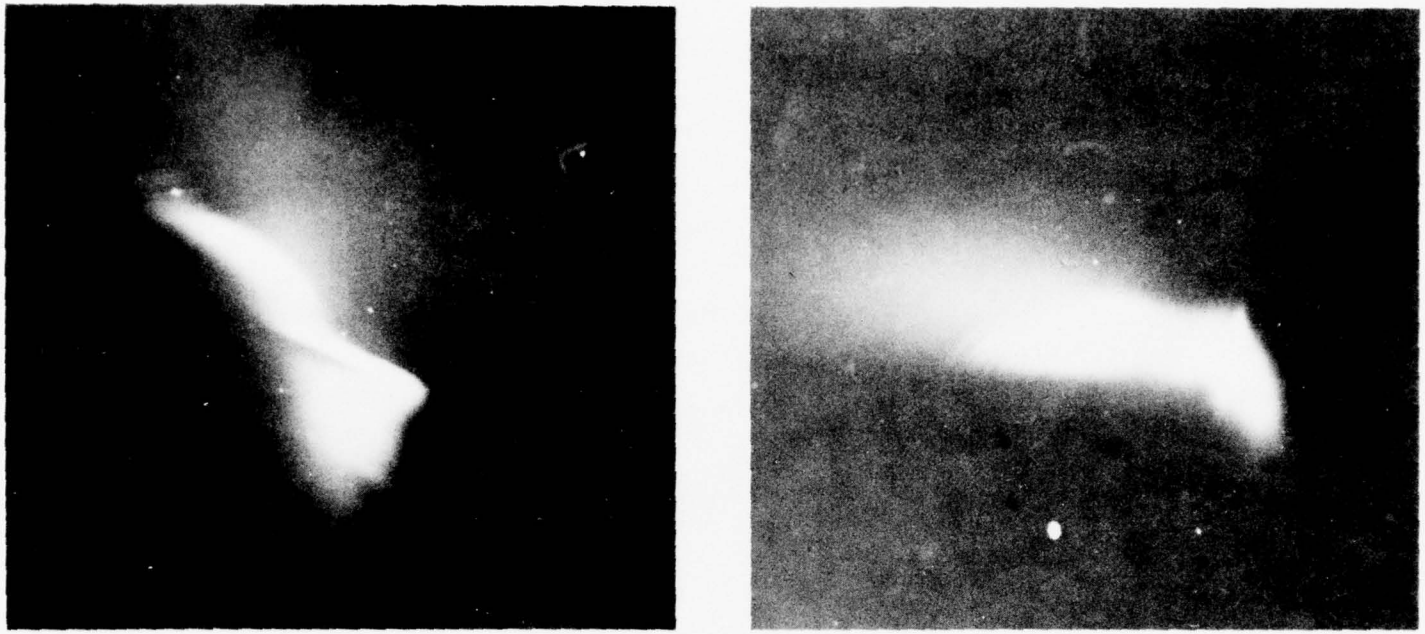

a) R + 34 min, Tyndall Site

b) R + 35 min, C-6 Site

Figure 5.8 Project STRESS, Event Dianne, Release Time 06:01:10 I.

The triangulated cloud tracks of Event Dianne are shown in Figure 5.9. The neutral center is plotted to R + 20 minutes. The foremost trailing edge striation is plotted to R + 32 minutes. The lower (northern) and upper (southern) ends of the edge most striation are shown for 15, 21, and 27 minutes after the hour. A dashed line connects the lower end of the striation with the corresponding position symbol for the leading edge at a given time. At 33 minutes an ensemble of 3 striations is shown -- also connected to the corresponding leading edge position by dashed lines. At this latter time, the lower end of the edge striation was triangulated to a height of 160 km and the upper end to a height of 210 km altitude.

5.6 Event Esther

Figure 5.10 shows the relative shapes of the Event Esther ion cloud at R + 1 hour 38 minutes as seen from the Tyndall and C-6 triangulation sites. Because of the nearly up the field line perspective of the Tyndall site the striation images from this site show remarkable definition and identity. It is worth remarking again that event Esther was the first of two events released significantly before sunset to ascertain the late time striation formation and longevity characteristics. While it was extremely difficult to identify common features from the C-6 and Tyndall perspectives, the gross cloud motion was able to be determined as a function of a group of trailing striations.

Figure 5.11 shows the results of the triangulation measurements of the late time Event Esther ion cloud. No neutral cloud was apparent throughout the observations. The motion of a group of 5 striations (later 4) from R + 1 hour 29 minutes (00:30) to R + 1 hour 41 minutes (00:42) at 150 km altitude is plotted. The position of the striation group at a given time is shown connected with dashed lines. The extent of the cloud at R + 1 hour 23 minutes (00:24) is also shown as a dashed line connecting the leading edge

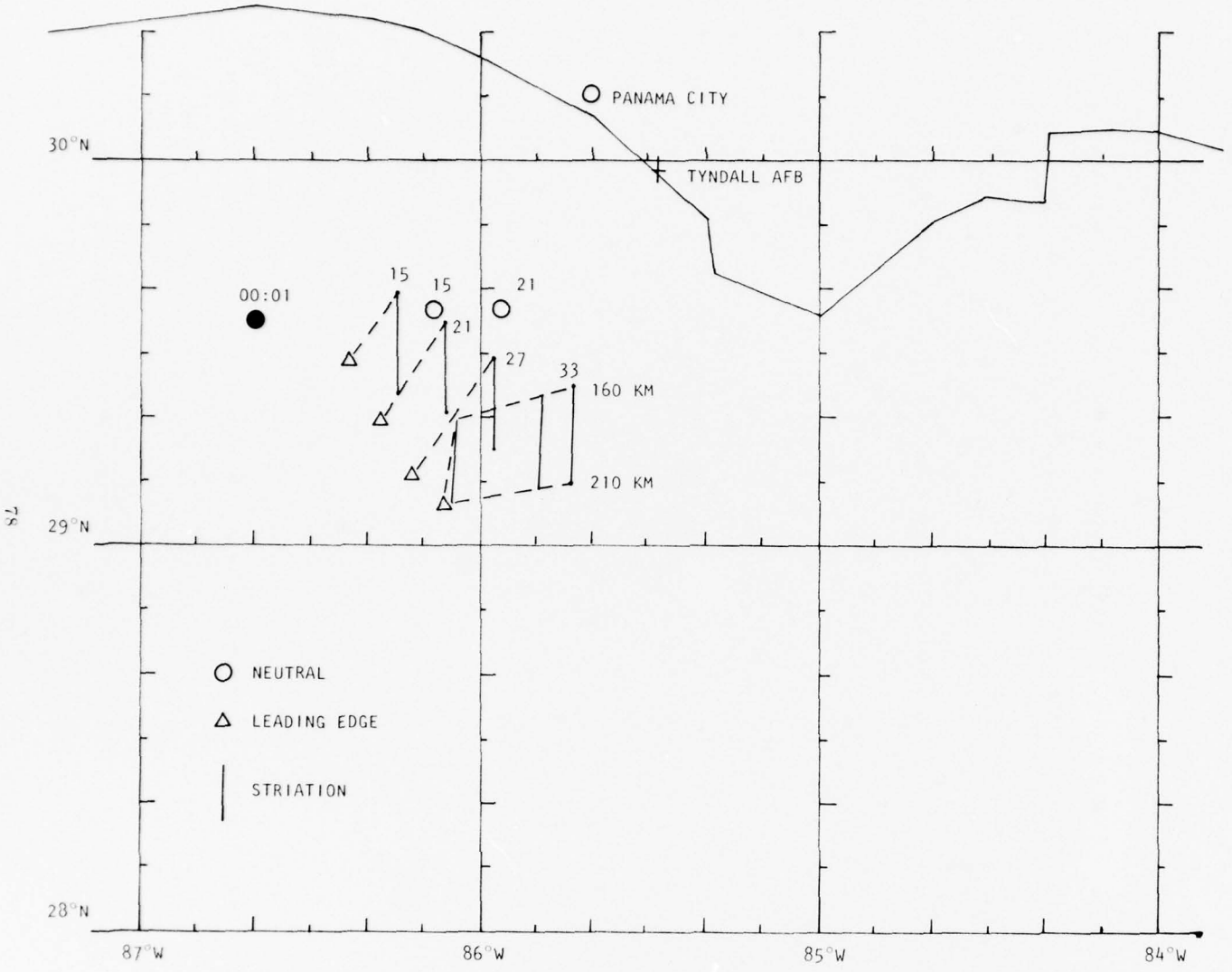

Figure 5.9 Event Dianne Cloud Tracks

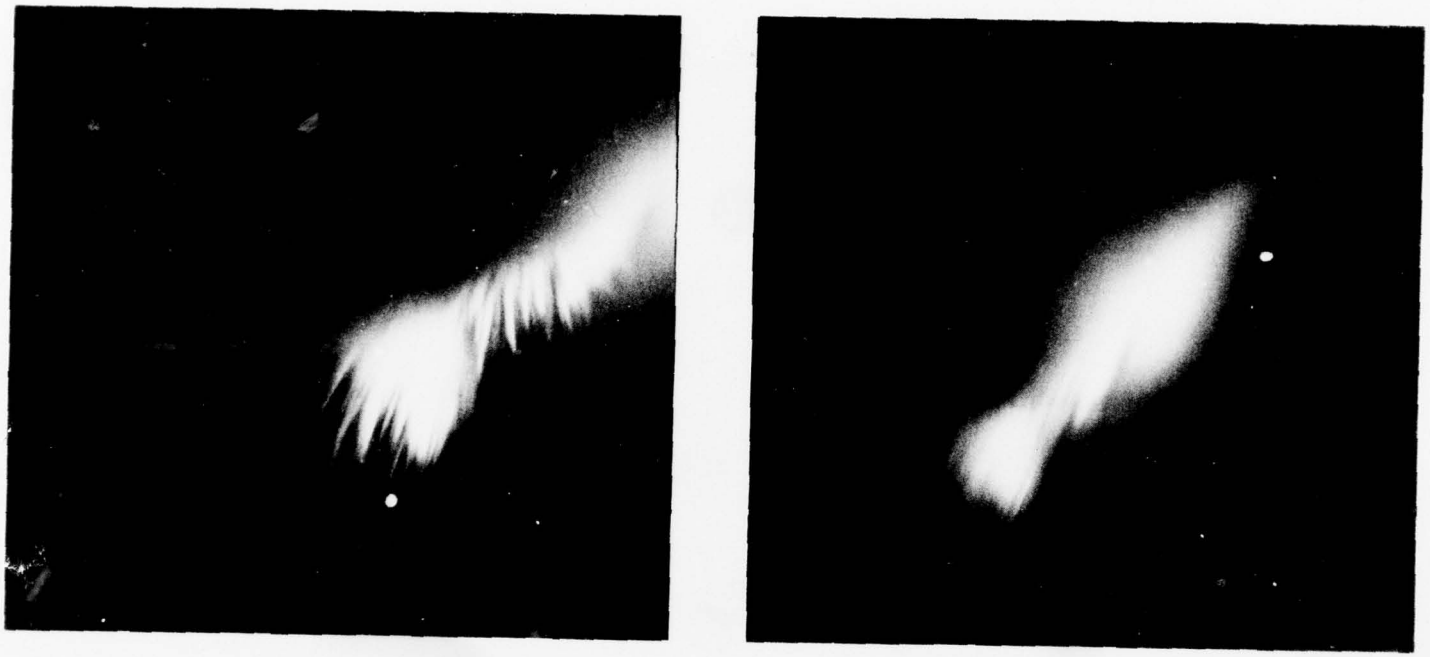

a) R + 1 hr 38 1/2 min, Tyndall Site

b) R + 1 hr 38 min, C-6 Site

Figure 5.10 Project STRESS, Event Esther, Release Time 05:01:08 I.

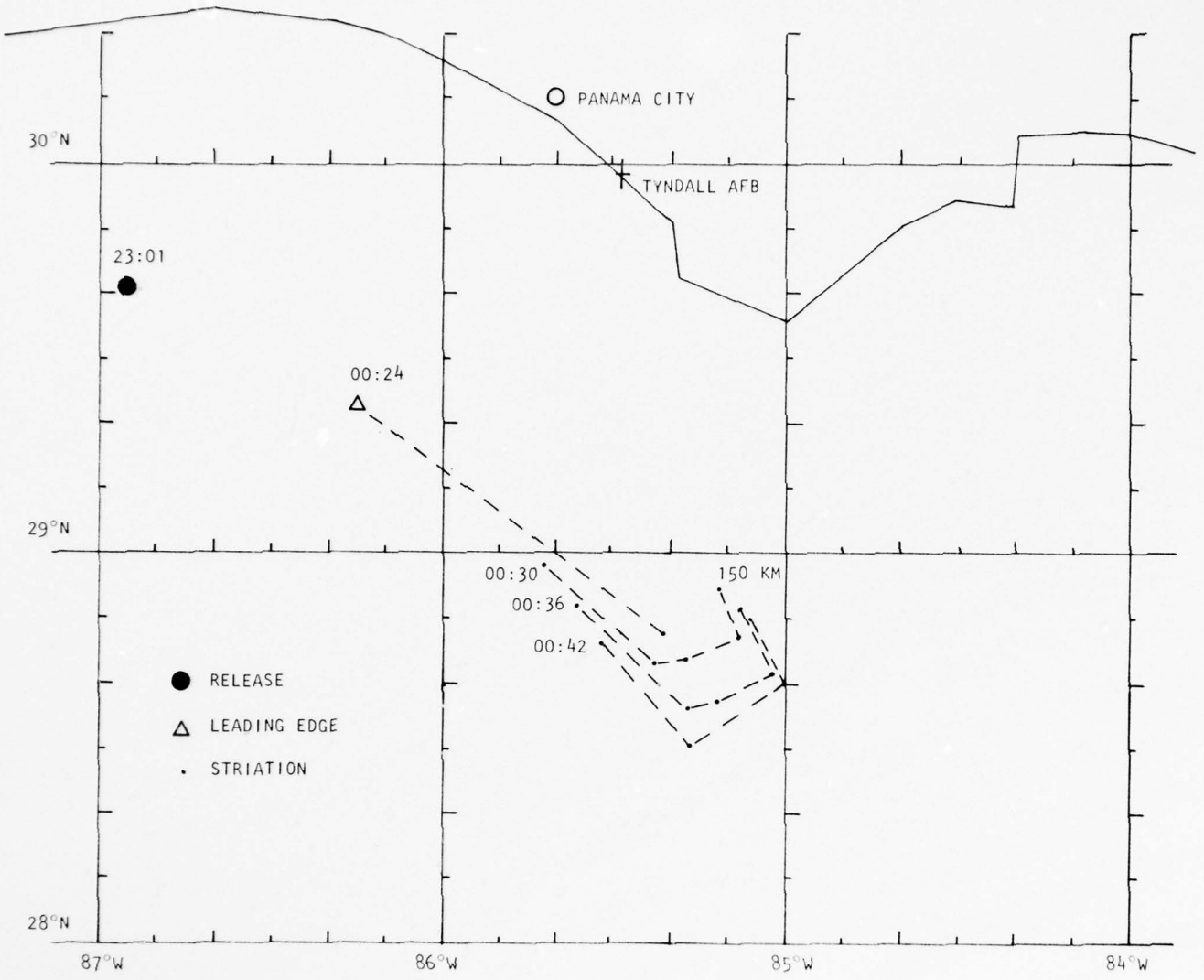

Figure 5.11 Event Esther Cloud Tracks

and a single striation.

5.7 Event Fern

The late time ion cloud of Event Fern is shown in Figure 5.12 at R + 1 hour 45 minutes and R + 1 hour 54 minutes from Tyndall and C-6 sites, respectively. The Fern ion cloud moved very slowly. From C-6 the cloud appeared very diffuse with undefined structure. From Tyndall, however, portions of the cloud located close to an up the field line perspective were much more definite. An example of this is the fine structure near the bottom left region of the ion image. Triangulation was possible only to the extent of following a few striations for limited times.

Event Fern, as in the case of Esther, did not exhibit a neutral cloud at the late times for which photographic coverage was obtained. Moreover, little structure was readily identifiable from two triangulation sites. Two significant striations were triangulated as best possible and are plotted in Figure 5.13, over a period of R + 1 hour 35 minutes to R + 1 hour 56 minutes. In general the ion cloud moved with a relatively slow velocity and was not as distinctive in structure as the prior events.

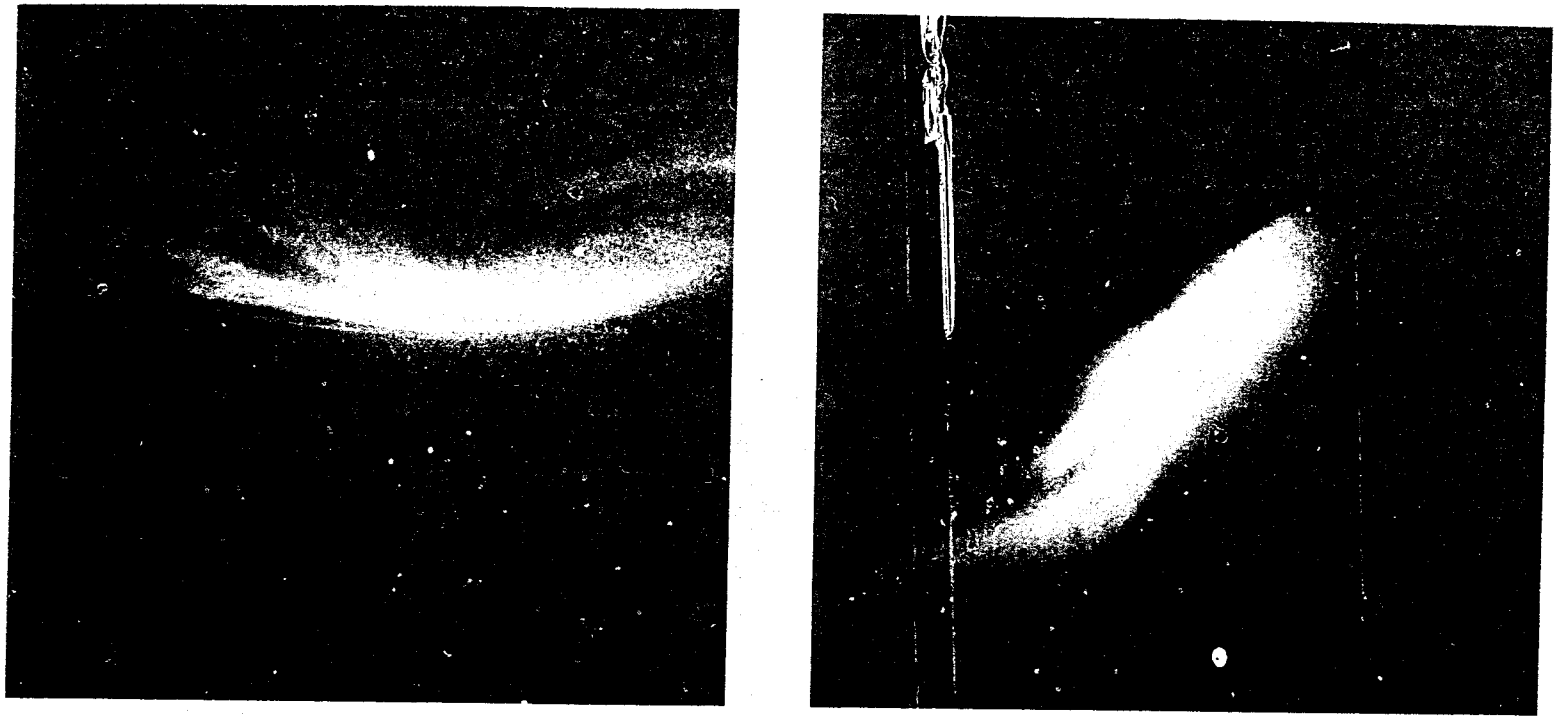

a) R + 1 hr 45 min, Tyndall Site

b) R + 1 hr 54 min, C-6 Site

Figure 5.12 Project STRESS, Event Fern, Release Time 04:46:09 L

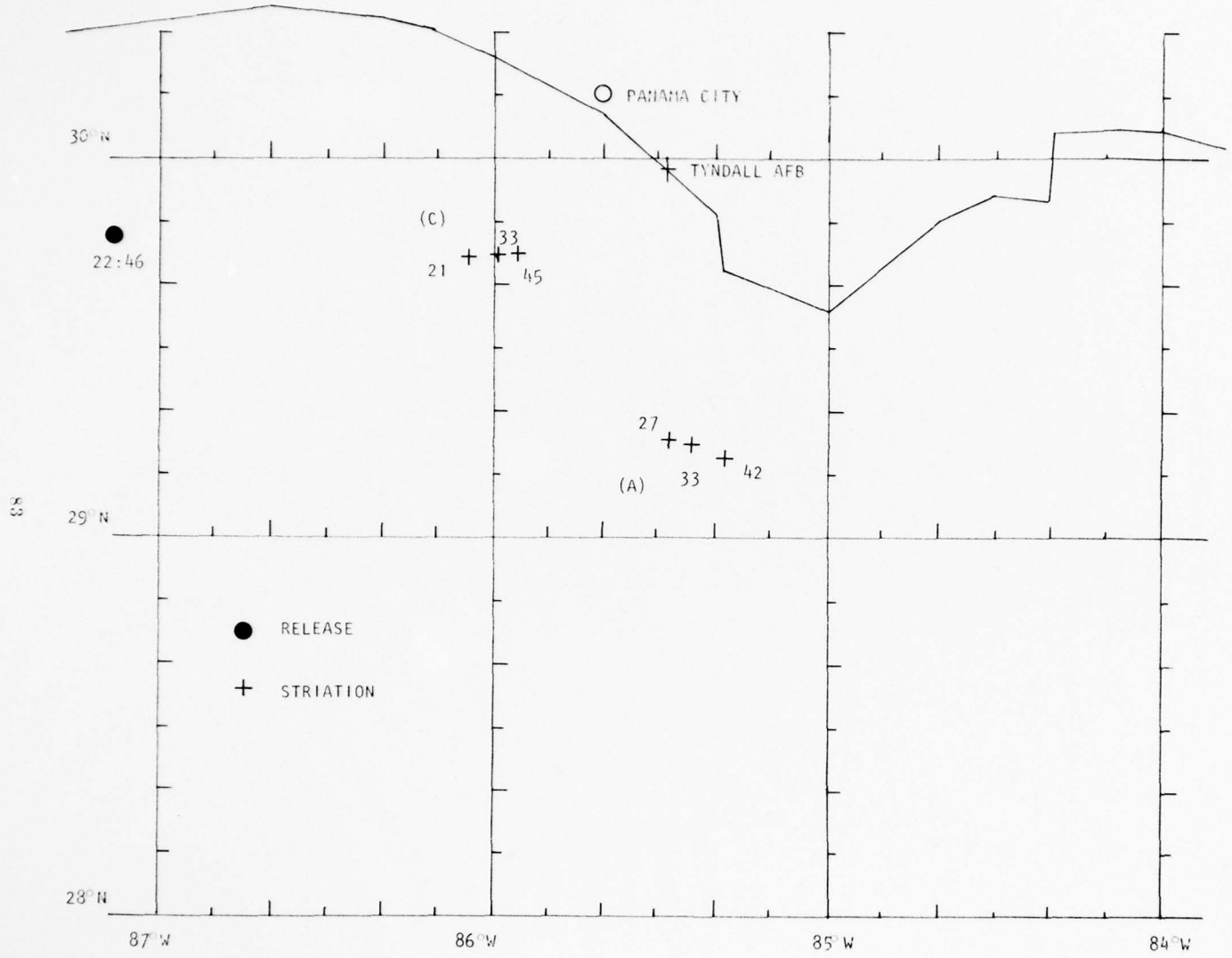

Figure 5.13 Event Fern Cloud Tracks

5.8 STRESS Velocity Summary

In order to provide a basis for comparing the relative motion of the STRESS clouds with each other and with corresponding measurements from other operations, the velocities of the clouds have been calculated. A summary of these velocity calculations is presented in Table 5.1 for, where possible, the neutral center, the trailing edge or region, and the cloud leading edge. Within each of these columnar groups are given the east-west velocity component, the total velocity (both in meters/second) and the velocity azimuth.

The velocity calculations were performed on tabulated triangulation data at times for which there was continuous data. Thus, in general, neutral cloud data (except Esther and Fern for which none was visible) was obtained during the earlier portion of the visible cloud history while the ion cloud data reflects cloud history representative of the mid to latter portion of the visible period. As a consequence, for this and other reasons related to the sometimes difficult task of defining a feature sufficiently and accurately from two widely separated sites, the resultant data must be used with an appreciation of the potential variance in the magnitudes given. An attempt was made for events Betty and Carolyn to define the accuracy of the calculations and these values might well be used as a guide to interpreting the remaining cloud data.

Table 5.1

STRESS CLOUD VELOCITY SUMMARY

	Neutral Center			Trailing Edge			Leading Edge		
	V_{E-W}	V_T	AZ	V_{E-W}	V_T	AZ	V_{E-W}	V_T	AZ
	(meters/sec)			(meters/sec)			(meters/sec)		
Anne	44	47	105°	22	27	126°	-11	-	-
Betty	36±7	42	60°	38±6	38	90°	17±9	18	106°
Carolyn	60±12	66	115°	60±7	69	120°	25±5	28	120°
Dianne	47	47	87°	43	54	127°	30	42	131°
Esther	-	-		~20	~36	146°	~10	-	-
Fern	-	-		(a)16±2	17	107°			
				(c)16±2	16	83°			

(Velocities Positive Easterly)

SECTION 6.

STRIATION SPATIAL FREQUENCY ANALYSIS

6.1 Analysis Procedure

High resolution black and white film records were made from the Eglin C-6 site for each of the STRESS barium ion clouds. Of these five events, four exhibited significant striations from this perspective as to be suitable for analysis. These were events Betty, Carolyn, Dianne, and Esther.

Data frames were selected from each of these events (two from Carolyn and one from each of the other three) as being most appropriate technically (and suitably representative of the event) for spatial frequency analysis. All data discussed here was obtained from a 300 mm camera system located at the Eglin C-6 site. The film used in this camera was Tri-X Pan and was developed to a D log E slope somewhat greater than unity.

The data frames were scanned on a transmission microphotometer with an effective scanning aperture of 50μ x 0.5mm. The long axis of the slit was oriented perpendicular to the direction of motion. The values of transmission vs image position were digitized with approximately 2000 data points being obtained over a typical dimension of 20 mm. The sensitometric processing curve was scanned subsequently and a density vs log exposure curve computed. With the aid of this curve the transmission profile of the image was then converted and plotted as relative radiance.

The relative radiance was next Fourier transformed with a large computer utilizing a Cooley-Tukey algorithm fast Fourier transform. The resulting data was then plotted as power (amplitude squared) vs log spatial frequency in lines/mm.

6.2 Spatial Frequency Results

The ion cloud data frames selected for analysis for spatial frequency content are tabulated in Table 6.1 by event, data frame number, and time after release. For each of the data the following is provided. First, a photographic plate showing the data frame scanned together with the region scanned (identified by two white lines between which the scan was made). Next is shown the computed relative radiance of the density scan as a function of distance on the film, given in millimeters. This intermediate step derives from the utilization of a calibrated step wedge exposed on the same kind of emulsion with which the data was exposed and, when plotted, provides a quantitative correlation of the visual striation image.

The third presentation is the corresponding Fourier transform, the spatial frequency as a function of optical power. It should be pointed out that no data filtering was performed in this analysis, as is sometimes done by some groups.

The data given above in lines/mm can be converted to object dimensions if the focal length of the lens and range to the object is known. Assuming a nominal range of 200 km and using a focal length of 300 mm, a spatial frequency of one, for example, would correspond to an object dimension of about 660 meters.

TABLE 6.1

SUMMARY OF DATA ANALYZED

Event	Data Frame	Time
Betty	73434-165	R + 39 min 47 sec
Carolyn	73534-142	R + 28 min 04 sec
Carolyn	73534-211	R + 37 min 08 sec
Dianne	73634-215	R + 37 min 26 sec
Esther	73734-114	R + 1 hr 31 min

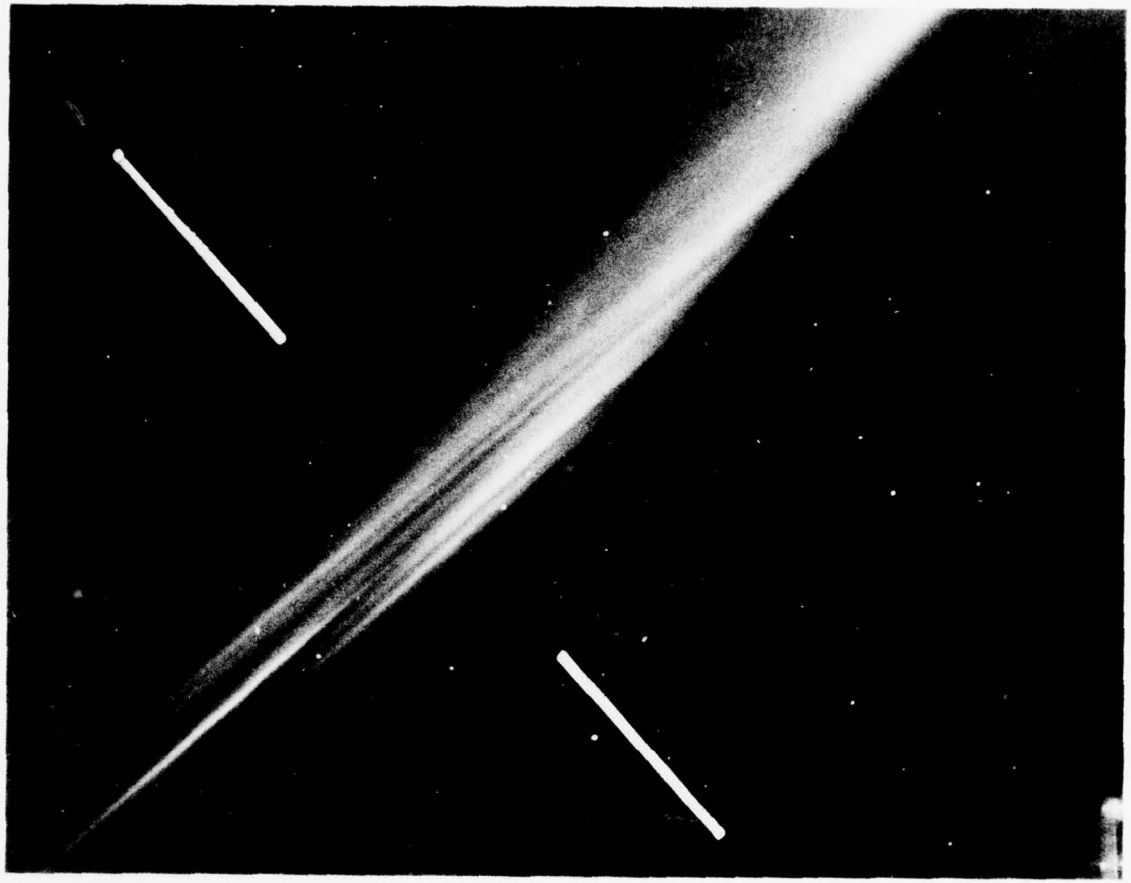

Figure 6.1 Event Betty, C-6 Site, R + 39 min 47 sec

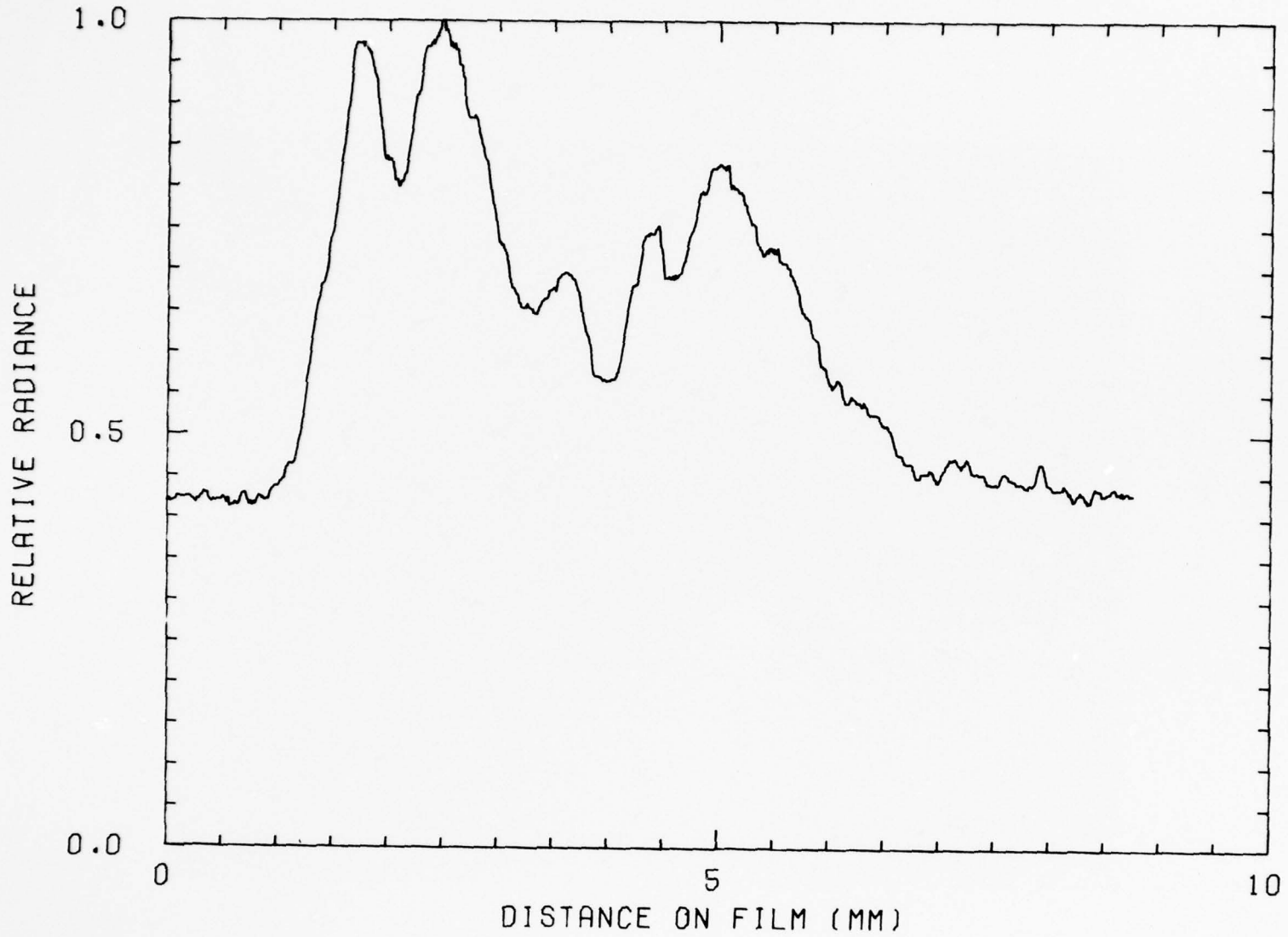

Figure 6.2 Event Betty Radiance Profile at R + 39:47, C-6 Site

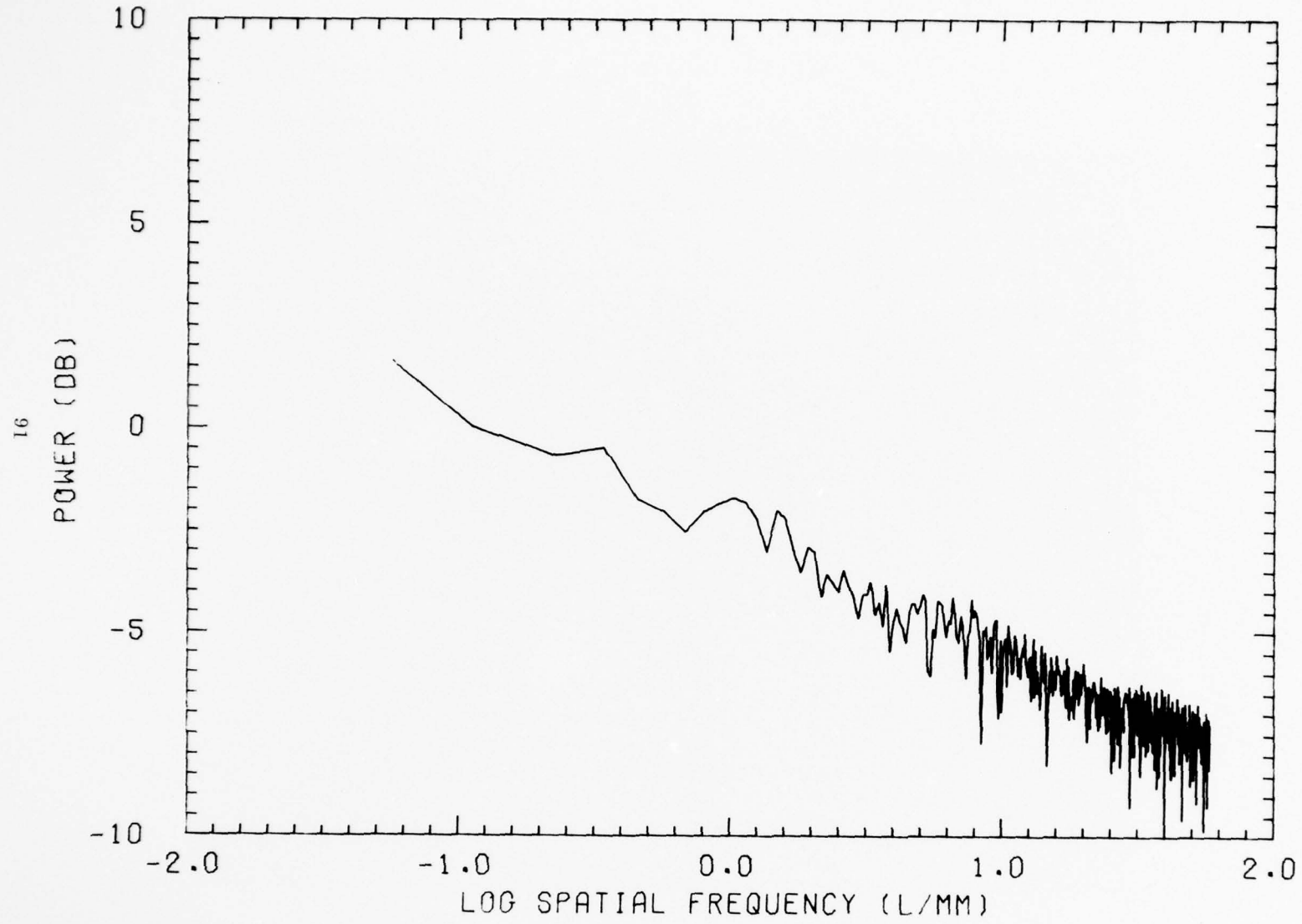

Figure 6.3 Event Betty Spatial Frequency Transform at R + 39:47

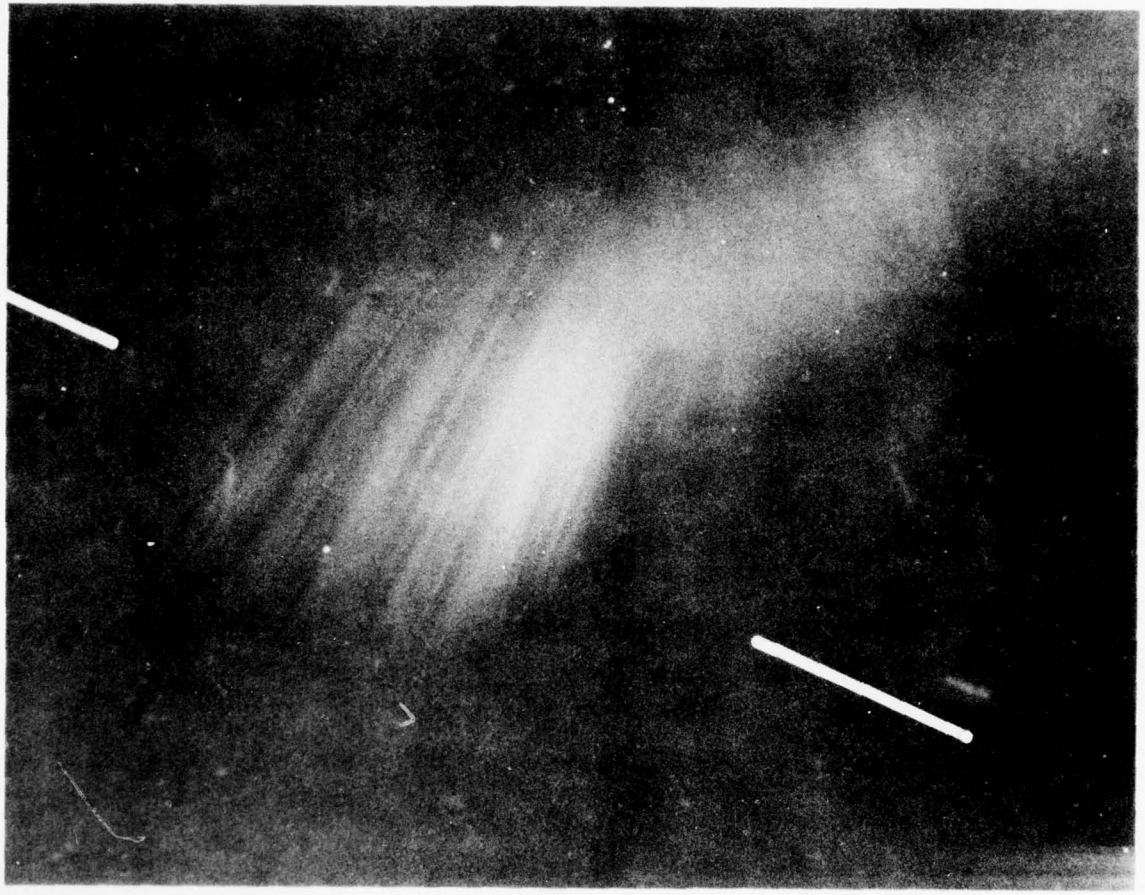

Figure 6.4 Event Carolyn, C-6 Site, R + 28 min 04 sec

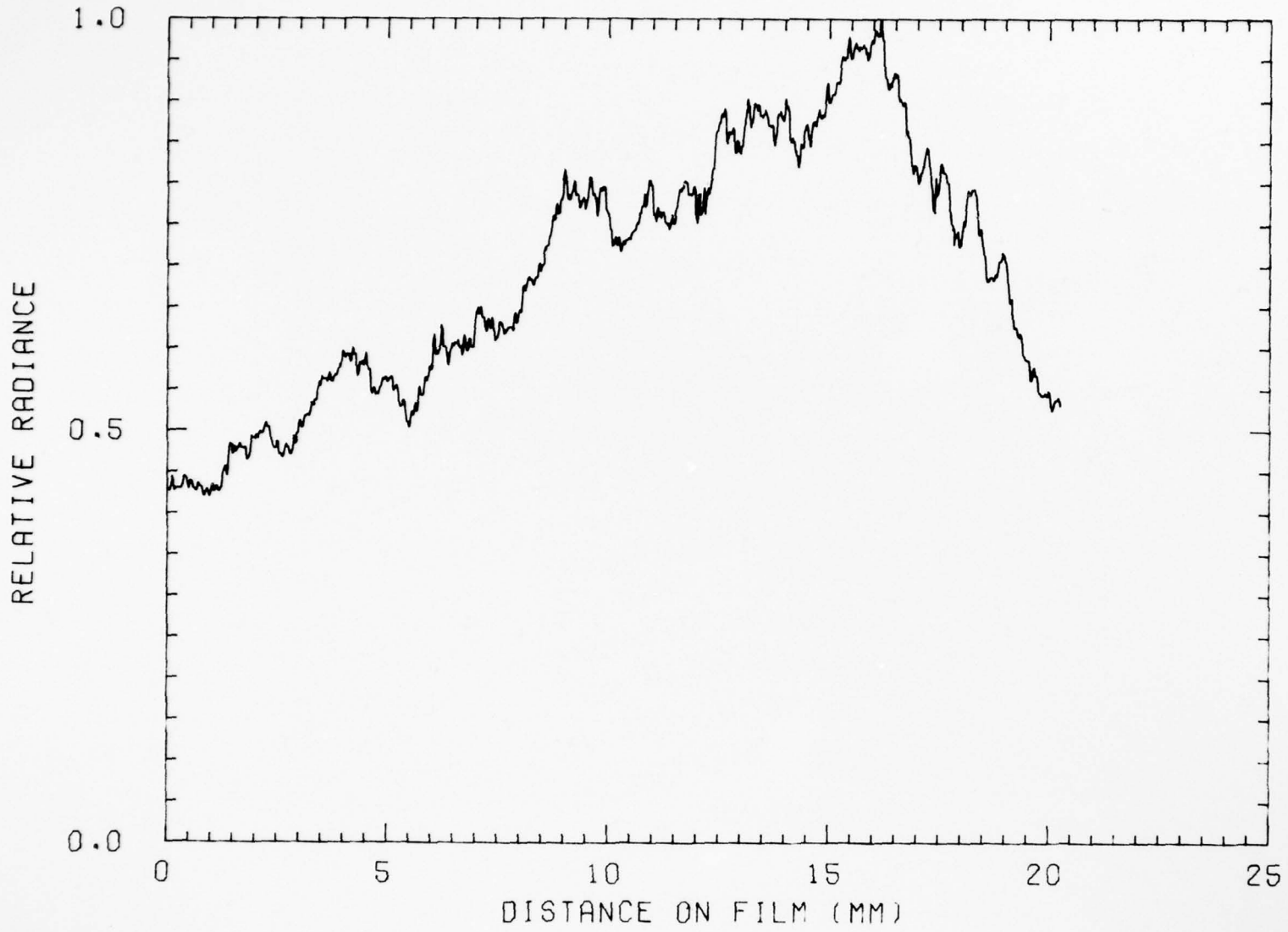

Figure 6.5 Event Carolyn Radiance Profile at R + 28:04, C-6 Site

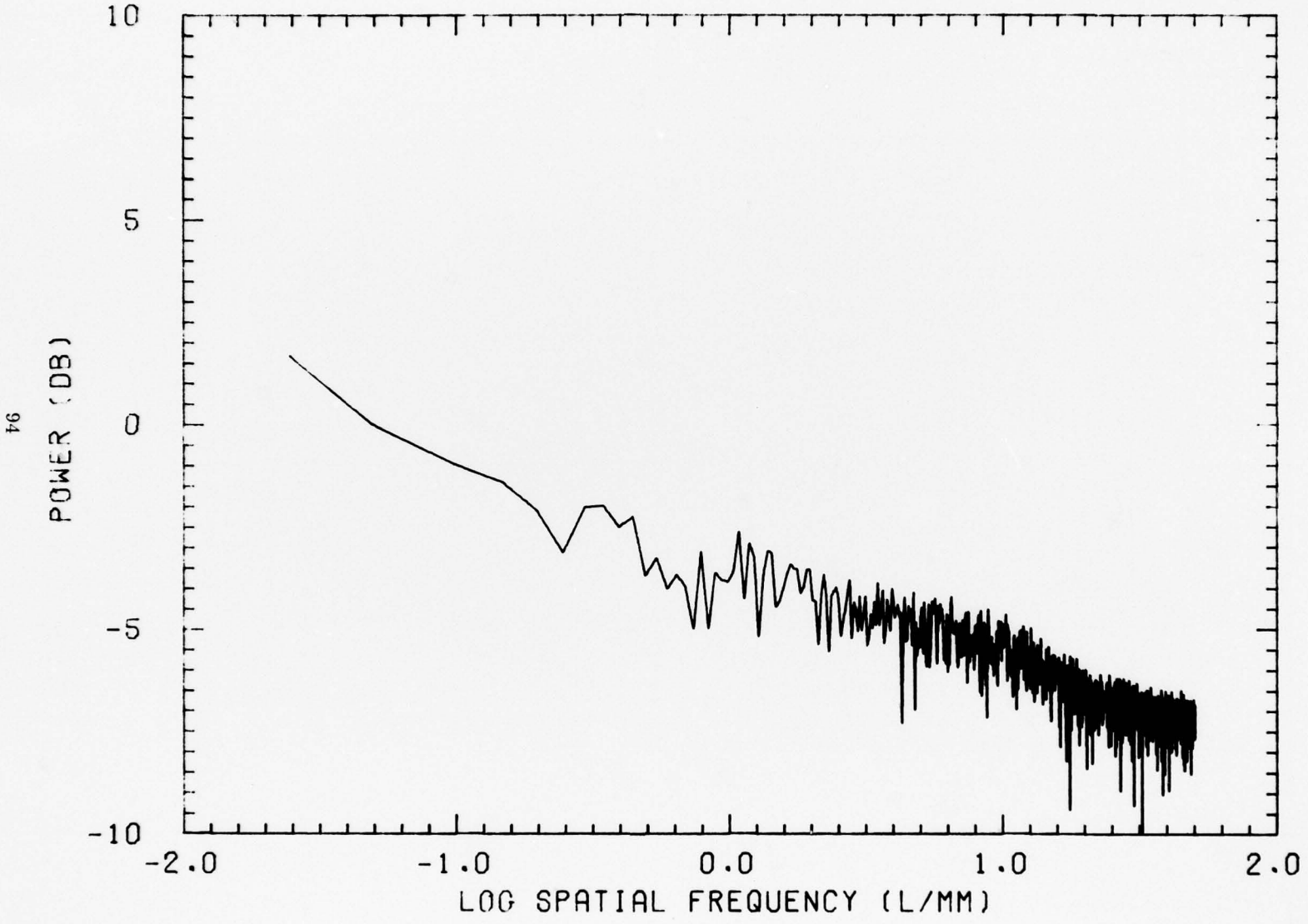

Figure 6.6 Event Carolyn Spatial Frequency Transform at R + 28:04

Figure 6.7 Event Carolyn, C-6 Site, R + 37 min 08 sec

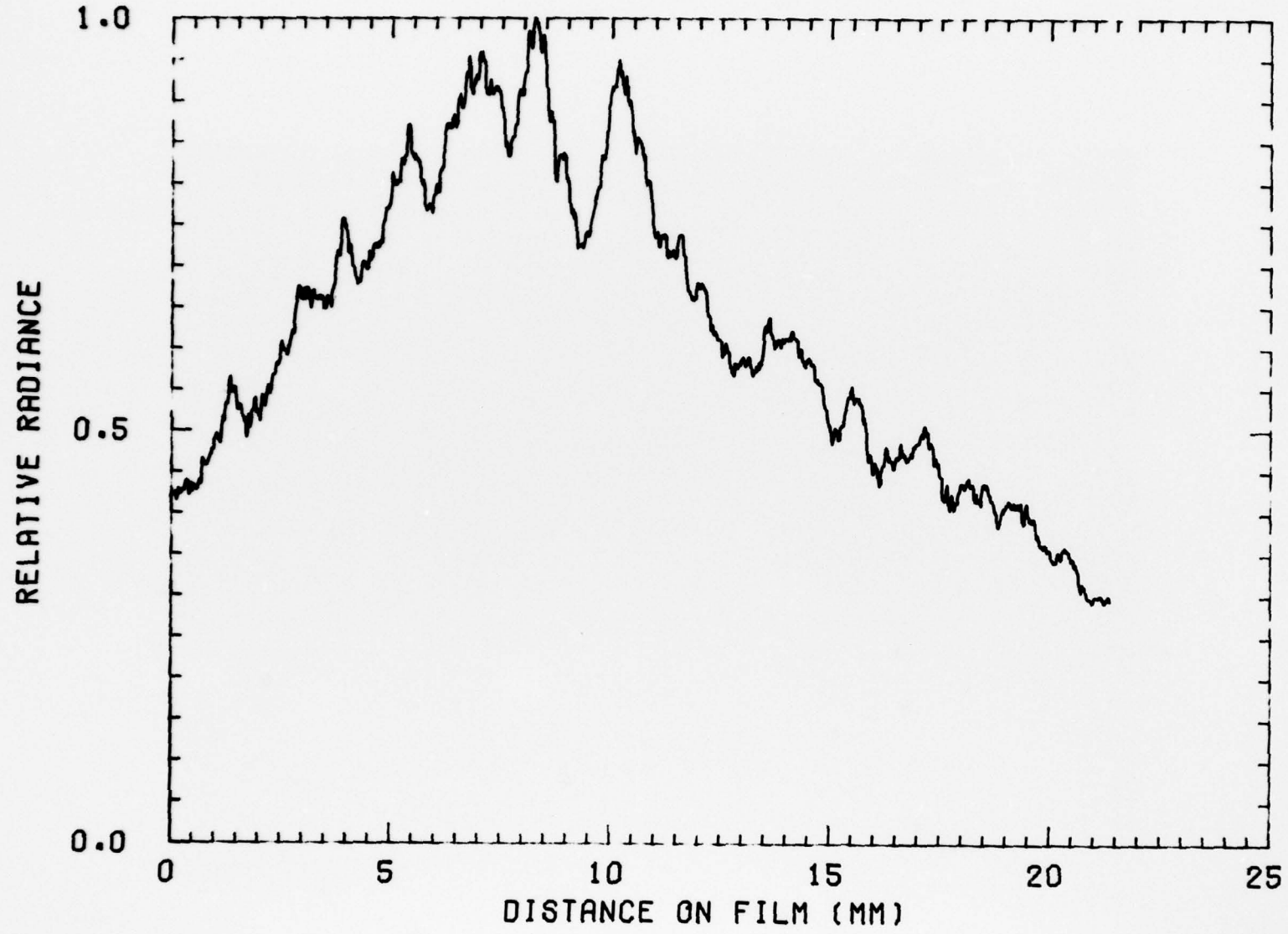

Figure 6.8 Event Carolyn Radiance Profile at R + 37:08, C-6 Site

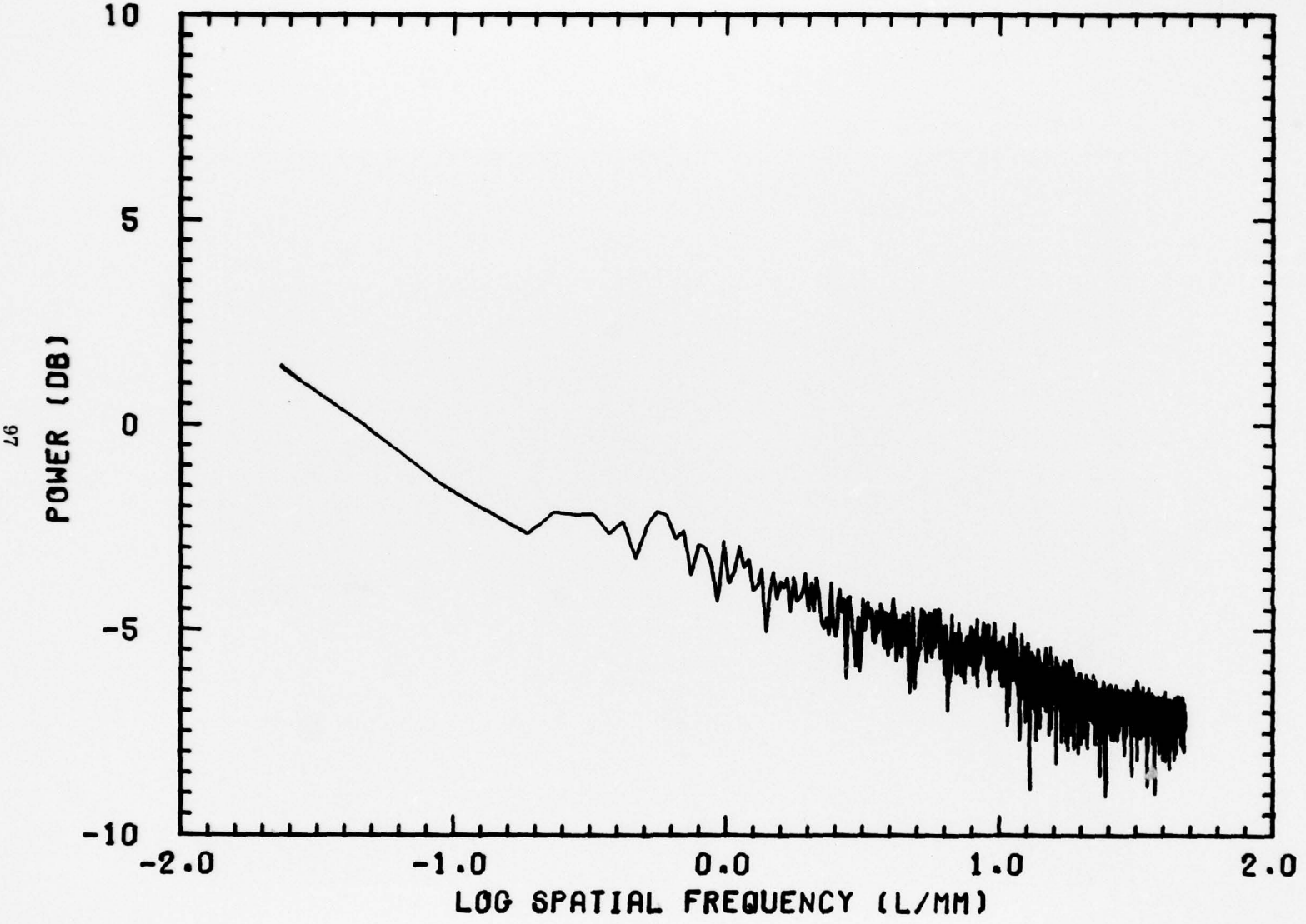

Figure 6.9 Event Carolyn Spatial Frequency Transform at R + 37:08

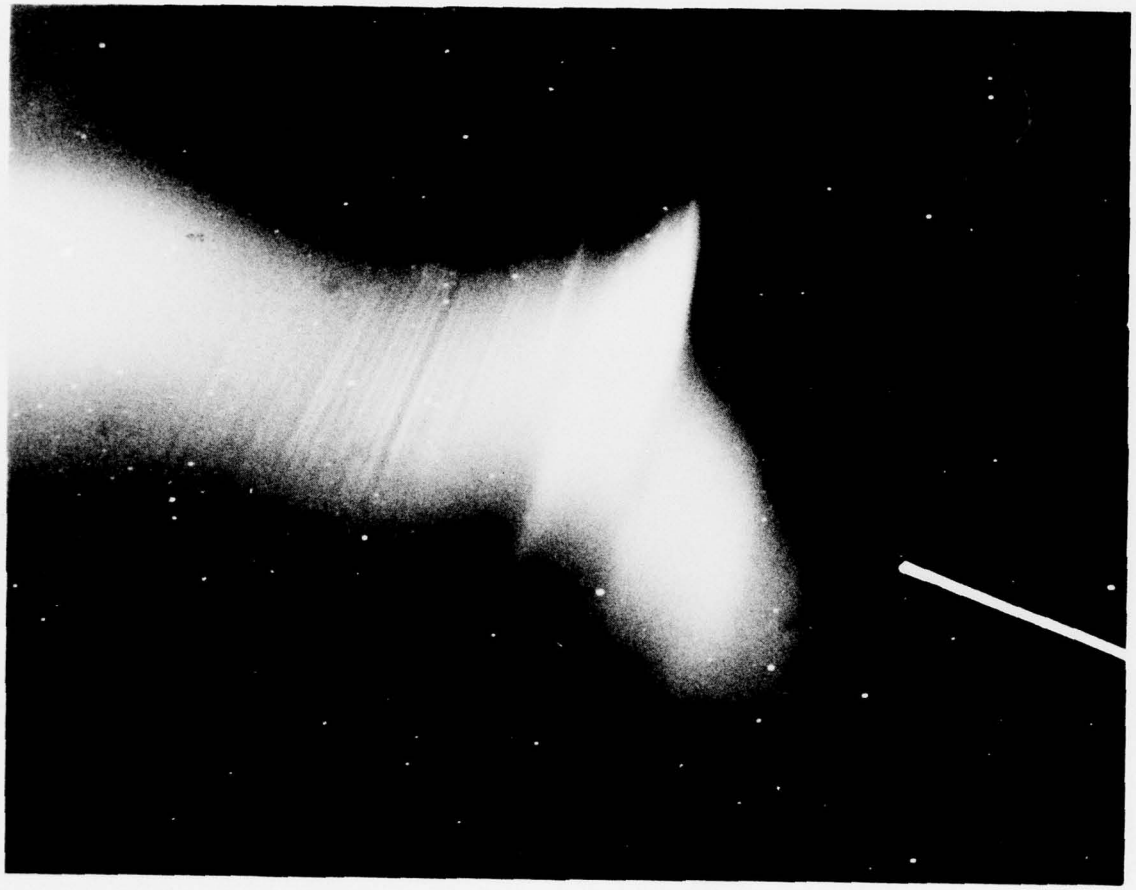

Figure 6.10 Event Dianne, C-6 Site, R + 37 min 26 sec

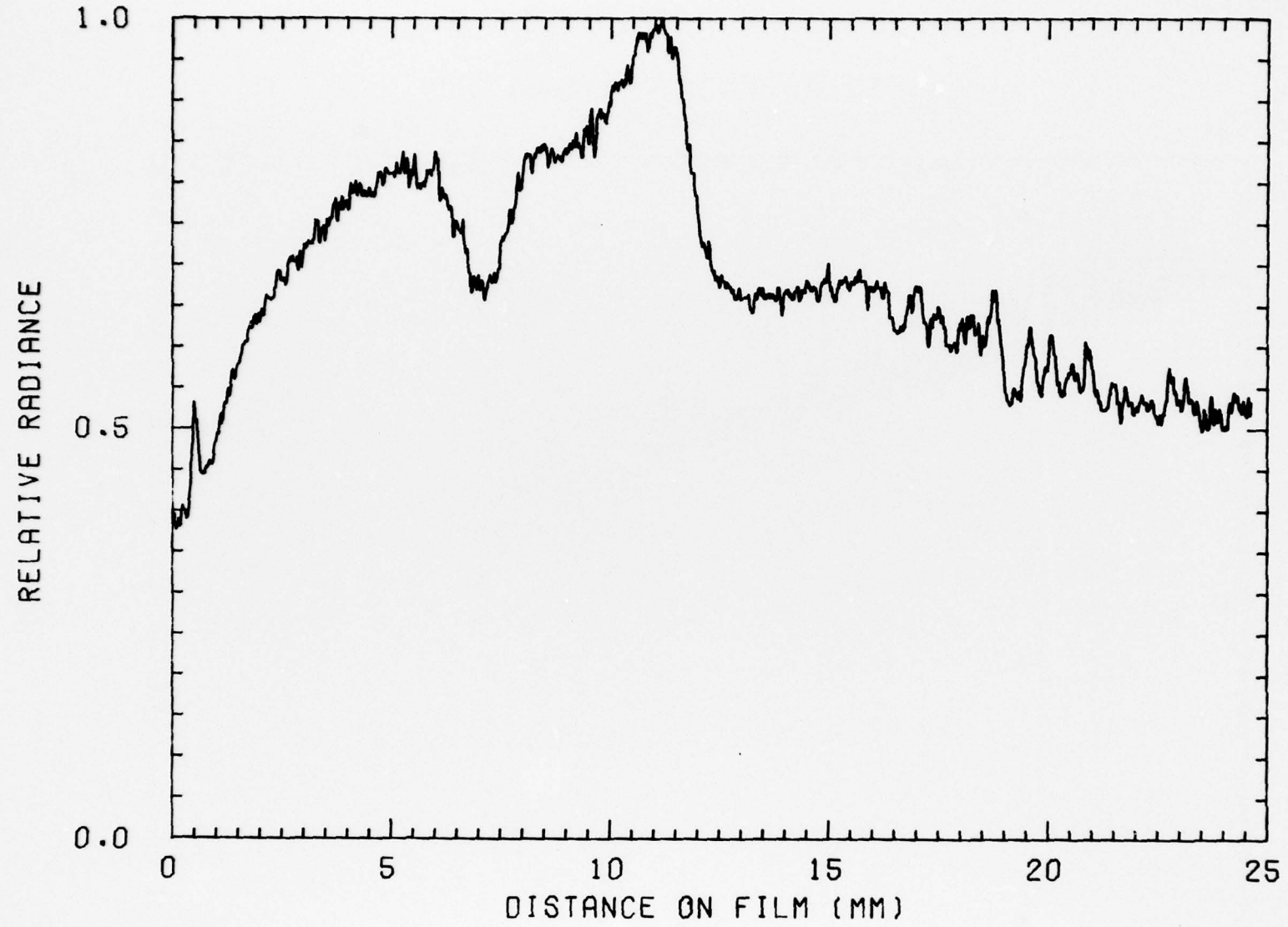

Figure 6.11 Event Dianne Radiance Profile at R + 37:26, C-6 Site

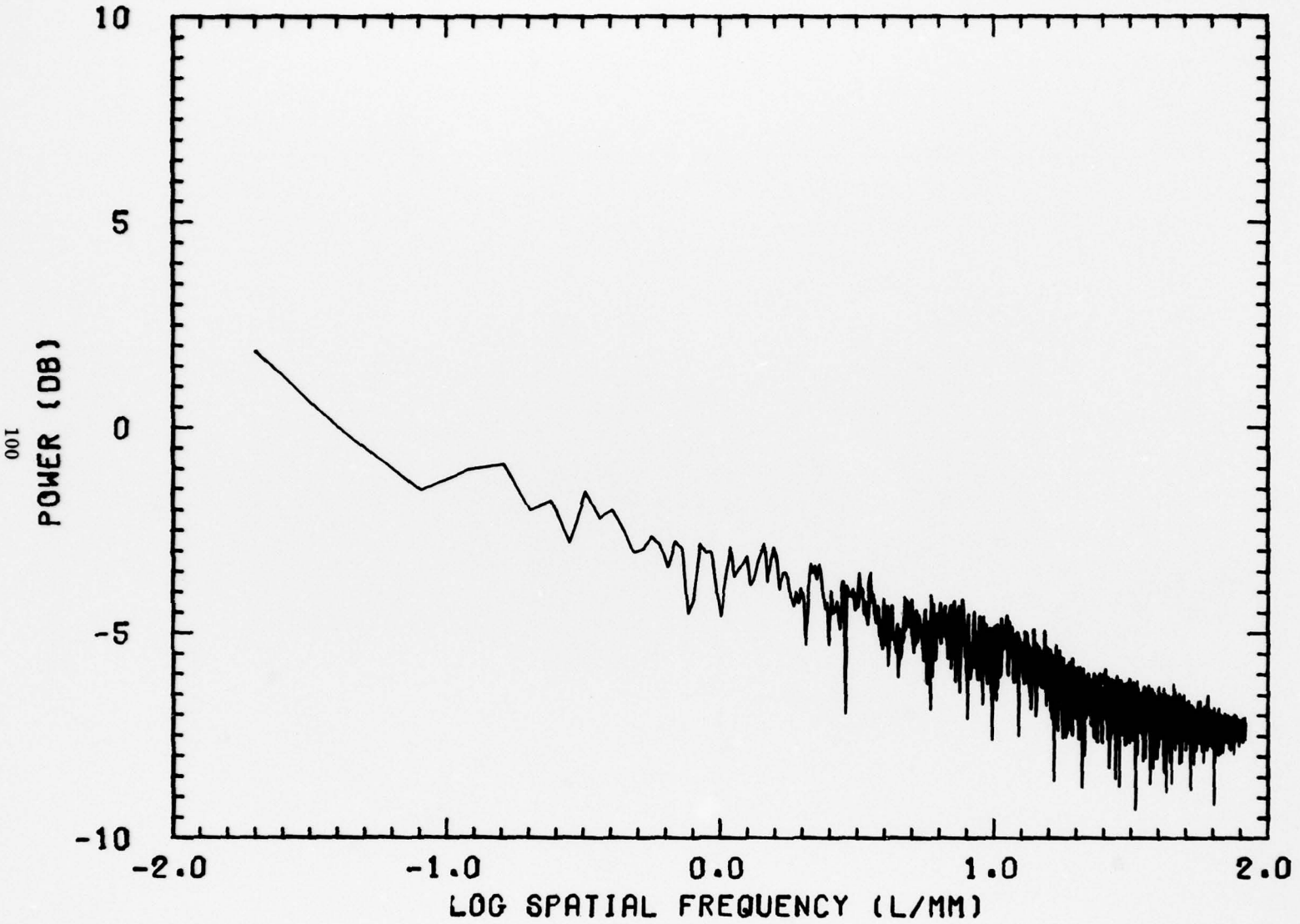

Figure 6.12 Event Dianne Spatial Frequency Transform at R + 37:26

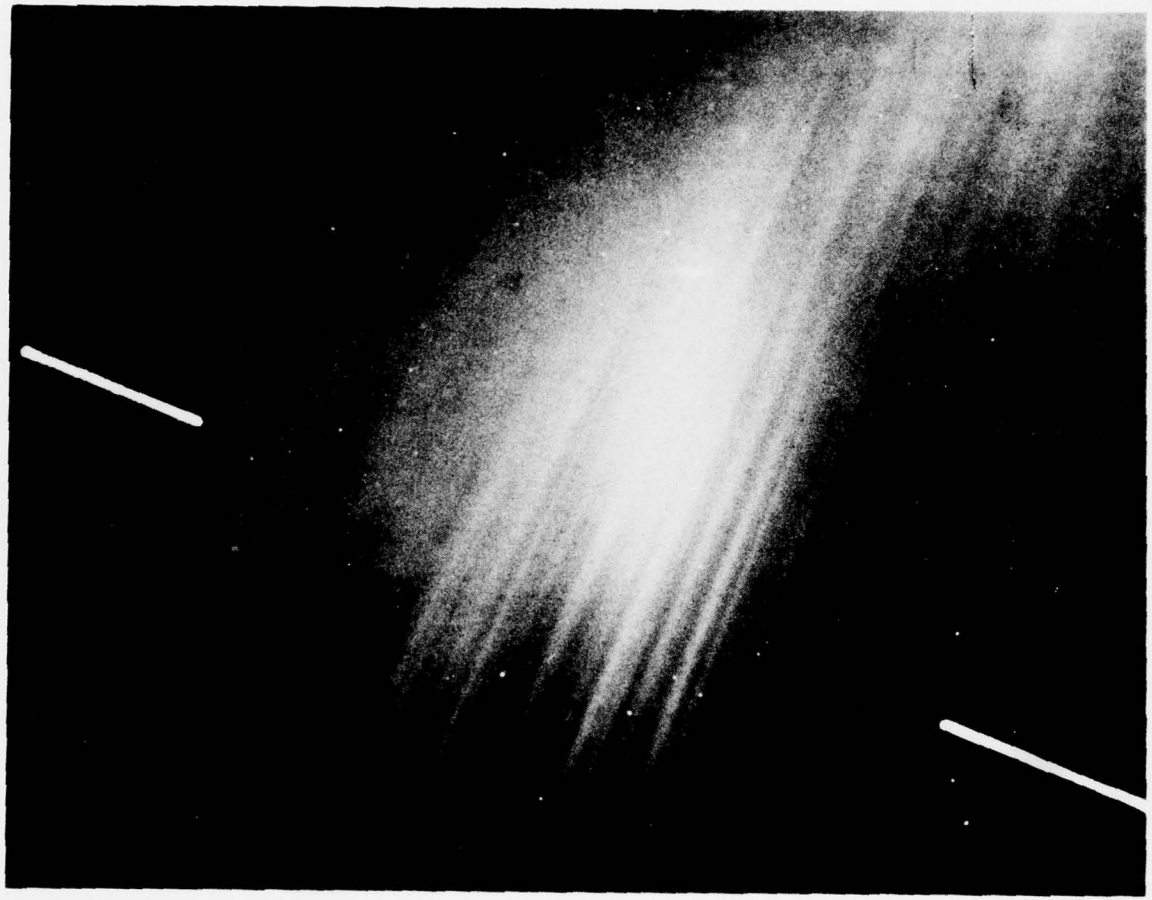

Figure 6.13 Event Esther, C-6 Site, R + 1 hr 31 min 16 sec

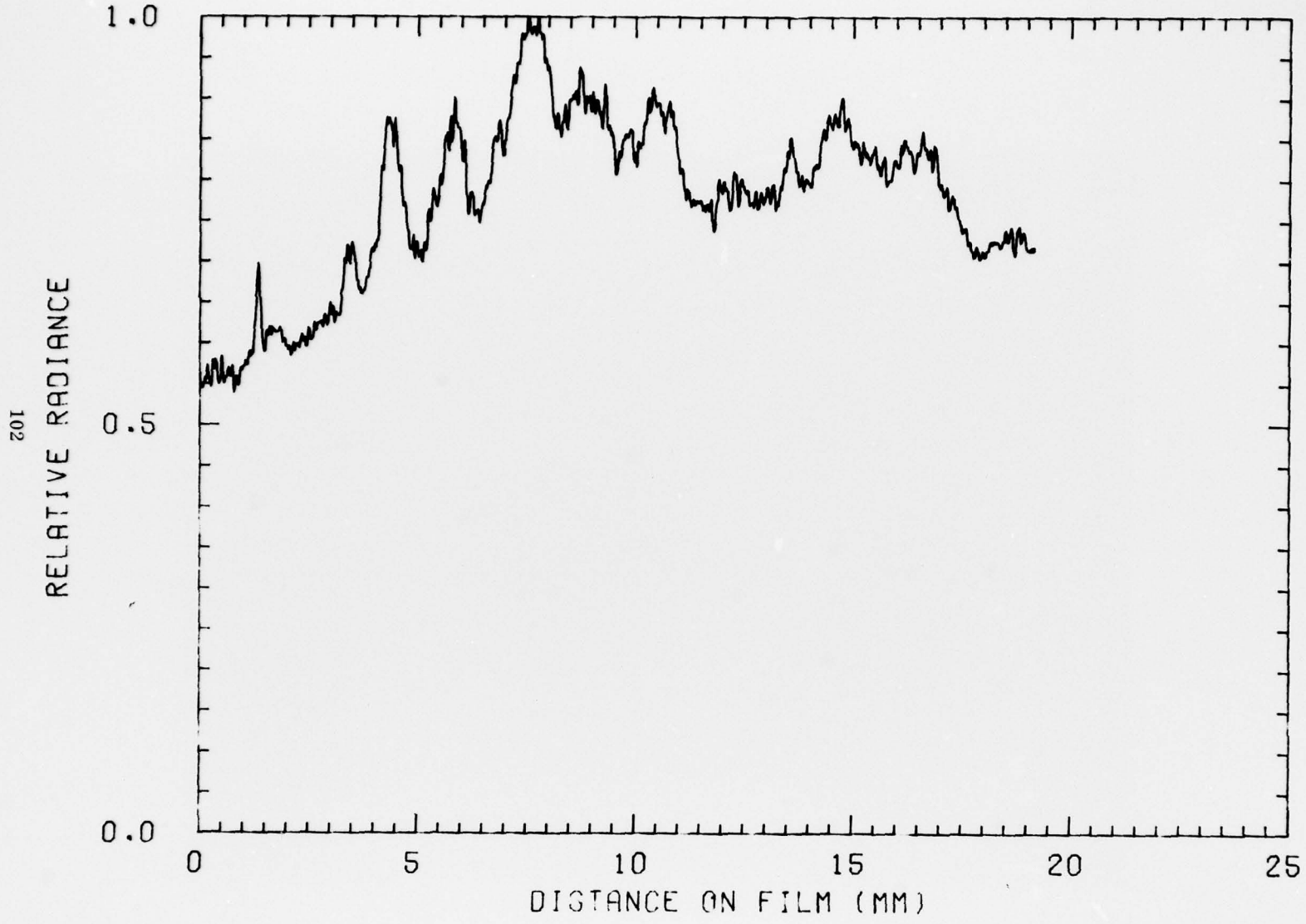

Figure 6.14 Event Esther Radiance Profile at R + 1.31:16, C-6 Site

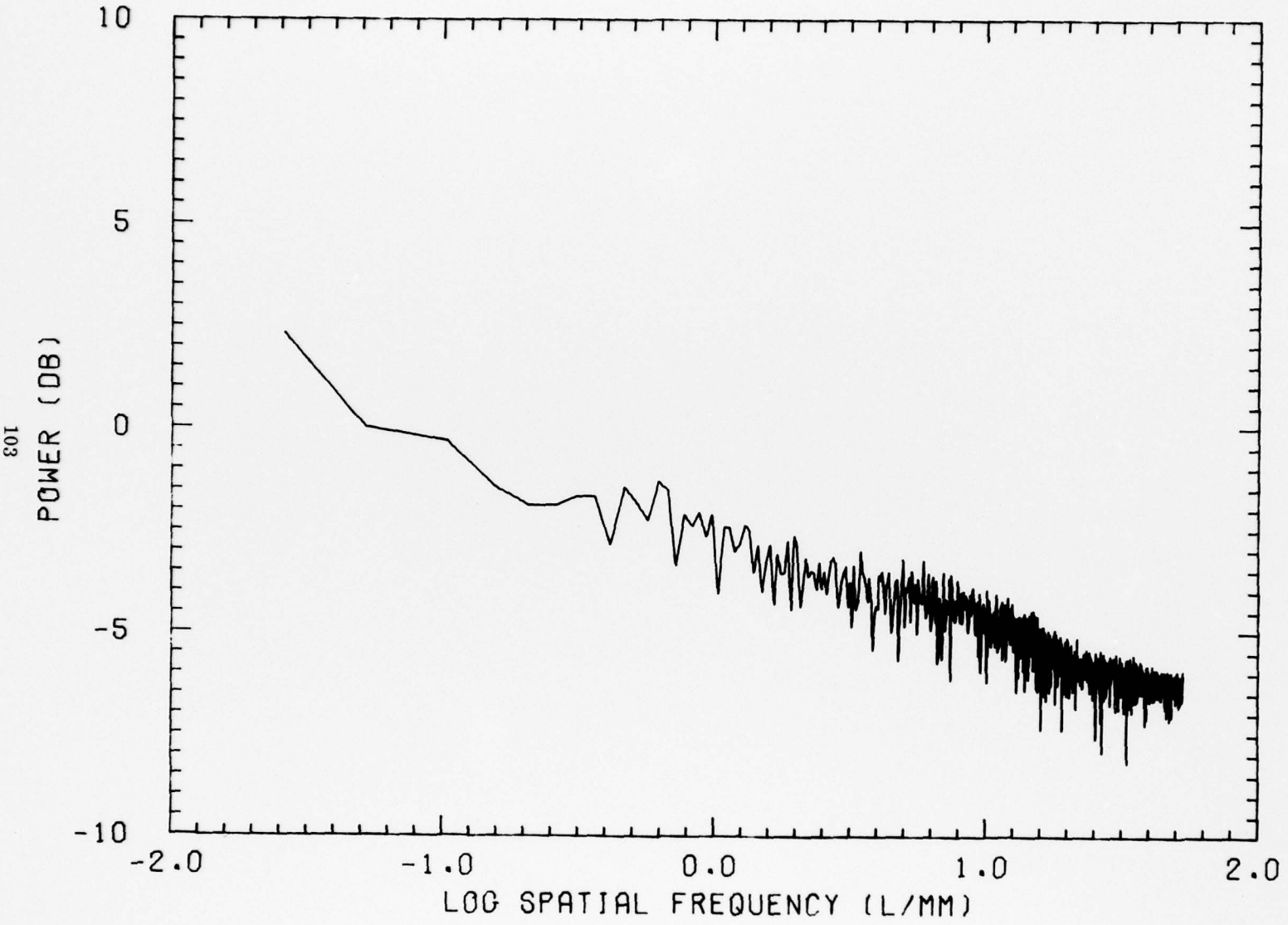

Figure 6.15 Event Esther Spatial Frequency Transform at R + 1:31:16

DISTRIBUTION LIST

DEPARTMENT OF DEFENSE

Assistant to the Secretary of Defense
Atomic Energy
ATTN: Executive Assistant

Command & Control Technical Center
ATTN: C-650

Defense Advanced Rsch. Proj. Agency
ATTN: NMRO
ATTN: STO

Defense Communication Engineer Center
ATTN: Code R410, J. McLean
ATTN: Code R820

Defense Communications Agency
ATTN: Code 103, M. Raffensperger
ATTN: Code 480
ATTN: Code 810, R. Rostron
ATTN: Code 101B

Defense Documentation Center
Cameron Station
12 cy ATTN: DD

Defense Nuclear Agency
ATTN: STVL
ATTN: DDST
ATTN: RAAE
4 cy ATTN: TITL

Field Command
Defense Nuclear Agency
ATTN: FCPR

Interservice Nuclear Weapons School
ATTN: TTV

Joint Chiefs of Staff
ATTN: J-3, WWMCCS Evaluation Office

Joint Strat Tgt. Planning Staff
ATTN: JLTW-2

Livermore Division, Field Command, DNA
Lawrence Livermore Laboratory
ATTN: FCPRL

National Security Agency
ATTN: R52, J. Skillman
ATTN: R5

NATO School (SHAPE)
ATTN: U.S. Documents Officer

Under Secretary of Defense for Rsch. & Engrg.
ATTN: Strategic & Space Systems (OS)

WWMCCS System Engineering Org.
ATTN: R. Crawford

DEPARTMENT OF THE ARMY

BMD Advanced Technology Center, Huntsville Office
ATTN: ATC-T, M. Capps

DEPARTMENT OF THE ARMY (Continued)

Harry Diamond Laboratories
ATTN: DELHD-NP
ATTN: DELHD-T1, M. Weiner

U.S. Army Comm-Elec Engrg. Instal. Agency
ATTN: EED-PED, G. Lane

U.S. Army Foreign Science & Tech. Center
ATTN: DRXST-SD

U.S. Army Satellite Communications Agency
ATTN: Document Control

U.S. Army TRADOC Systems Analysis Activity
ATTN: ATAA-SA

DEPARTMENT OF THE NAVY

Naval Electronic Systems Command
ATTN: Code 5011

Naval Intelligence Support Center
ATTN: STIC 12, Mr. Dubbin

Naval Ocean Systems Center
ATTN: Code 532

Naval Research Laboratory
ATTN: Code 6700, T. Coffey
ATTN: Code 5430
ATTN: Code 7127, C. Johnson
ATTN: Code 5400, B. Wald

Naval Surface Weapons Center
ATTN: Code F31

Navy Space Systems Activity
ATTN: Code 52

Office of Naval Research
ATTN: Code 461

Strategic Systems Project Office
ATTN: NSSP-2722, F. Wimberly
ATTN: NSP-2141

DEPARTMENT OF THE AIR FORCE

Air Force Avionics Laboratory
ATTN: AAD, A. Johnson

Air Force Geophysics Laboratory
ATTN: OPR-1, J. Ulwick
ATTN: PHP, J. Aarons
ATTN: PHD, J. Buchau
ATTN: PHD, J. Mullen

Air Force Technical Applications Center
ATTN: TN

Air Force Weapons Laboratory
ATTN: DYC, J. Barry
ATTN: SUL
ATTN: DYC, J. Kamm
ATTN: DYT, M. Fry

DEPARTMENT OF THE AIR FORCE (Continued)

Foreign Technology Division, AFSC
ATTN: NICD Library

Rome Air Development Center, AFSC
ATTN: Documents Library/TSLD

Space & Missile Systems Organization/MN
ATTN: MNNL, Lt Col Kennedy

Space & Missile Systems Organization/SK
ATTN: SKA, M. Clavin

Space & Missile Systems Organization/YA
ATTN: YAT, L. Blackwelder

Strategic Air Command/XPFS
ATTN: NRT
ATTN: ADWATE, B. Bauer
ATTN: XPFS, B. Stephan

DEPARTMENT OF ENERGY

Lawrence Livermore Laboratory
ATTN: Doc. Con. for Technical Information Dept.

Los Alamos Scientific Laboratory
ATTN: Doc. Con. for R. Jeffries
ATTN: Doc. Con. for J. Wolcott
ATTN: Doc. Con. for J. Zinn

Sandia Laboratories
ATTN: Doc. Con. for W. Brown
ATTN: Doc. Con. for J. Martin
ATTN: Doc. Con. for T. Wright
ATTN: Doc. Con. for D. Dahlgren

OTHER GOVERNMENT AGENCIES

Central Intelligence Agency
ATTN: RD/SI, Rm. 5G48, Hq. Bldg. for OSI/PSTD

Institute for Telecommunications Sciences
National Telecommunications & Info. Admin.
ATTN: W. Utlaut

NASA
Goddard Space Flight Center
ATTN: P. Corrigan

DEPARTMENT OF DEFENSE CONTRACTORS

Aerospace Corporation
ATTN: N. Stockwell
ATTN: I. Garfunkel
ATTN: SMFA for PWW
ATTN: J. Carter

Berkeley Research Associates, Inc.
ATTN: J. Workman

Boeing Company
ATTN: D. Murray
ATTN: G. Keister

Charles Stark Draper Lab., Inc.
ATTN: D. Cox
ATTN: J. Gilmore

DEPARTMENT OF DEFENSE CONTRACTORS (Continued)

Computer Sciences Corporation
ATTN: J. Spoor
ATTN: C. Nail

Cornell University
Department of Electrical Engineering
ATTN: D. Farley, Jr.

Electrospace Systems, Inc.
ATTN: Security

ESL, Inc.
ATTN: J. Marshall
ATTN: C. Prettie

General Electric Company
ATTN: F. Reibert

General Electric Co.-TEMPO
Center for Advanced Studies
ATTN: W. Knapp
ATTN: DASIAC

General Research Corporation
Santa Barbara Division
ATTN: J. Ise, Jr.
ATTN: J. Garbarino

Geophysical Institute
University of Alaska
ATTN: Technical Library

University of Illinois
Department of Electrical Engineering
ATTN: K. Yeh

Institute for Defense Analyses
ATTN: E. Bauer

International Tel. & Telegraph Corp.
ATTN: Technical Library

JAYCOR
ATTN: S. Goldman

Johns Hopkins University
Applied Physics Lab.
ATTN: T. Potemra
ATTN: Document Librarian
ATTN: J. Dassoulas

Kaman Sciences Corporation
ATTN: T. Meagher

Linkabit Corporation
ATTN: I. Jacobs

University of Lowell Rsch. Foundation
ATTN: K. Bibl

MIT Lincoln Lab.
ATTN: D. Towle

McDonnell Douglas Corporation
ATTN: Technical Library Services

Mitre Corporation
ATTN: W. Foster
ATTN: W. Hall

DEPARTMENT OF DEFENSE CONTRACTORS (Continued)

Mitre Corporation
ATTN: W. Sen

Mission Research Corporation
ATTN: R. Hendrick
ATTN: R. Kilb
ATTN: R. Bogusch
ATTN: F. Fajen
ATTN: D. Sappenfield

R&D Associates
ATTN: W. Karzas
ATTN: C. MacDonald
ATTN: R. Lelevier
ATTN: B. Gabbard

Rand Corporation
ATTN: E. Bedrozian
ATTN: C. Crain

DEPARTMENT OF DEFENSE CONTRACTORS (Continued)

Science Applications, Inc.
ATTN: D. Hamlin
ATTN: L. Linson
ATTN: D. Sachs

SRI International
ATTN: C. Rino
ATTN: W. Chesnut
ATTN: V. Gonzales
ATTN: R. Hake, Jr.
ATTN: D. McDaniels
ATTN: R. Leadabrand

Technology International Corp.
ATTN: W. Boquist
ATTN: T. Fitzgerald
ATTN: G. Best